MS Tribometer

Variable environment friction
and wear testing machine

Final Report

MEAM 445/446 Senior Design
Team 11
September 2017 - April 2018
Submitted: April 30, 2018

Darryl Beronque
Reciprocating Motion

James Buser
Machining

Sabino Padilla
Loading and Machining

Ben Riedel
Project Management

Omar Rizkallah
Sensors and Controls

Kai Wang
Temperature Control

Project Advisors and Stakeholders

Dr. Robert Carpick
Faculty Advisor
John Henry Towne Professor and MEAM Department Chair
B.Sc., M.A., Ph.D.

Dr. Andrew Jackson
Faculty Advisor
Professor of Practice, MEAM
B.Sc., Ph.D.

Dr. Harman Khare
Faculty Advisor, Stakeholder
Research Project Manager, Carpick Nanotribology Group
B.E., Ph.D.

Abstract

Friction is the bane of any mechanical device. It is responsible for suboptimal operation of engines, massively contributing to CO_2 emissions, and causing millions of dollars' worth of losses. At a glance, a tribometer measures this ever-changing force to assist industry experts and researchers in predicting frictional effects. However, most tribometers exhibit price-tags of 5-figures or more, making them cost-prohibitive to small companies and labs. In addition, current tribometers are manufactured to be all-in-one solutions, entirely non-customizable and with limited testing environments.

This team has designed a small-scale tribometer that is a fraction of the cost of existing tribometers and is able to operate in a variety of different settings. The design process consisted of quantitative downselection and extensive prototyping in the device's subsystems. The subsystems of the MS Tribometer are loading, temperature, motion, and data acquisition. The instrument is able to test contact pressures of 0.05 GPa to 2 GPa in liquid baths and at temperatures ranging from -30°C to 200°C. This instrument enables researchers to test in extreme conditions where friction behaves in peculiar ways. The team hopes that armed with this instrument, researchers will make strides in understanding friction.

Contents

1 Executive Summary

The importance of understanding friction cannot be understated. In a typical car, only 21.5% of the fuel is used to put the car into motion; the rest is lost, largely due to friction [1]. However, friction in the engine is a double-edged sword. If one attempts to increase the viscosity of the oil in order to decrease contact friction, hydrodynamic friction arises [2]. Under high pressure and temperature (as one would find in an engine), a tribolayer may form. A tribolayer is a boundary layer between the interacting materials that is comprised of entirely new compounds. Countless hours of research have been conducted on this phenomenon and the related problems of lubricants.

Tribologists are researchers and academics who attempt to gain understanding of interacting surfaces in relative motion. This field is a bridge between the mechanical engineering of forces and motion, the materials science of the test substances, and the chemical engineering of oils and lubricants. Tribologists use devices named tribometers to conduct tests and collect data. At a glance, a tribometer consists of a point contact, a loading force on that contact, an oscillatory drive, and a frictional transducer (Fig. 1). The point contact is driven in a reciprocating motion under a set load and the resistance to motion (the frictional force) is measured and outputted. Often, but not always, tests are conducted in lubricant baths in order to assess the impact of lubricants on the friction between the two materials, as well as any compounds that arise.

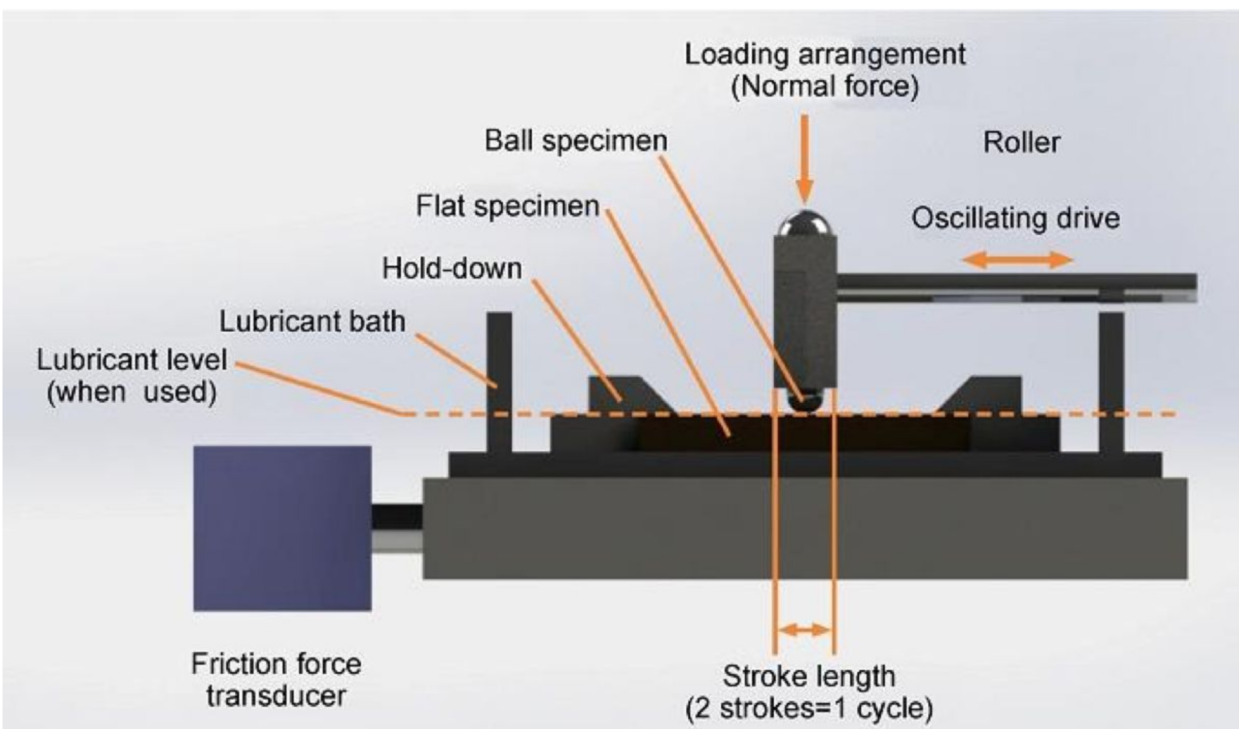

Fig. 1: The basic elements of a tribometer

However, tribology is a small field which only has a select few commercial tribometers available. These tribometers are often limited in their ability to represent certain environments, such as that of a car engine. Stress profiles, relative motion and velocity, and temperature can all widely affect results. Combine this concern with a lack of customizability in these tribometers, and it is reasonable to see why most research labs choose to build their own. Moreover, these commercial tribometers consistently exhibit price tags of greater than $50,000, which limits many firms from doing the required tests on their products. The Carpick Group is a renowned tribology research group at Penn that has expressed its need for a tribometer that is able to simulate car engine environments.

This senior design team was inspired by this shared need in multiple market participants. It set out to design a tribometer with three overarching qualities: affordability, ease of use, and reliability. Through constant communication with the Carpick Group and others, the team established design parameters for the MS Tribometer relating to loading, motion, temperature, and other aspects. After having carefully downselected technologies and prototyped rigorously, the MS Tribometer attains nearly all the goals the team set for its final device while still leaving ample room for customization.

The MS Tribometer (Fig. 2) utilizes technologies such as a twin double-leaf cantilever, thermoelectrics and resistive heaters, a micropositioning stage, a stepper motor and carriage assembly, and a testing base designed to easily integrate with current industry standards. The MS Tribometer is able to comfortably test in ranges of -30°C to 200°C, under loads of 1 mN to 15 N, at frequencies of 0.5 - 10 Hz over 5 mm, all while accommodating any lubricant in a bath. The normal and frictional loads output through LabVIEW, and coefficients of friction are measured over tests ranging from 10 seconds to 10 hours. This all coalesces in a device able to measure coefficients of friction ranging from 0.05 to 0.50 in a wide range of harsh environments.

In its final form, the MS Tribometer will be used by the Carpick Group in the foreseeable future. The team hopes that the Group will make strides in understanding friction and wear using the MS Tribometer, and that the engineering accomplishments achieved in this design will influence the Group's future tribometers.

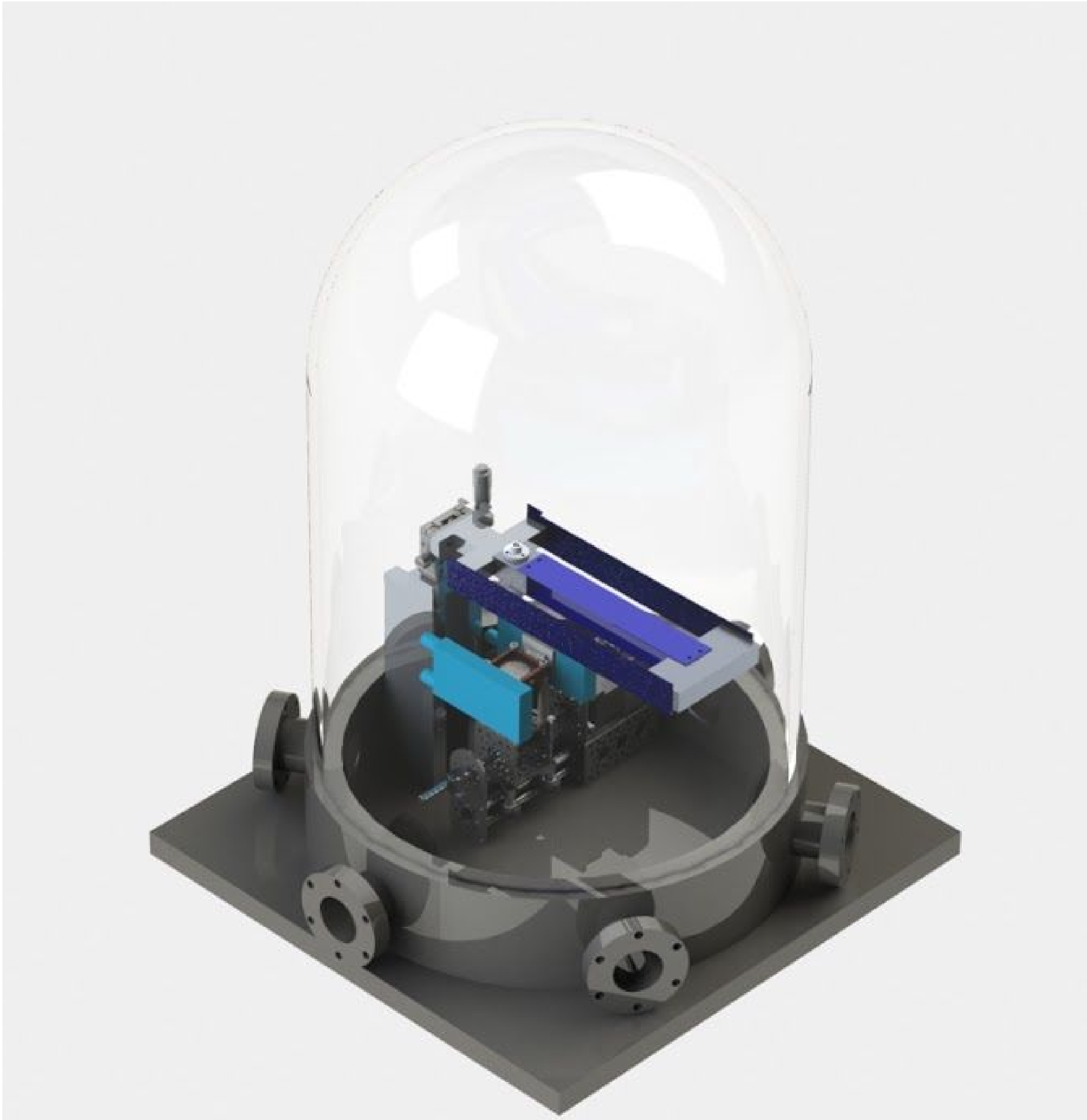

Fig. 2: The MS Tribometer

2 Statement of Roles and External Contributions

2.1 The Team

Darryl Beronque - Chief Motion Officer

Darryl's main responsibility was designing, selecting, and optimizing the linear motion system. Along with the motion system, Darryl took on programming responsibilities regarding the software necessary for the motion and data acquisition systems. In the Fall, Darryl worked on the first prototype, specifically, on the linear reciprocation of the system. Some duties included designing the linear reciprocation system, manufacturing its components, and developing and integrating the software with the team's first prototype. In the Spring, Darryl continued working on the linear motion subsystem. Based on feedback from the team's advisors, Darryl redesigned the linear motion subsystem and developed a new program to drive the linear reciprocation of the system. Darryl also designed and programmed the first iteration of the data acquisition system GUI and worked with Omar Rizkallah to integrate the data acquisition hardware with MATLAB and LabVIEW.

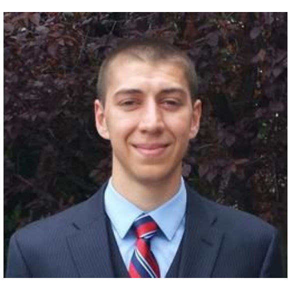

James Buser - Chief Machining Officer

James was primarily in charge of machining and assisting on the temperature subsystem. During the fall semester he designed the first testing base and worked closely with Kai on the temperature subsystem. In the spring, the testing base design was updated and remachined. James also machined the parts that interacted with the micropositioning stage. He also machined the piece that interfaced the micropositioning stage and the cantilever. James worked with Darryl Beronque to perform tests with the final system.

Sabino Padilla - Chief Cantilever Officer

Sabino was primarily in charge of the cantilever system. In the fall semester he designed and built the initial L shaped cantilever prototype and worked with Darryl Beronque in order to connect the first prototype to the motion system. Sabino was also initially in charge of determining how to load the system and contributed in the efforts to learn about and select strain gauges. In the Spring, his work consisted of first verifying spring steel as a viable cantilever material through MTS testing. Based on the initial design idea provided by Dr. Bennett (see below) Sabino created SolidWorks parts and compiled an assembly of the folded double leaf cantilever used in the final iteration of the machine and worked as the mechanist in charge of producing said designed parts. Once the cantilever was completed and assembled, Sabino developed the calibration tests used to convert the electric signals read into the system into forces.

Ben Riedel - Chief Executive Officer

Ben took responsibility of managing the project in its entirety. He oversaw each subsystem design process, in constant communication with each team member, and acted as a leader for the year. Ben also designed the loading subsystem in its entirety. He took an active role in scheduling meetings and ensuring good channels of communication amongst the team. Ben directed the team's Gantt chart creation and maintenance. In addition, he was the lead point of contact for interested third-parties such as advisors, sponsors and industry engineers. He maintained relations with Dr. Carpick and Dr. Jackson and scheduled the monthly advisor meetings.

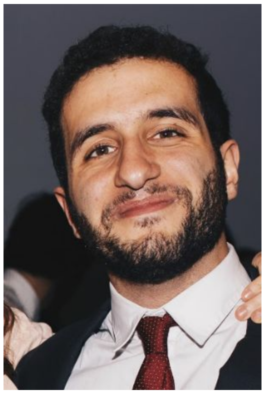

Omar Rizkallah - Chief Acquisition Officer

Omar was responsible for the design of the data acquisition subsystem.This includes the circuitry hardware, ranging from the choosing and installation of the strain gauges to the design of the amplification circuit as well as the circuit designed to measure temperature into the data acquisition board. He was responsible for learning labVIEW and implemented a project file on the software side to collect, process and present the force and temperature data.

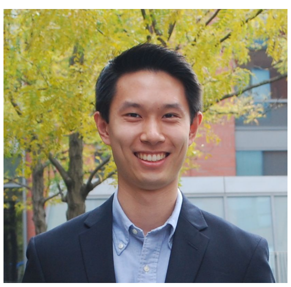

Kai Wang - Chief Temperature Officer

Kai was responsible for designing and assembling the temperature subsystem. This responsibility included modeling heating and cooling processes, designing the testing base to minimize external heat transfer, selecting heating and cooling devices to reach the target temperatures, conducting tests to reach the temperatures, and assisting in integrating temperature into the data acquisition and control subsystem.

2.2 Advisors and external contributions

Dr. Robert Carpick, Faculty Advisor

John Henry Towne Professor, MEAM Department Chair

Dr. Carpick served as one of two primary faculty advisors. Dr. Carpick provided valuable advice on how tribometers function and connecting the team with members of the Carpick Group who furthered the team's understanding of the tribometer subsystems.

Dr. Andrew Jackson, Faculty Advisor

Professor of Practice, MEAM

Dr. Jackson was one of two primary faculty advisors. Dr. Jackson provided the team with knowledge about the current industry as well as the impact of tribology as a field of study. Dr. Jackson's input formed a strong portion of the team's ultimate need statement.

Dr. Harman Khare, Technical Advisor / Stakeholder

Research Project Manager, Carpick Nanotribology Group

Dr. Khare served as the team's primary contact with the Carpick Group. Dr. Khare was instrumental in connecting the team with relevant experts within the Group as well as offering his guidance on what data would be useful for the full system to output.

Dr. Alex Bennett, Technical Advisor / Stakeholder

Postdoctoral Fellow, Carpick Nanotribology Group

Dr. Bennet aided the team in discussions on how to go about constructing the final tribometer. Dr. Bennett provided the initial idea for a folded double leaf cantilever system that was later on realized by the team.

The team would also like to recognize the Argonne National Lab who provided the data used for data matching and verifying the device.

3 Need and Background

3.1 Tribometers and Their Uses

The field of tribology is commonly known as ‘the branch of science and technology concerned with interacting surfaces in relative motion and with associated matters,’ and deals with the study of friction, wear, and lubrication [3]. Its contributions to the world’s engineering progress cannot be understated, as nearly every mechanical system is affected by the contacts of two surfaces. The field’s findings extends to such non-intuitive areas as medical devices, food science, and cosmetics.

In many cases, low friction is desirable to minimize the superfluous work done overcoming the opposing force. Examples of such applications include biological joints, bearings, gears, and myriad other mechanical components. However, in many other cases, such as brake discs or clutches, there exists a predictable large frictional force. Whenever surfaces move in contact with each other, wear will occur--a progressive loss of material from one or both surfaces. Wear is often detrimental and can lead to an unwanted increase in freedom of movement, vibrations, or mechanical stresses among other issues. Although, controlled high wear rates are sometimes desirable in capacities such as grinding or polishing. A key method of reducing friction and minimizing wear is to lubricate the system. Thus, the science of lubrication is closely related to the study of friction and wear in the overarching field of tribology.

All surfaces are uneven at a sufficiently small scale. An element of the smoothest stainless steel may be polished for hours, yet still show irregularities. Many methods of examination of the topography of sample surfaces exist currently, including optical measurements, the contact of a fine stylus, and the most accurate, atomic force microscopy (AFM). Fig. 3 shows an example of the disparities that can be seen on otherwise identical steel samples.

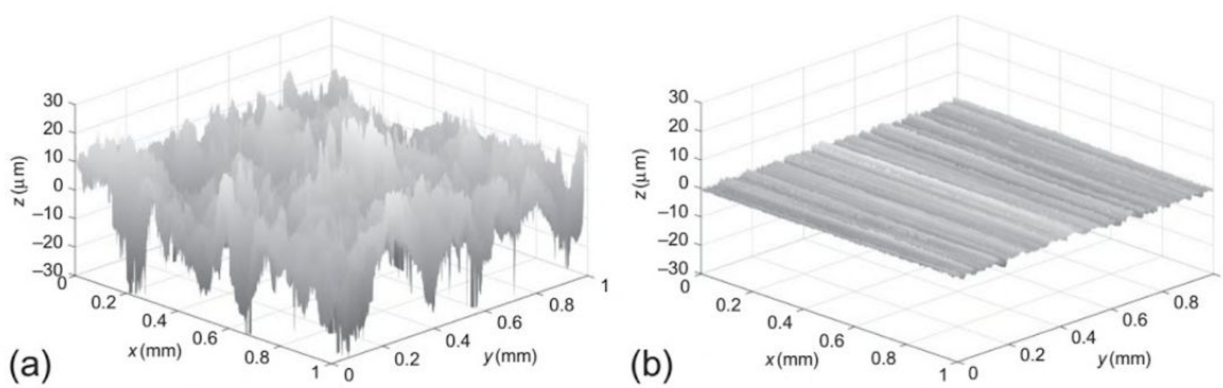

Fig. 3: Three dimensional plots of (a) a grit blasted steel surface; (b) a ground steel surface [1]

However, tribology is the study of surfaces in contact with one another, so the discussion must turn to the meaning of *asperities*. Asperities are the microscopic points at which two surfaces two surfaces touch when brought gently together. Fig. 4 displays the interaction and subsequent deformations of asperities on two solids. The asperities in contact are responsible for supporting the applied normal load and generating any frictional forces. It is also at these points that stress concentrations arise. Due to the asperity's small area, the resulting pressure can be very high. The mathematical analysis of these stresses was first addressed by Heinrich Hertz and is referred to as *Hertzian contact mechanics* [3].

Fig. 4: The top image shows asperities under no load. The bottom image depicts the same surface after applying a load [4].

Hertz simplified the random surface imperfections to gain mathematical insight using two elastic spheres under a normal load *W*, as seen in Fig. 5. Contact occurs of a circle of radius *a*, given by:

$$a^3 = \frac{3WR}{4E^*} \tag{3.1.1}$$

Where *R* is the relative radius of curvature of the contacting bodies:

$$\frac{1}{R} = \frac{1}{R1} + \frac{1}{R2} \tag{3.1.2}$$

And E^* is the reduced modulus, which depends on the Young's moduli of the two bodies, E_1 and E_2, and on their respective Poisson ratios.
The pressure *p(r)* in the contact varies with distance *r* from the center of the contact as:

$$p(r) = Po\sqrt{1 - \frac{r^2}{a^2}}, r \leq a \tag{3.1.3}$$

Where *Po* is the maximum pressure that occurs at the center of the contact. It can also be shown:

$$Po = \frac{6WE^{*2}}{\pi^3 R^2} \tag{3.1.4}$$

This type of contact is commonly referred to as a *point contact*, as opposed to a *line contact*, which is applicable to two cylindrical surfaces with parallel axes. Attempting to simulate contacts is outside the scope of this project, as the market need is specialized to point contact simulations, detailed below.

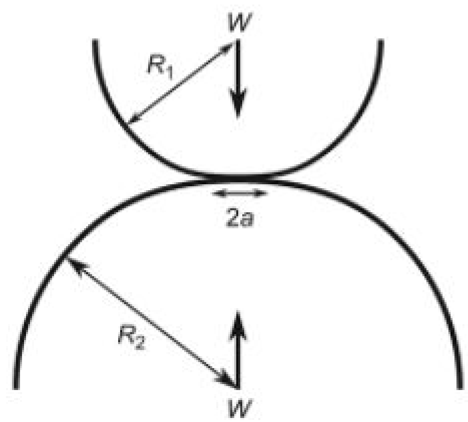

Fig. 5: Elastic deformation between two spherical surfaces under normal load *W* to form a contact circle with radius *a* [3]

These and other equations guide tribology experts when conducting research and guided the team when designing the MS Tribometer.

3.2 Intended Use of the MS Tribometer at Penn

The principal use of the MS Tribometer is to aide research conducted in University of Pennsylvania's tribology research lab: the Carpick Nanotribology Group ("the Group"). Robert Carpick, the Group's head and a faculty advisor to the team, has expressed the lab's need for a small, macroscopic tribometer. The Group has achieved breakthroughs in the nanoscale using special instruments such as ultrahigh vacuum (UHV) tribometers, and atomic-force microscopy (AFM). The Group also utilizes a specialized tribometer, restricted to simulating line contacts. However, the renowned Group lacks a small-scale point contact tribometer to simulate contacts at the macroscale.

Fig. 6: The Carpick Group [5]

Dr. Carpick and the broader team have had success studying interactions in the nanoscale. In a 2015 publication, the Group addressed the frictional losses of the anti-wear additive, zinc dialkyldithiophosphate, or ZDDP. The Group investigated the creation of a ‘tribofilm,’ a thin, solid layer that adheres to the surfaces in contact and further protects them from wear [6], and its chemical relation to the mechanical stresses inherent in an engine.

The Group often uses tribometers to test automotive lubricants and engine performance. In light of the introduction presented above, engines are complex mechanical systems with many moving parts in contact. As such, a large field of tribology is dedicated to simulating the contacts in engines and the efficacy of automotive lubricants. Friction losses in these systems are very important. They drastically affect efficiency and life of an engine, which in turn have large implications for the world’s energy use. “Our overall motivation is to more efficient and sustainable," Carpick said. "Considering the massive use of vehicles, a small gain in efficiency has a big impact in saving energy and reducing carbon emissions annually" [7]. There exists a huge potential to reduce carbon dioxide emissions by striking a balance between its viscosity and the frictional contact of engine components [7]. The Group also studies the tribology involved in electro-mechanical switches and geological processes.

The MS Tribometer will enable the Group to test the desired physical scale at extreme temperatures. It will be able to test at temperatures ranging from -30°C to 200°C in order to represent conditions of an engine’s exposed parts during a harsh winter and its typical operating temperature. The desired normal force range applied is 10mN to 10N, meant to study coefficients of friction ranging from 0.05 to 0.5, with a transducer noise less than 5%. The substrate will reciprocate back and forth along a track length of 5 mm at frequencies between 0.5 and 10 Hz. The MS Tribometer has the ability to test in a bath of lubricant or other liquid. In addition, the team has a reach goal of varying the ball contact’s roll to slide ratio. This will truly be a novel characteristic in a tribometer. To the team's knowledge, current solutions only have a stationary or rotary ball, but are unable to simulate tests in a middle ground. In many field applications, however, contacts rotate as well as slide.

3.3 Competitive Market Landscape

However, market research was not limited to academic research conducted at Penn. The team contacted tribology research labs around the country and internationally to learn about the needs of the team's customers. In total, the team received responses from researchers at six different labs about their tribometer use. A summary of their responses is available in Table 1 below.

Table 1: Academic research landscape

				Temp (C)		Force (N)		Stress (GPa)	
Professor	**University**	**Liquid Testing?**	**Flowing liquids?**	**Low**	**High**	**Low**	**High**	**Low**	**High**
Dr. Robert Carpick	*Univ. of Penn.*	*Yes*	*Yes*	*-50*	*200*	*0.01*	*10*	*0.05*	*2*
Dr. Bart Raymaekers	University of Utah	Yes	No	18	37			0	0.002
Dr. Jeffrey Streator	Georgia Tech	Films only	No	20	200			0	couple GPa
Dr. Q Jane Wang	Northwestern	Yes	Yes	20	700	0.001	13000	0.5	1
Dr. Chaunlin Tao	Oakland Univ.	Yes	No	20	120	0.5	1000		
Dr. Alison Dunn	UI - Urbana Champaign							0.000001	1
Dr. Ngaile Gracious	North Carolina State	No	No		100		1.00E+06		

			Implied Speed (m/s)					
Professor	**Track dimensions**	**Frequency (Hz)**	**Low**	**High**	**Drive**	**Make vs Buy**	**Variable roll/slide**	**Transdu-cer noise**
Dr. Robert Carpick	*5 mm*	*0.5-10*	*0.005*	*0.1*	*Linear reciprocating*	*Make*	*Yes*	*5%*
Dr. Bart Raymaekers			0	2	Linear reciprocating			
Dr. Jeffrey Streator	up to 2m		0.0025	several m/s	Linear reciprocating	Make	Yes	5-10%
Dr. Q Jane Wang					Pin on disk, journal bearings	Buy		
Dr. Chaunlin Tao		1.0 -10			Linear reciprocating, rotary	Buy		
Dr. Alison Dunn						Make		
Dr. Ngaile Gracious					Ring compression, ball penetration, spike test	Make	No	

From the responses that were received, the team found that researchers were fairly split on whether they built or bought tribometers. While Dr. Wang from Northwestern University preferred to buy commercial tribometers due to the months of effort needed to build tribometers, Dr. Streator, Dr. Dunn, and Dr. Gracious preferred to build their own tribometers because of the high cost, often tens of thousands of dollars, and the unique requirements of their tests. However, several commonalities emerged among the responses:

1) Testing in liquids was a common requirement due to the use of lubricants in mechanical systems to decrease wear. Fluid flow in particular was desired to effectively simulate the movement of lubricants in those systems. In addition to lubricants, liquid testing would also help simulate biological surfaces for researchers interested in friction and wear in nature.
2) Contact stresses varied from miniscule values to several GPa, which corresponds to the yield strength of the strongest metals
3) Temperatures generally ranged from room temperatures to several hundred degrees Celsius, which can simulate engine-like environments. However, low temperature capability was also requested in order to simulate extreme cold weather conditions.
4) Linear reciprocating drives and pin on disk / rotary drives were most common because of their similarity to the sliding and rotating motions in mechanical systems

On the other hand, liquid flow and varying the slide-to-roll ratio of the contact ball were relatively niche requirements. Ultimately though, these results verified that there was indeed demand in labs for tribometers with requirements similar to those proposed by Dr. Carpick.

At the same time, the team examined existing tribometers on the market to see if they fulfilled all of the requirements. While the team found a number of tribometers currently on the market that fulfilled some, there were none which fulfilled all of the requirements. Through website browsing and emailing support staff, the team was able to identify 8 different tribometers from 5 manufacturers. The team automatically excluded tribometers which clearly did not possess a majority of the required capabilities. A list of the tribometers and their capabilities compared to the team's needs is available in Table 2 below.

Table 2: Current tribometers and their functions

				Temp (C)			Force (N)		
Manufacturer	Model	Flowing liquids?	Interchangeable head?	Low	High	Humidity	Low	High	Simultaneous?
Desired		*Yes*	*Yes*	*-50*	*200*	*Controlled*	*0.01*	*10*	*Yes*
Rtec Instruments	Universal Tribometer	No	Yes	-60	1000	Controlled	nN	500 0	N/A
Rtec Instruments	Nano Tribometer	No					uN		N/A
Anton Paar	Pin on disk	No		-	-	Controlled		10	-
Anton Paar	High Temp	No			1000			10	N/A
Anton Paar	Nano Tribometer	No				Sensor	5 uN	1	N/A
PCS	MTM	No	Yes	20	150		0	75	N/A
Nanova	T50	Limited to drops	Yes	-40	1000 (150 w/ liquids)	Controlled	0.1	40	Yes
Lewis Research	LRI-1A	No	No	-	-	-	-	-	-

	Ball DIA (mm)					Implied Speed (m/s)			
Manufacturer	Low	High	Type of contact?	Track dimensions	Frequency (Hz)	Low	High	Drive	Variable slide/roll ratio
Desired	*2*	*12*	*Ball*	*5 mm length*	*0.5 - 10*	*0.005*	*0.1*	*Linear reciprocating, rotary*	*Yes*
Rtec instruments								rotary, reciprocating, block on ring, four ball	
Rtec instruments								rotary, linear, piezo	
Anton Paar				60 mm disk				rotary	
Anton Paar								rotary	
Anton Paar					.01 - 10			linear reciprocating, rotary	
PCS	6	19		46mm DIA disk				rotary, rotary reciprocating	Yes
Nanovea	1	10	Ball, Pin	20 mm track	2 - 60	0.08	2.4	Linear reciprocating, rotary disk, and block on ring	No
Lewis Research	-	-	Ball	-	-			Linear and rotary	No

A key finding from Table 2 is that fluid flow is a rare capability for tribometers. Many tribometers can handle pools of liquid or thin layers of lubricants. However, fluids and lubricants in an engine cannot be modeled precisely through these relatively static forms of testing. The T50 tribometer manufactured by Nanovea comes close through the use of liquid drops, but is lacking in other areas such as temperature and speed ranges for their linear reciprocating drive. Although the breadth of current tribometers covers the entire range of operating conditions required by Dr. Carpick, there is no single tribometer that can operate in all the conditions simultaneously.

While novel and innovative, perhaps the most important aspect of the MS Tribometer is the price. Current comparable tribometers made by manufacturers cost more than \$50,000, an undoubtedly prohibitive price for any small research lab. To purchase a tribometer, even large research labs must obtain a generous grant. Many labs or companies designing components that should be friction or wear-tested, are not conducting the tests due to the price of a tribometer. The team would like to remedy that. The price of MS Tribometer will be an order of magnitude smaller than the leading solutions. With the important implications of tribology for greenhouse gas emissions, the problem of cost must be remedied in the near term.

3.4 Problem statement

Lubricants exist in many mechanical systems, and their frictional properties must be tested using tribometers in order to optimally design systems and reduce friction losses. Tribometers are currently commercially sold and built internally by labs, but commercially sold tribometers don't cover the entire range of required environments for small-scale lubricant studies, and internally built tribometers typically take months of effort. The team proposes building a linear-reciprocating tribometer that costs under \$10,000 and is able to recirculate fluid flow, operate in temperatures between -50°C and 200°C, deliver loads between 10 mN and 10 N, reciprocate at frequencies between 0.5 and 10, and operate on a track length of at least 5 mm, while maintaining transducer noise below 5%.

4 Objectives

4.1 Design Specifications

Based on the conversations with the Carpick Group and with other research groups, the team finalized the objectives listed in Table 3 below. The low-end of the basic goal for temperature range was revised up to -30°C from the -50°C target requested by the Carpick Group to be more realistic and in-line with capabilities of commercial tribometers. Load and ball diameter variation were finalized to be able to result in a contact stress range of 0.05 GPa to 2 GPa to be able to test metals up to their yield strength. The viscosity range was set make sure lubricants of all viscosities, including lubricants at the low and high end of temperature ranges, would be able to flow through the contact surface. Friction coefficient detection ranges were chosen to roughly match the capabilities of commercial tribometers and ranges that the Carpick Group has historically explored. The < 5% transducer noise goal was also determined to roughly match commercial tribometers. Reciprocation frequency and length were finalized to result in speeds of 0.005 m/s to 0.1 m/s, which would be common in mechanical systems. Finally, a capability of varying the roll/slide ratio of the ball was a reach goal as this can provide interesting data for a ball contact as opposed to pin contacts.

Table 3: Final objectives for MS Tribometer

Parameter	Subsystem	Basic Goals	Reach Goals
Load Variation	Loading	10mN - 10N	
Ball Diameter Variation	Loading	2 - 12mm	
Roll-Slide Capability	Loading	Roll or slide	Adjustable roll-slide ratio
Linear Reciprocation Frequency	Motion	0.5 - 10 Hz	
Reciprocation Length	Motion	> 5 mm	
Temperature Range	Temperature	-30°C to 200°C	-50°C to 200°C
Fluid Testing	Fluid	Static fluid	Flowing fluid
Viscosity Range	Fluid	1 - 2500 cSt	
Friction Coefficient Detection	Data Acquisition	0.05 - 0.5	0.01 - 0.5
Transducer Noise	Data Acquisition	< 5%	< 1%

4.2 Engineering Standards

There are a few standards established by the American Society for Testing and Materials (ASTM) which apply to the testing methods related to the use of tribometers. The current ASTM standards that apply to the team's build of the tribometer are listed and described below.

Linearly Reciprocating Ball-on-Flat Sliding Wear (ASTM G133) **[8]:**

ASTM G133 standard defines a linearly reciprocating configuration of a tribometer with a ball-on-flat interface. This apparatus should contain a spherical tip that allows a back and forth movement across a flat surface. During the motion, either the flat surface or the spherical tip can perform the back and forth motion. Either configuration is accepted. The spherical tip is sometimes replaced by a ball bearing. If using a ball bearing, it must be tightly clamped onto the pin as to prevent any slippage during the oscillating motion. To measure friction coefficients and forces, tension-compression load cells or similar devices are used. Moreover, some tribometers have to consider the effects of humidity and temperature. Humidity and temperature sensors should be present to actively measure both properties. Humidity sensors should be as close to the test specimens as possible to avoid the effects of air flow on the relative humidity readings. Additionally, it is required to measure the humidity at an accuracy of +/- 3%. The measurement of temperature should be in Celsius and in tests with lubrication submerged test specimens, the liquid temperature should also be recorded. An example of a configuration that this standard applies to is shown below (Fig. 7).

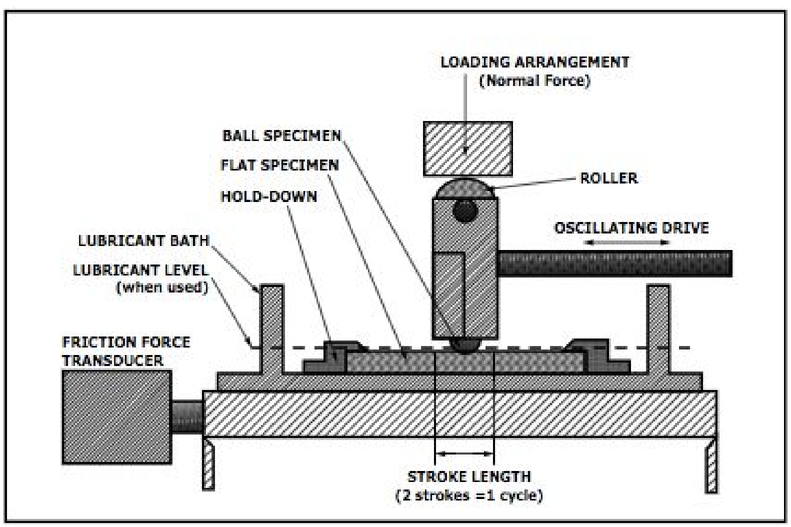

Fig. 7: Linearly reciprocating schematic

Three parts of the apparatus require calibration: loading system, motor drive, and friction force sensor. With the loading system, the applied normal load should not vary more than 2% of its magnitude (i.e. 10 N load shouldn't var +/- .2 N). Both the motor drive and friction force sensor should be periodically checked so that the oscillation and the normal load applied is consistent throughout the test. Furthermore, a method to provide a calibrating force designed to adjust the friction and normal forces should be present. Calibration checks and the use of sensors may pose a problem at extreme temperature values due to the proximity requirement that allows accurate measurements.

***Wear Testing with a Pin-On-Disk Apparatus (ASTM G99)* [9]:**

Similar to the linearly reciprocating configuration, the pin-on-disk apparatus (Fig. 8) can have a ball-on-surface interface. Additionally, either the pin holding the ball and the surface or disk can move (while the other remains static) to perform the friction tests. Thus, either the pin can rotate around the disk, creating a circular track or the disk itself rotates about its center while the pin remains still. According to ASTM G99, this apparatus should contain a motor drive (changes the rotational speed of the disk), revolution counter (counts the number of revolutions performed by the disk), pin and lever arm system (holds the pin and ball in contact, in place during the disk rotations), and wear measuring systems (record the amount of wear from the test specimens). For the team's tribometer design, the configuration will instead contain a linear stage, as opposed to a circular disk and the base will be driven linearly by a motor where the oscillation is linear rather than circular.

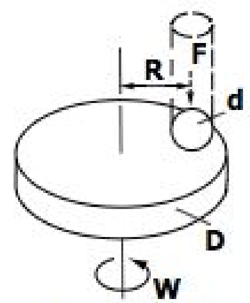

Fig. 8: Pin-On-Disk Schematic

***Measuring and Reporting Friction Coefficients (ASTM G115)* [10]:**

ASTM G115 standard serves as a guide to properly choose the correct tribosystem to measure friction coefficients. Both the pin on disk and linearly reciprocating systems were approved as proper test configurations to measure friction coefficients and wear.

***Data Acquisition in Wear and Friction Measurements (ASTM G163)* [11]:**

ASTM G163 describes the necessary components to successfully acquire the desired data from the tests. The main components needed to acquire data include hardware such as sensors (force transducers or strain gauges for example), data acquisition system such as filters, analog to digital converters or other electronic circuits, and a controlling computer. Additionally, software should be present to handle the data acquired from the hardware. In the team's case, the software used was LabView, as the Carpick Group is accustomed to using LabView in tests.

Measuring Rolling Friction Characteristics of Spherical Shape on a Flat Horizontal Plane (ASTM G194) **[12]:**

ASTM G194 describes the sliding friction as the sum of the forces from deformations of surface features, atomic and molecular attractive forces, and the interactions between film and particulates on both surfaces. Additionally, it establishes that rolling friction is the sum of the aforementioned forces with the added effects of the different characteristics of the ball rubbing on the surface. Thus, it concludes that the best way to evaluate rolling friction is to develop a test in which the material of interest (as a sphere or ball) is rolled upon the desired counterface.

5 Design and Realization

5.1 Loading Subsystem

5.1.1 Design Loading

The various options for this subsystem were judged on numerous criteria. The most important is the ability to not only span the desired load range (10mN - 10N) in an incremental manner. The variation of the loading force works in tandem with the size and material of the ball attached to the end of the system in order to determine the area of contact, which in turn determines the pressure distribution and stress forces at the contact point as it moves. Other factors considered were repeatability of the process, the ease of implementation and the potential challenges a system would pose for collecting accurate data.

The team saw two overarching possible methods in the design space of the vacuum chamber to induce a force:

1. A weight or actuator acting on the pin itself
2. A displacement using the spring quality of the cantilever to create a force

The solutions considered were:

Piezo Actuators

Piezoelectrics are materials that convert mechanical energy into electrical energy. These materials are capable of working in reverse (i.e. converting electrical energy into mechanical energy) [13]. Piezoelectric actuators are capable of providing large loads of force depending on the voltage applied with minimal displacement. These components also take up minimal space and can be integrated into the system easily.

Fig. 9: Piezoelectric actuators [13]

Implementing this system would be a matter of installing it into the physical beam in order to displace it and apply a load. Piezoelectrics have a long lifespan and the movements are repeatable and precise [13]. The thin wire connections required to operate the device would cause negligible vibrations to the system. However, piezoelectrics are limited by a small maximum displacement and a relatively difficult ease of use.

Linear Actuators

A linear actuator pushes a piston out based on an electric voltage.

Fig. 10: Linear actuator [14]

This system is capable of loading in a continuous manner, like the piezoelectric version, however, this system cannot be integrated into the beam system and requires the build of a system to suspend the actuator over the beam so it can push down on it when activated. Since the beam system itself would be moving, the actuator would need to remain in contact and move with the beam.

Discrete mass loading

The simplest system would be to weigh down the end of the system with a combination of objects with known masses. For a range of loads, the masses would need to range from 1 gram to 1 kilogram. While such sets are available for purchase, the issue with such a system would be that it is a discrete loading system dependent on the quantity of smallest masses available. Loading this system would potentially take more time than the previously discussed systems. The dimensions of the masses would also be larger than that of the beam meaning there is potential for uneven loading as well as a top-heavy system that may affect the readings of the sensor as the entire system moves back and forth.

Micropositioning stage with spring

A compression spring could be loaded above the system and the force applied would be determined by Hooke's law. Utilizing the spring steel in the cantilever would give it a dual purpose: first, to displace to measure a force and second, to apply the force. A micropositioning stage designed to displace the cantilever very accurately in the normal direction would need to be set at the beginning of a test. This means however that the load is subject to human error.

Table 4: Design downselection of loading mechanisms

	Desired load range (0.1 N to 10 N)	**Ease of use**	**Resolution**
Linear Actuator	**Satisfies**	**Poor -** Must control using software and a circuit + controller	**Good**
Masses	**Satisfies**	**Medium –** Must switch out masses and maintain a set	**Poor**
Piezoelectric Actuators	**Fails -** Limited displacement is unable to induce the correct strain in cantilever	**Poor -** Must control using software and a circuit + controller	**Good**
Micropositioning Stage	**Satisfies**	**Good -** Able to simply the turn dial to adjust load and utilizes cantilever	**Good**

5.1.2 Realization Loading

The team ultimately chose the micropositioning stage due to its reliability, ease and high resolution. The micropositioning stage utilizes the spring steel leaves of the cantilever to create a force when displaced. See Fig. 11 for a pictorial depiction of the mechanism. A strain is then induced in the horizontal leaves, measured by the strain gauges, and outputted by the data acquisition system. This system is advantageous due to its reliability, ease of use, and small topological footprint.

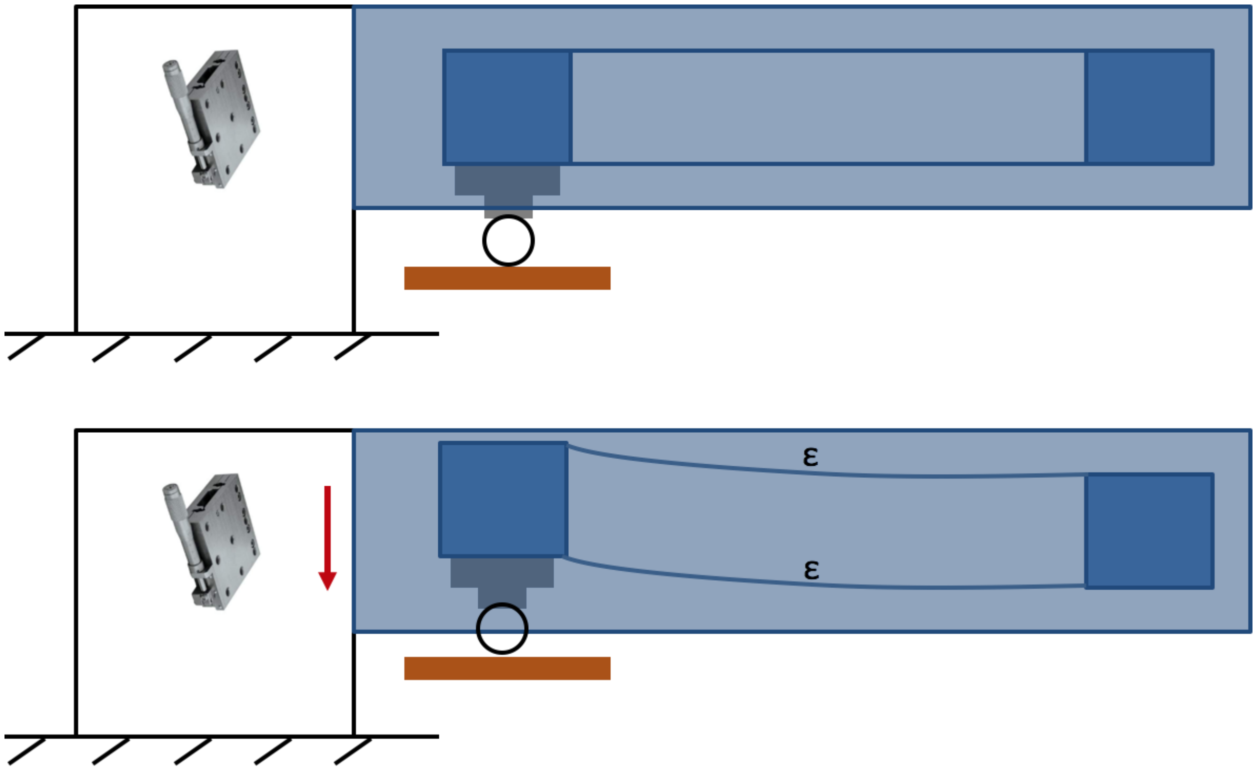

Fig. 11: Before the system is loaded (top), and the system under loading (bottom).

Integration challenges with the z-axis translation micropositioning stage centered around the attachment to the vacuum chamber. In order to relieve concerns regarding the load transfer and torque that the interface would experience, the team purchased a micropositioning stage with a horizontal angled bracket mount. This enabled the team to directly affix the micropositioning stage to the raised platform without worries of undue torque to parts not designed to handle the load.

The team purchased a 40 mm x 40 mm OptoSigma TADC-SZ horizontally mounted micropositioning stage, seen in Fig. 12. Upon testing with the cantilever, the team was delighted to find that the maximum load was 15 N, rather than the requested 10 N. This means that the MS Tribometer is able to test at higher stress profiles than originally requested, which opens up a larger range of coefficients of friction.

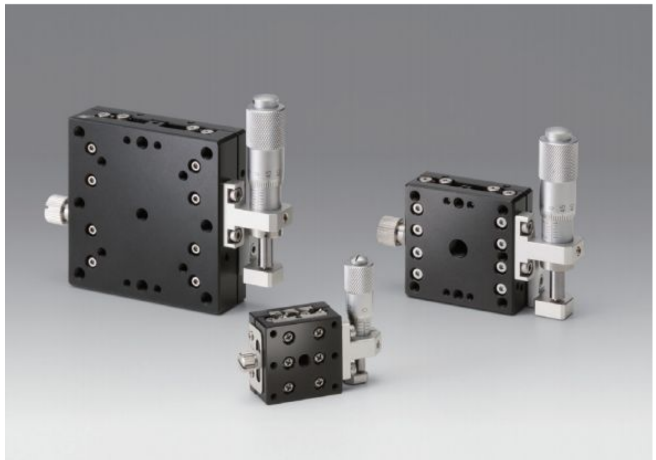

Fig. 12: Micropositioning stages of varying sizes; chosen 40 mm size seen in the top right.

5.1.3 Design Cantilever

There were three overall designs considered for the cantilever system. The first design was the design utilized in the first prototype which consisted of two rectangular beams in an L-shape such that each beam was rigid in every plane except the plane in which it was meant to bend. Planar views of the system can be seen in Fig. 13 below.

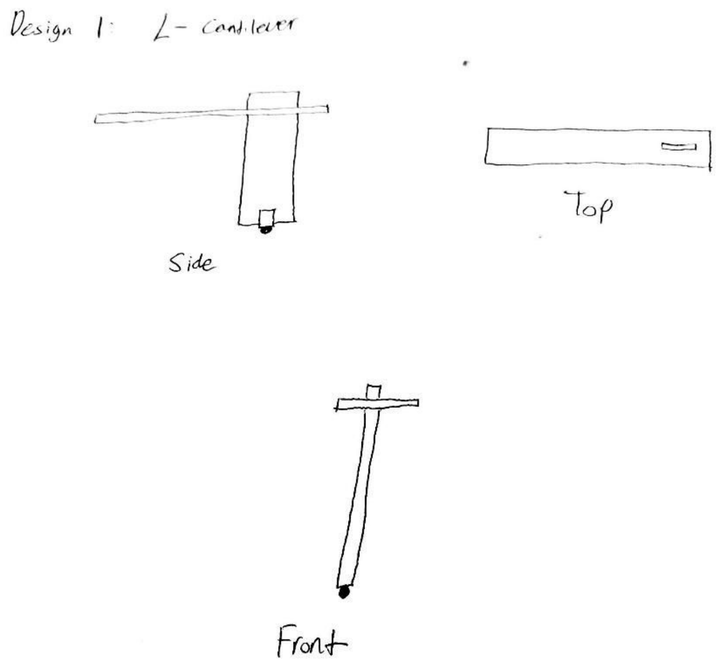

Fig. 13: L-Shaped cantilever design

The second design considered, though never physically made, was the initial double leaf cantilever system where two sets of two beams coupled to one another in a parallel configuration. These beams would be connected in a line such that the one set of beams would bend when a normal load was applied to it, while the other set bent in the direction perpendicular to the direction of the normal load. The system described can be seen in Fig. 14 below.

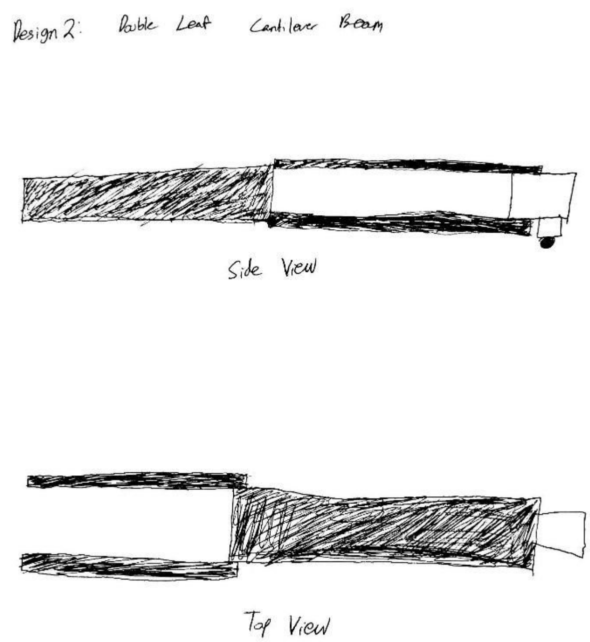

Fig. 14: Initial double leaf cantilever design

The final design chosen was a variation of the second design where instead of a straight line, the cantilever folded in on itself such that the beams that were loaded normally were between the beams that bent laterally. This final design was chosen because not only did the coupling prevent displacement in unwanted directions as seen in the initial design but the folded over nature of the beam meant that the system could be made such that one beam spanned the length of the vacuum chamber as opposed to dividing that length between the two beams. By doing this, the overall rigidity of the beam is lessened allowing the beam pairs to bend significantly even at low loads, allowing for better force sensing. The realized design was generated on Solidworks and can be seen in Fig. 15 below

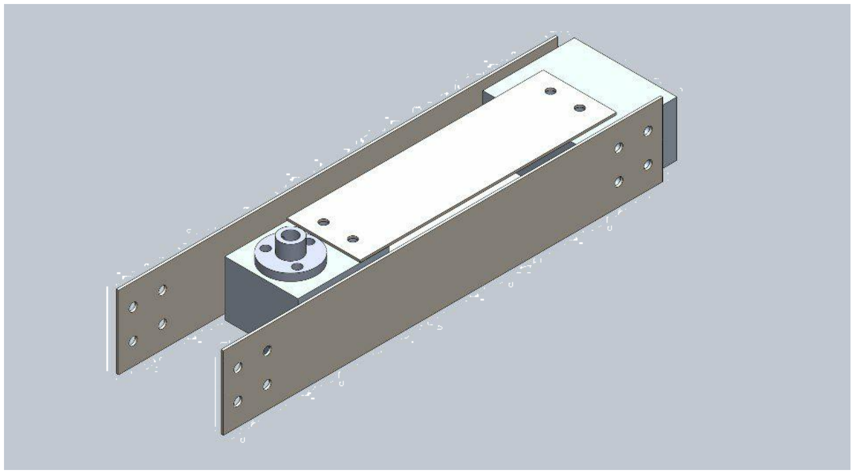

Fig. 15: Folded double leaf cantilever design

A summary of design considerations can be found below in Table 5.

Table 5: Different design considerations

	Undesired Deflections	Sensitivity	Number of Parts	Manufacturing Time
L-Cantilever	**High -** Torsion not constrained, there is potential for translation as opposed to bending	**Low -** Due to material choice	2	**Low** - Lasercut
Double Leaf Spring	**Low -** Coupled beams prevent torsion and translation	**Medium –** Length constrained by the chamber	8	**High** - CNC manufacturing required
Folded Double Leaf Spring	**Low -** Coupled beams prevent torsion and translation	**High-** Can span the full length of the chamber	8	**High** - CNC manufacturing required

5.1.4 Realization Cantilever

The cantilever beam itself consists of eight manufactured parts and two additional components. The eight parts are the two normal cantilever beams, two perpendicular beams, one positioning cube, one loading cube and two hub pieces used to load balls in place.

The cantilever beams were manufactured out of 1/40” 1095 Spring Steel. The normal cantilever beam was 6’’ long by 1’’ wide while the lateral beams were 8’’ long by 1’’ wide. The spring steel stock was cut to dimension using a stomp shear. Due to the nature of the tool, there were deviations to the actual dimensions of the beam, however, these were accounted for in future manufacturing processes. The holes cut in the piece were dimensioned from the center of the measured width as opposed to the dimension stated in the engineering drawings. The holes were cut using a 0.125” endmill with a carbide insert. On the normal beam, the holes were located on either side, .150’’ from the edge and ±.200’’ from the center line. On the lateral beams, one side has a square pattern of holes, one hole ±.200’’ from the center line at 0.200’’ and 0.600’’ from the edge. On the other side, there are two holes on the center line at 0.200’’ and 0.600’’.

The positioning cube is made of 6061-Aluminum, with 0.6000 thickness, 3.000’’ long and 1.000’’ in width. Holes located on the positioning cube align with one set of holes on the normal beam and with the square pattern holes on the lateral beams. The holes are tapped to fit 4-40 screws to a depth of 0.250’’. The loading cube is a 0.600’’ x 1.00’’ x 1.25’’ prism made of 6061-Aluminum. 4-40 screw holes to a depth of 0.250’’ were made on the top and bottom faces 0.200’’ from one edge to accommodate the hole pattern on the normal beam. In addition to this, a through hole of 0.188’’ diameter was drilled 0.650’’ above the midpoint between the two holes. A circular 4-40 screw hole pattern with a 0.500’’ diameter and 0.750’’ diameter from the center of the through hole on the top and bottom face respectively.
The top hub is made primarily on a lathe. 0.300’’ of 6061-Aluminum stock is turned to a diameter of 0.700’’. Of this, 0.200’’ is further turned to 0.300’’ diameter and a hole of 0.1875’’ diameter is drilled through the center. The piece is then transferred to the mill where a circular 4-40 screw hole pattern is drilled in a circle with a 0.500’’ diameter from the center and a 4-40 set screw hole is made on the 0.300’’ diameter portion.

The final hub is made in a similar manner, however, the overall hub length is 1.0125’’ where 0.8125’’ is turned to a 0.560 diameter and the remaining 0.200’’ are turned to 0.2’’. This hub is used to hold the steel ball used during testing in place and as such, the dimension of the two holes drilled on the center line will vary depending on the ball dimension used. The first hole is a through hole just under the diameter of the ball to be inserted and the second hole is a hole large than the diameter of the ball, that is drilled to 0.95’’. The piece is then transferred to the mill where a circular 4-40 screw hole pattern is drilled in a circle with a 0.750’’ diameter from the center.

The remaining parts required for the cantilever are the ball to be used in testing and a .1875 steel cylinder that is long enough to go from the top of the first hub and push the steel down and hold it in place, as well as all the necessary screws. The assembly of the cantilever involves first loading the desired steel ball into the appropriate bottom hub before attaching hubs to the loading cube and then securing the normal beams to the loading and positioning cubes. The lateral beams are then put on and the steel rod pushed through the top hub and secured using the set screw. The open end of the cantilever is used to connect to the loading system and is discussed in another section.

5.1.2.1 Roll - Slide Ratio

Roll to slide was a reach goal that was attempted to be implemented through the loading system. To allow the ball to roll, movement would have to be constrained in the vertical direction and have variable lateral direction restrictions. In the design shown in the figure below, the design made use of set screws to restrict lateral movement.

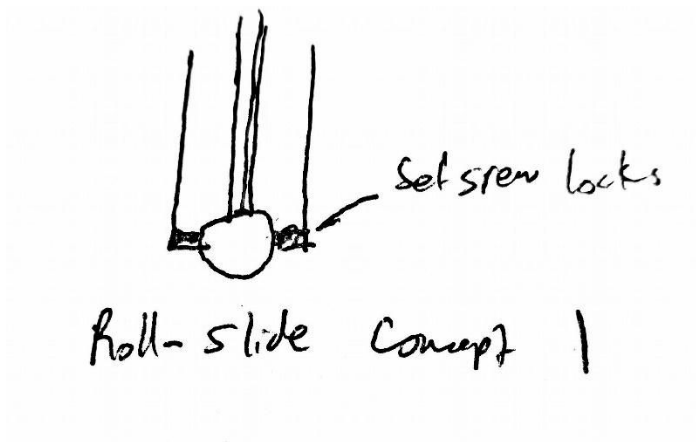

Fig. 16: Roll/Slide Design

This design was ultimately not fully realized due to time restrictions. The hub made in the cantilever section had the capability to create a downwards force, but due to the design of the system, set screws could not be implemented.

5.2 Motion Subsystem

5.2.1 Design Motion Subsystem

During the downselection for the linear motion subsystem, there were two overarching variables to consider in the design. First, there was the placement and configuration of the driving mechanisms relative to the other components in the tribometer. The decisions for the positioning of linear motion subsystem relied on the current iteration design of the other subsystems. Second, there was the actual implementation of the linear reciprocation. The design process included down selecting from different driving mechanisms and types of motors.

5.2.1.1 Placement of Subsystem

The placement of the linear motion subsystem was important in that it will determine the full configuration of the tribometer and dictate how much vibration the system will experience during operation. There were two placements considered: under the base of the beam and under the testing base. Placing the linear reciprocation system under the beam was advantageous in that it will avoid any circuitry and wires that the team anticipated to have near the testing base. Moreover, this placement will reduce the mass that the motor needs to drive. On the other hand, placing the linear reciprocation system under the testing base will avoid the need to integrate any loading mechanisms the tribometer may have at the end of the cantilever beam base. Additionally, there would be less noise experienced at the testing base since the testing base is more compact in its size.

From these two placement options, the team initially decided to place the linear motion subsystem under the base of the cantilever beam. This decision was made based on the aforementioned advantages of this placement. In the first functioning prototype of the tribometer, the cantilever beam was driven while the testing base was kept still. During that iteration of the team's tribometer, the data acquisition circuitry covered most of the real estate that linear motion subsystem would have filled if it was placed underneath the testing base. After a few test runs on the reciprocation system, the team observed a significant amount of vibration which would likely lead to some noisy data. Because of this, the team switched to the placement under the testing base. In addition to the aforementioned advantages to the testing base placement, the second design iteration of the testing base allowed more room for a linear reciprocation system underneath the testing base.

The final placement of the linear motion subsystem was underneath the testing base, just below the components necessary for the testing base temperature control and out of the way of the wire connections between the cantilever beams and the data acquisition circuitry.

5.2.1.2 Implementing the Linear Reciprocation

The team down selected from four main mechanisms for the linear reciprocation. Each mechanism uses a different type of driving system and reciprocated the testing base. Below is the list of mechanisms the team down selected from and each system's advantages and disadvantages.

The first mechanism uses mechanical linear actuators (Fig. 17) and a guiding rail. In this design, there would be two types of configuration. The first configuration utilizes one linear actuator attached to the testing base, screwed on to the guiding rail, such that a "push" and "pull" action generated by the actuation, would result in a reciprocating motion. The second configuration utilizes two linear actuators which alternatively pushed the testing base to create the reciprocation. The main advantage of this mechanism is the relatively lower price range of the mechanical actuators compared to the other mechanisms. Additionally, there wouldn't be much of a need to manufacture parts for the system.

Fig. 17: Mechanical linear actuator

The second mechanism uses piezoelectric actuators (Fig. 18) with the guiding rail. Piezoelectric actuators work by actuating by deflection based on an input current. The linear motion system would be configured such that a current is run through two piezoelectric components which leads to two alternating deflections that results in a pushing the testing basing back and forth along the guiding rail. The piezoelectrics' size would allow more real estate for another necessary circuitry that may be needed by the temperature control system or the data acquisition system.

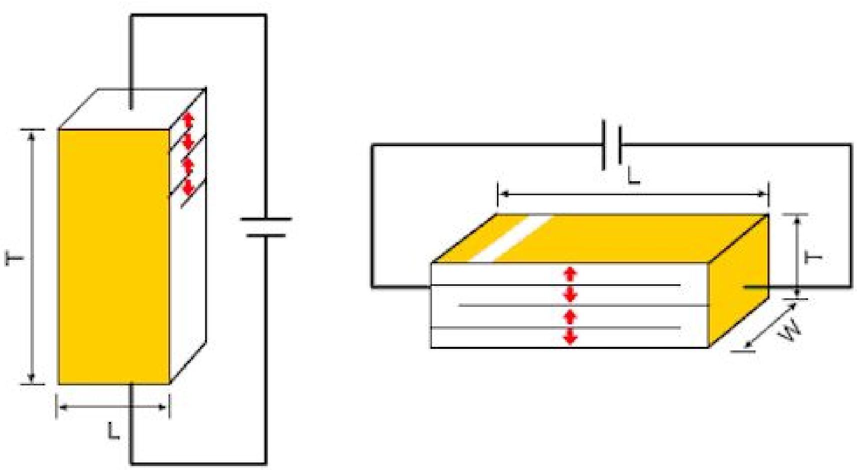

Fig. 18: Piezoelectric actuators

The third mechanism uses a stepper motor linear actuator (Fig. 19) with a lead screw and guiding rail system. This works similarly to the mechanical linear actuator but instead of pushing the testing base, a conversion of rotational motion to linear motion occurs to translate the testing base across the guiding rail. There are two main subassemblies in this mechanism. First are the stepper motor and lead screw components. In this subassembly the stepper motor interfaces with a lead screw such that the rotation of the stepper motor results in a rotation of the lead screw. The second subassembly is the testing base, anti-backlash nut, and the guiding rail system. This mechanism works by constraining the testing base onto the lead screw and anti-backlash nut. As the lead screw rotates, the constraint between the testing base and the anti-backlash nut will force a linear translation to the testing base. To generate the reciprocation the tribometer needs, the stepper motor will simply need to rotate clockwise and counterclockwise alternatively. Using a stepper motor to drive the lead screw and the translation gives the team a higher resolution in the linear motion.

Fig. 19: NEMA 14 stepper motor

The last mechanism uses a servo, belt system (Fig. 20), and guiding rail to translate rotational motion into linear motion. In this mechanism, there are two belt pulleys, a belt, and one servo interfacing with one another. One belt pulley interfaces with the servo gear such that the rotation of the servo gear leads to the rotation of the belt pulley. The belt is wrapped around both belt pulleys. When the belt pulley interfacing with the servo starts rotating, the other belt pulley will begin to rotate as well. Either the testing base or the cantilever beam base can interface with this rotation by attaching to the belt such that the linear translation experienced by the belt would also be experienced by the system. Reciprocation can then be achieved by alternating clockwise and counterclockwise rotations. A key advantage of this mechanism was its ability to easily interface with MATLAB which allows users to input specific angles for a corresponding linear translation.

Fig. 20: Belt driven actuator

The four most important categories Table 6 the team evaluated these mechanisms against were functionality, noise, resolution, and price. After some initial research on piezoelectric actuators, it was found that the max displacements that can be achieved by piezoelectric actuators were in the magnitude of micrometers. The tribometer's system characteristics defined the need for a 5 mm displacement which can't be achieved with the use of piezoelectric actuators. Next, is the noise. Of all the mechanisms, the belt driven system is more susceptible to noise since it relies on how taut the belt is, wrapped around the belt pulleys. The most notable disadvantage of the belt driven system and the mechanical actuators was the resolution. Compared to the stepper motor actuator, the resolution of these two mechanisms is low. During the team's down-selection process, the team found that most expensive but most reliable mechanism would be the stepper motor linear actuator. Due to the team's relationship with the Carpick Group, the team was able to acquire a stepper motor linear actuator which was later used in the second iteration of the tribometer.

Table 6: Advantages and Disadvantages of Linearly Reciprocating Mechanisms

	Functionality	Noise	Resolution	Price
Mechanical Linear Actuator	**Good** - able to travel 5 mm	**Medium** - larger motor could cause more vibration	**Medium** - good for displacements in cm range	**Medium** ~ $100-$300
Piezoelectric Actuator	**Poor** - limited to displacements in um	**Good** - pure displacement from current (no motor)	**Good** - performs displacement in the um	**Poor** ~ $500-$700
Stepper Motor Actuator	**Good** - able to travel 5 mm	**Good** - small vibrations	**Good** - performs displacement in the um	**Good** ~ Donation from lab ($800)
Belt-Driven	**Good** - able to travel 5 mm	**Poor** - belt has to be taunt	**Poor** - noise in conversion from rotation to linear displacement	**Good** ~ $50-$70

5.2.2 Realization Motion Subsystem

In the final iteration of the tribometer, the linear motion subsystem drove the testing base using a stepper motor linear actuator. Below are the specifications of the manufacturing of the linear motion subsystem and the development of the software required to run the system.

5.2.2.1 Guiding Rail System

All the parts for the guiding rail system (Fig. 21) were ordered from a company called ServoCity. The main components of the guiding rail system were the carriage, rail, and motor stand. The carriage component was made up of a 1'' x 1'' L-shaped pattern bracket and a 1'' x 1'' square bracket. The L-shaped pattern bracket contained a 0.5'' hole diameter that allowed the anti-backlash nut from the lead screw to press fit and screwed into. Additionally, it had a four wheel set that allowed the carriage to slide into the rail. The wheels contained ball bearings to allow smooth translations along the guide rail. The rail was T-slotted and hollow with a length of 3''. The face of the rail had a dimension of 0.75'' x 0.75'' with four 6-32 screw holes which allowed the motor mount to attach to the one end of the guiding rail. On the opposite end of the rail was another bracket that screwed onto the rail and contained a 0.25'' diameter hole that allowed the lead screw to fit into. To allow the lead screw to rotate freely within the bracket hole, a combination of a shaft collar, bearing, spacer, and shaft couplers were used. Lastly, the motor stand contains an elongated 1'' x 1'' L-shaped bracket with a square bracket used to interface with the guide rail. This component served as a stand that allowed the motor to sit on top it and interface via a motor mount bracket. Both ends of the guiding rail (the motor mount and the shaft bracket were screwed onto the surface of the tribometer's vacuum chamber.

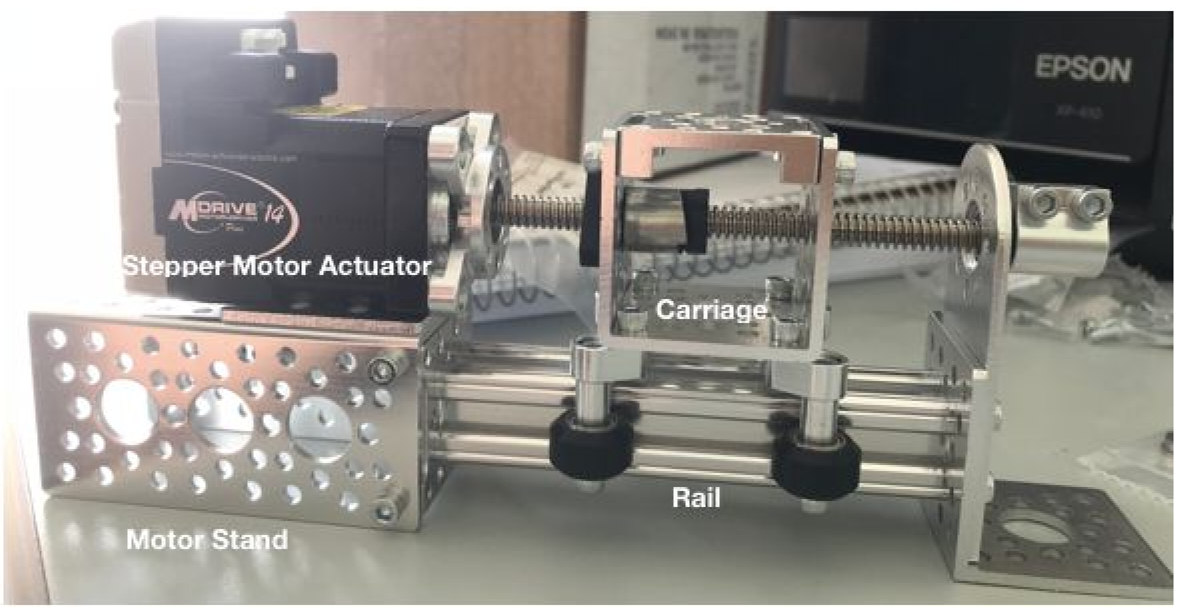

Fig. 21: Guiding rail system

5.2.2.2 Stepper Motor Linear Actuator

The stepper motor linear actuator used was the MLI3 NEMA 14 External Linear Programmable Motion Control IP20 [15] from Schneider Electric and was provided to the team by the Carpick Group. This actuator uses a NEMA 14 stepper motor and came with an attached lead with a 0.25’’ diameter and an anti-backlash nut that screwed into the lead screw. This anti-backlash nut, as previously mentioned, interfaces with the carriage through screws so the rotation is constrained and forced into a linear translation as the motor rotates. The motor itself was initially mounted on top of the motor stand using the motor mount bracket. Due to some screw hole misalignments, electric tape was instead used to keep the motor in place on top of the motor stand.

5.2.2.3 Motion System Software

The main software used to interface with the NEMA 14 stepper motor was the Lexium Software Suite [16]. The motor connected to a laptop via a USB and came with another cable that connected the motor to a power supply. The software is initialized by inputting an M-Code program in a form of a text file. To run the motor the software allows the user to transfer the code to the stepper motor and the program is executed by typing in “EX Program_Name” in the terminal window (Fig. 22).

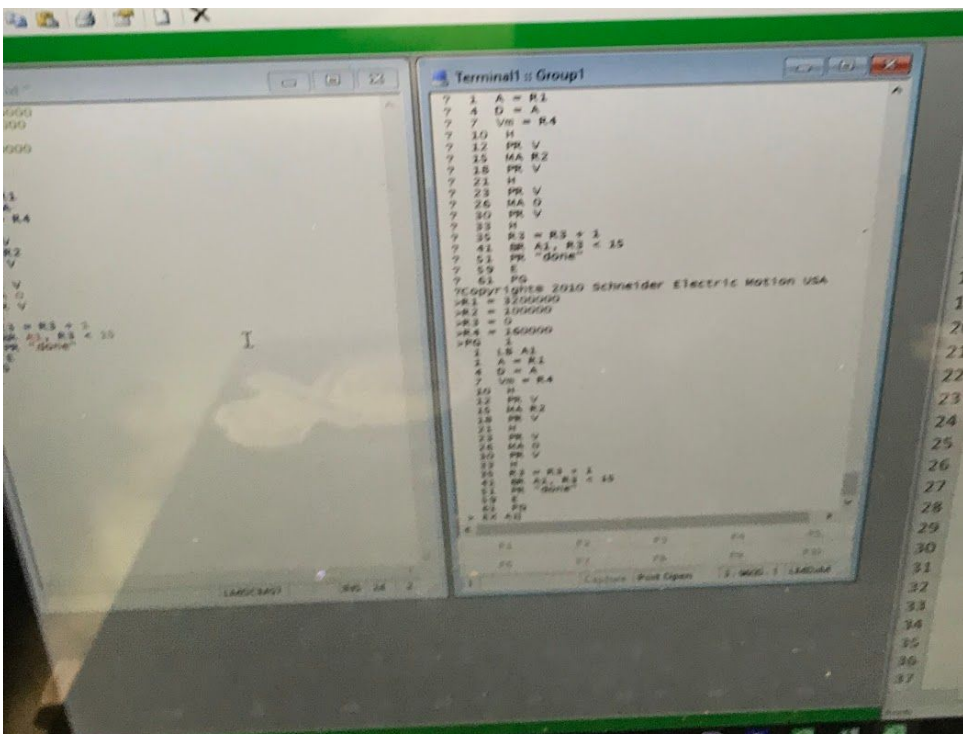

Fig. 22: Transferring code to the terminal

```
// Linear Reciprocation Program

R1 = 3200000
R2 = 100000
R3 = 0
R4 = 160000

PG   1
LB A1
  A = R1
  D = A
  Vm = R4
  H
  PR V
  MA R2
  PR V
  H
  PR V
  MA 0
  PR V
  H
  R3 = R3 + 1
  BR A1, R3 < 3
  PR "done"
  E
PG


```

Fig. 23: Linear reciprocation program

As seen from the code above (Fig. 23), there are four registers that are tracked during the program: R1, R2, R3, R4. These serve as input variables to the program. R1 stores the acceleration and deceleration of the stepper motor in microsteps per second^2. R2 stores the rotational displacement of the lead screw. R3 stores the number of cycles that has occured, where one cycle is an oscillation of 5 mm back and forth. R4 then stores the velocity of the stepper motor in microsteps per second. To summarize, the program shown makes the stepper motor accelerate to the velocity value set in R3 using the acceleration R1 and as it approaches the end one stroke (5 mm), the motor decelerates to zero using the same R1 magnitude. This is repeated for each stroke until the total number of cycles R3 reached the set amount in the program.

5.3 Temperature Subsystem

5.3.1 Design Temperature Subsystem

In order to reach -30°C and 200°C, the team saw the necessity of creating separate heating and cooling processes to change the temperature of the testing base. In addition, the team needed to carefully design the testing base to minimize heat transfer from or to the testing surface and control the humidity in the system to prevent condensation from forming on the testing surface during low temperature tests. Thus, there were four major components to this subsystem: humidity control, the cooling system, the heating system, and the testing base.

5.3.1.1 Humidity Control

To control the humidity of the air around the testing base, the testing base needed to be enclosed in an air-tight container. Since the Carpick Group had a vacuum chamber available (Fig. 24), the team decided to use their vacuum chamber due to the stable base that it could provide for the rest of the tribometer and the pre-built feedthroughs. Further conversations with Dr. Carpick revealed that nitrogen purging, which involves connecting a nitrogen tube into the vacuum chamber and pushing out the existing air, is the standard method in the field to reduce relative humidity. Thus, the team decided to simply manufacturer new feedthroughs for the nitrogen tube to enter the chamber and an exit hole for the existing air.

Fig. 24: Vacuum chamber loaned by the Carpick Group

5.3.1.2 Cooling

The team identified three different potential solutions for the cooling system: liquid nitrogen cooling, thermoelectric coolers, and low temperature freezers.

5.3.1.2.1 Liquid Nitrogen Cooling

By connecting an insulated pipe to a pressurized liquid nitrogen dewar, liquid nitrogen can be transported into the vacuum chamber at a steady rate to directly cool the bottom of the testing base through a cooling plate or nozzle. A probe and controller would be used to measure the material temperature and would adjust the flow rate of the nozzle to change the cooling rate. This solution is depicted in Fig. 25.

5.3.1.2.2 Thermoelectric Cooler

Through the use of the Peltier effect, thermoelectrics act as heat pumps and produce hot and cold ends. By adding thermoelectric coolers on the sides of the testing base, the team can directly cool the material using electricity without intermediate components. A probe connected to a controller would continuously measure the temperature of the surface and adjust the current to maintain the desired temperature. The setup is shown in Fig. 26 below.

5.3.1.2.3 Low Temperature Freezer

Certain low temperature freezers are able to operate at temperatures around -30°C or -50°C. By enclosing the vacuum chamber in a commercial low temperature freezer, the team could maintain the entire system at a range of low temperatures depending on the setting the team selects. The setup is shown in Fig. 27 below.

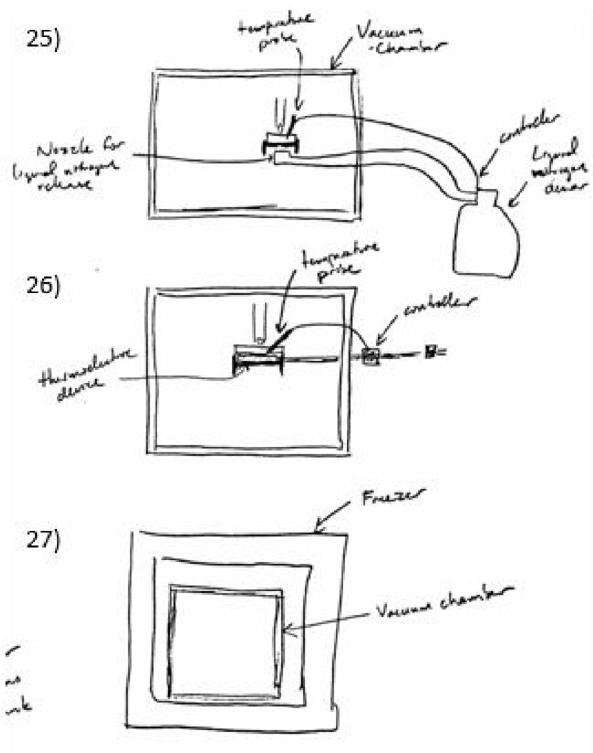

Fig. 25-27: Sketches of the various cooling options. 25) Liquid nitrogen cooling 26) thermoelectric cooler 27) freezer.

A summary of the team's down selection process is shown in Table 7 below.

Table 7: Advantages and disadvantages of cooling systems

	Cost	Ease of use	Sensor interference	Energy efficiency	Temperature range
Liquid Nitrogen	**Poor** – requires > $1,000 nitrogen dewar	**Poor** – requires constant supply of liquid nitrogen	**Good** – minimal interference	**Good** – only controller needs energy	**Good** – boiling point is well below -50°C
Thermoelectric Cooler	**Good** – modules typically cost < $100	**Good** – only requires electricity	**Good** – no moving parts	**Medium** – low temperatures may need high power	**Medium** – may have trouble reaching -50°C from 20°C

Low temperature freezer	**Poor** – typically costs >$1,000	**Good** – only requires electricity	**Poor** – vibrations could affect measurements	**Poor** – require large amounts of electricity	**Good** – some freezers can reach -50°C

Based on the low cost, high ease of use, and the lower potential for interference with sensors, the team chooses to use thermoelectric coolers to reach the low end of the temperature range. During use, the thermoelectrics would be connected to power supplies that would maintain a certain heat load.

5.3.1.3 Heating

To determine the most optimal method of heating, the team explored three different devices: induction heating coils, joule heating plates, and gas burners.

5.3.1.3.1 Induction Heating Coil

Induction heating is the process of heating up an electrically conducting object through the use of rapidly alternating magnetic fields, which generate eddy currents and thus heat inside the conductor. To heat the contact surface, the team proposed to surround an extended portion of the contact material with an electromagnetic coil connected to an electronic oscillator and power supply to generate the alternating current. The temperature could be adjusted by the amount of power supplied to the system and a temperature probe connected to a feedback loop would maintain the desired temperature by adjusting the power supplied or switching on and off. This setup is shown in Fig. 28 below.

5.3.1.3.2 Joule (Resistive) Heating Hot Plate

Joule heating is the process of heating by running an electric current through a conductor. To heat the contact surface, the team proposed to add a miniature electric hot plate between the motion system and the testing material. This setup is shown in Fig. 29. A temperature probe would be in contact with the testing material and connected to the control system, which would regulate the current to the hot plate or switch it on and off. The heat produced through Joule heating is characterized by the formula:

$$P = I^2 R \tag{5.3.1.3.2.1}$$

5.3.1.3.3 Gas Burner

Our third option was to connect a gas hose to a gas tank and place it underneath the reciprocating base structure. The gas would then be ignited using a flint spark lighter or similar device. The reciprocating structure would have a hole in the middle to allow the flame to directly contact the testing material. A temperature probe would be in contact with the testing material and connected a controller, which would regulate the gas inflow into the hose. This setup is shown below in Fig. 30.

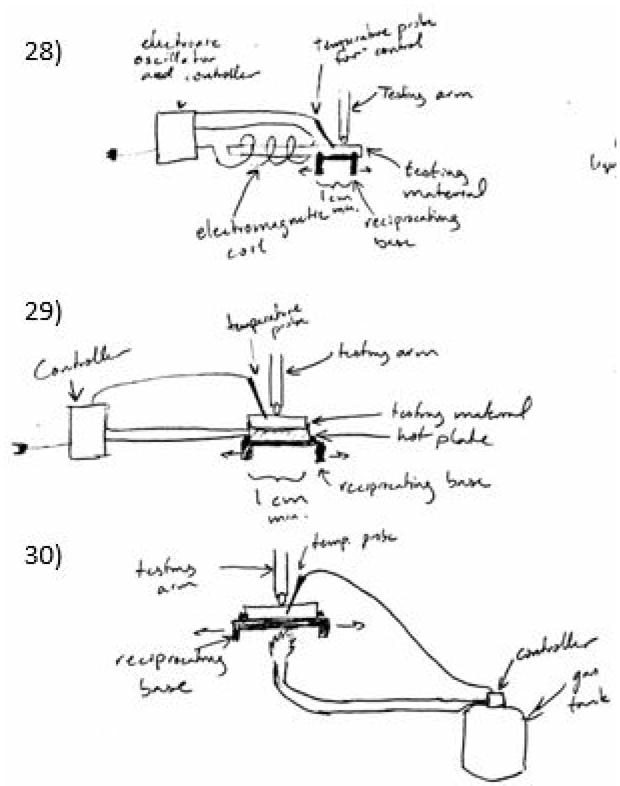

Fig. 28-30: Sketches of the various heating options. 28) Induction heating coil 29) Joule heating hot plate 30) gas burner.

A summary of the team’s down selection process is shown in Table 8 below.

Table 8: Advantages and disadvantages of each heating method

	Ease of Integration	Energy Efficiency	Ease of Use	Safety
Induction heating coil	**Poor** – requires larger testing base	**Good** – heat generated inside testing base	**Good** – only needs electricity	**Medium** – testing base is heated
Joule heating hot plate	**Good** – works with small heating plate	**Medium** – heat must be conducted to base	**Good** – only needs electricity	**Medium** – testing base is heated
Gas burner	**Poor** – open flame may cause damage	**Poor** – heat comes from flame	**Poor** – need gas tank	**Poor** – open flame hazard

Due to easier integration with other subsystems and ease of use, the team decided to use a joule heating hot plate to heat the testing base. To control the desired temperature, the team planned to use an RTD sensor connected to a PID temperature controller with a mechanical relay. The RTD sensor was chosen over thermocouples based on its more stable voltage outputs and thus readings. The team chose to use a temperature controller due to its autotuning features that would allow the user to easily set a temperature with minimal hassle and little fluctuation, rather than have to experiment with different proportional, integral, and derivative values. The team determined that programming a new controller with Matlab or LabVIEW with similar capabilities would not be most efficient use of time. Finally, the mechanical relay was chosen since it had the highest current rating of all the different relay options for the controller. The intention ultimately was for the heater to control the temperature during both the heating and cooling processes since thermoelectrics degrade quickly under the continuous cycling that the controller would cause.

5.3.1.4 Testing Base

Initially, the team planned on creating a steel testing base, since steel was the testing surface that the Carpick Group would most likely use. The size was determined by the thermoelectrics, as the initial plan estimated the use of three thermoelectrics, two on the sides and one on the bottom. However, conversations with the Carpick Group affected the design process.

During the conversations, the team found that it was standard in the research field for friction tests to be done on a small tab of material, typically 11 mm in diameter and 2-3 mm thick. Thus, the team decided to design a testing base to hold the tab in place and provide a contact area for the heating and cooling systems. To maximize heat transfer within the base, the team chose copper to be the primary material since it has the highest thermal conductivity out of common materials (385 W/m·K) and relatively low specific heat (0.385 J/g·K). Set screws were chosen to hold the tab in place during testing since tape would not be secure enough during high stress and adhesives would not allow the tab to be replaced after tests.

The team also designed the size of the testing base to be as small as possible to minimize heat capacity and heating times. As a result, the base was designed to be square-shaped with a side length just longer than the tab diameter to provide a small wall to keep fluid in, and just thick enough to accommodate a couple millimeters of fluid with the tab set in. The testing base design is visible in engineering drawing 446-12. In order to isolate the testing base from the vacuum chamber and minimize heat transfer, the base was designed to sit on top of 1.5’’ L5 ceramic spacers, which could be threaded onto a reciprocating carriage. L5 ceramic was chosen as it was one of the few materials with low thermal conductivity (2.9 W/m·K) that could withstand high heat and low temperatures. As a result of these design changes, a new temperature model suggested that the team could use two thermoelectrics rather than three.

5.3.1.5 Temperature Modeling

After the initial downselection, the team modeled out the projected temperature of the testing base over time for both high and low temperature systems to see if the testing surface could reach the team's stated goals. Using the dimensions and thermal conductivities of the different materials around the testing base, the team calculated the thermal resistance values of the ceramic spacers and screws, and convection with nitrogen or air using the following equations:

$$R_{cond.} = \frac{L}{kA} \quad (5.3.1.5.1)$$

$$R_{conv.} = \frac{1}{hA} \quad (5.3.1.5.2)$$

To calculate the temperature of the testing surface, the team assumed lumped capacitance for the testing base since the Biot number, which is the ratio of thermal resistance inside over versus at the surface of a body, was less than 0.1. The Biot number equation is given below:

$$Bi = \frac{L_c h}{k} \quad (5.3.1.5.3)$$

As a result, the team used the transient heat equation to solve for the testing base temperature:

$$\dot{E}_{in} - \dot{E}_{out} = \dot{E}_{st} = \rho V c \frac{\partial T}{\partial t} \quad (5.3.1.5.4)$$

Using this model, the team was able to determine the required heat loads and outputs required by the thermoelectrics and resistive heaters and found that SP2402 thermoelectrics from Marlow and 5 Ω Heat Scientific metal ceramic heaters were projected to satisfy the requirements. The team also modeled higher heat or cooling dissipation values to be conservative about the temperature capabilities. The initial results of these models are in Fig. 31 and Fig. 32 below.

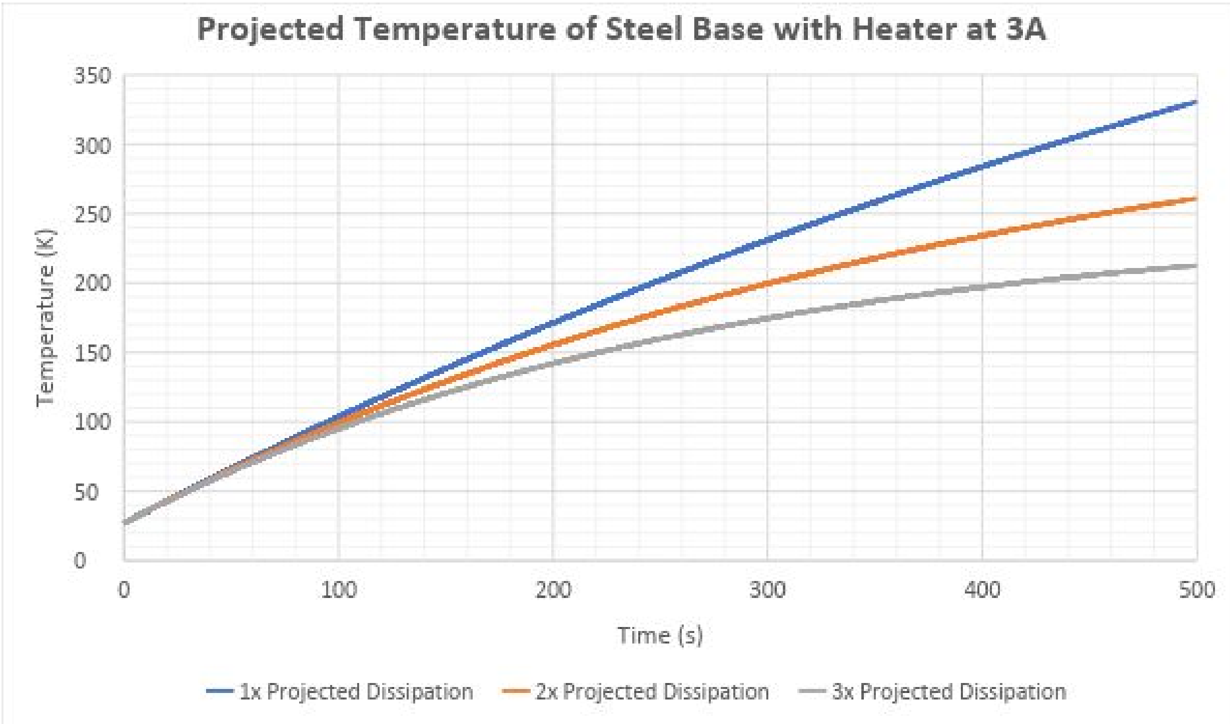

Fig. 31: Predicted testing base temperature over time during heating process

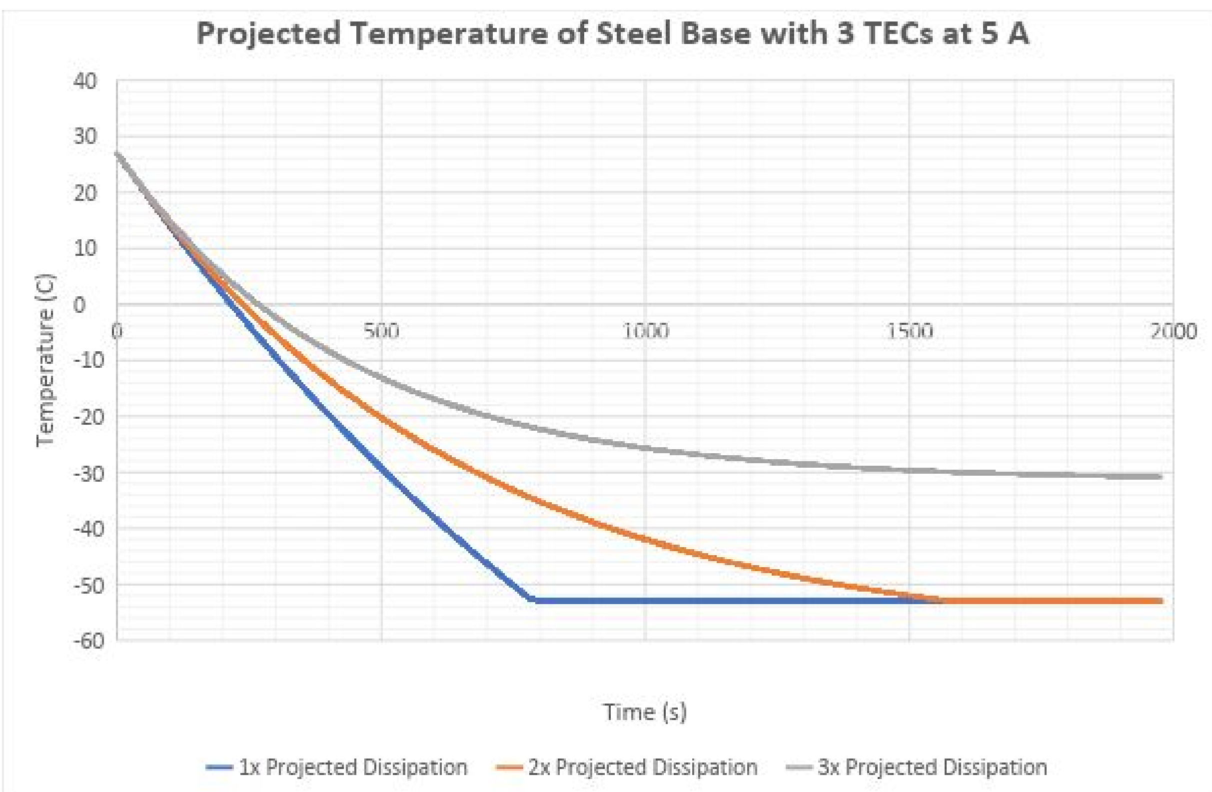

Fig. 32: Predicted testing base temperature over time during cooling process

5.3.2 Realization Temperature Subsystem

When manufacturing and assembly the temperature subsystem, the team made some changes in terms of configuration and design details. However, the main components of each subsystem remained the same.

5.3.2.1 Humidity Control

For the final tribometer, the team stuck with the vacuum chamber that the Carpick Group provided. However due to the unreliability of some of the vacuum feedthroughs and the vast number of wires required by the temperature and data acquisition subsystems, the team decided to replace many of the pre-existing feedthroughs with laser-cut 0.25'' acrylic port covers with central holes for wires (engineering drawing 446-13). A special acrylic port cover was also laser-cut for the nitrogen tube, two water tubes for the thermoelectrics, an RTD temperature sensor, and a hygrometer, which could be used to measure relative humidity inside the chamber (engineering drawing 446-14). During cooling tests, the team used electrical tape to seal off remaining gaps and preserve the nitrogen concentration in the chamber. While this setup was not ideal, the relative humidity in the chamber did remain low enough to prevent condensation and icing during cooling tests.

5.3.2.2 Testing Base

The final testing base was machined out of solid copper according to the initial design plans. The team purchased set screws, L5 ceramic spacers, and screws for the spacers from McMaster Carr. To lock the temperature sensor in place during testing, the team cut down one of the set screws to half the length, which provided enough space between the tab and the set screw without having the set screw stick out.

5.3.2.3 Heating System

The team purchased 3.5 Ω, 15 mm x 15 mm x 1.5mm Heat Scientific metal ceramic heaters to serve as resistive heating elements. The team selected the heater primarily so it could fit on the underside of the testing base, where the available area was less than 1'' x 1''. 5 Ω was one of the larger resistances available and was selected since 3.5 Ω and 3 A, which was the current limit for mechanical relays in temperature controllers, was predicted to be more than enough to heat the testing base. To secure the heater to the testing base, OMEGABOND 200, a thermally conductive epoxy that could survive continuous testing up to 260°C, was applied and cured for 8 hours at 250°F. Finally, the leads on the heater were soldered to wires that ran through the feedthrough ports to a 30 V DC power supply. Due to a malfunctioning temperature controller and lack of time, the team was unable to autonomously control the temperature and had to manually adjust current to stabilize the temperature. Instead of an RTD sensor, a K-type thermocouple was slotted between the set screw and tab during tests and was connected to a thermocouple reader to display temperature.

5.3.2.4 Cooling System

For the cooling system, the team used two sets of thermoelectrics, two SP2402s from Marlow (Fig. 33), and two ET Series from Laird (Fig. 34). Since the heat generated by the hot side of the thermoelectrics was too high for simple convection and air-cooled heat sinks with fans would significantly increase heat convection to the base, water-cooled aluminum heat sinks were purchased for each thermoelectric. The SP2402s were originally purchased for use with simple copper heat sinks but were kept once the team transitioned to ice water-cooled heat sinks. The ET Series was then purchased as better and cheaper alternatives with higher heat loads at the lower temperature differences provided by the ice water. 80mm x 40mm heat sinks were initially used for the SP2402 thermoelectrics and to eliminate further bulk, 40mm x 40mm heat sinks were chosen for ET Series. While copper would have been preferable due to higher thermal conductivity, copper versions of the heat sinks were not readily available for purchase. The heat sinks were then connected to 5/16’’ inner diameter plastic tubing, which was then connected to a 145 GPH Maxesla submersible pump to constantly recirculate the water between the heat sinks and an ice water reservoir consisting of a plastic container outside the vacuum chamber (see Fig. 35).

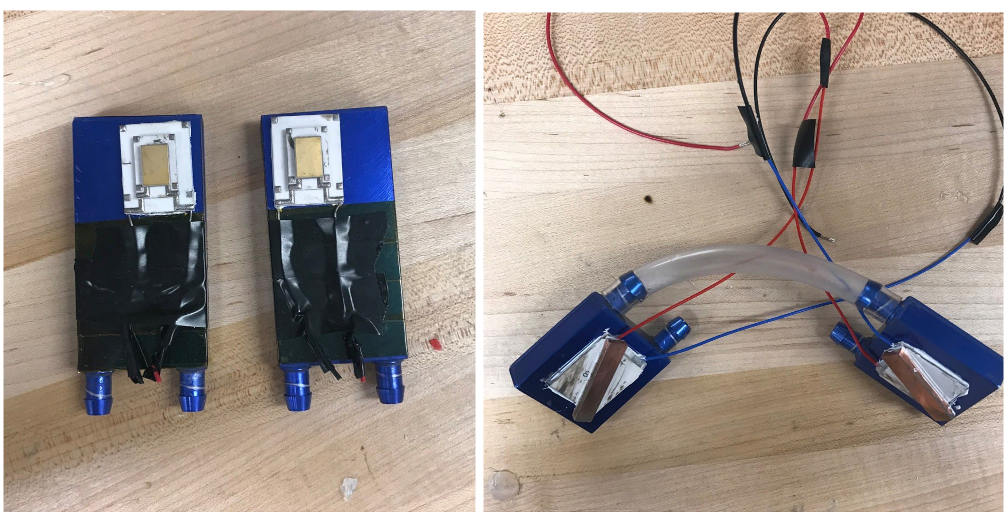

Fig. 33-34: Thermoelectrics with heat sinks 33) SP2402 thermoelectrics 34) ET Series thermoelectrics

To permanently connect the heat sinks to the thermoelectrics, Halnziye thermal adhesive was used. Finally, the team used Arctic Silver 5 thermal paste to maximize thermal conductivity between the thermoelectrics and the testing base. During testing, the two thermoelectrics would be placed on opposite sides of the testing base with a 6’’ plastic clamp holding them in place as seen in Fig. 36 The clamp was needed to secure the thermoelectrics because a non-permanent solution was required. If the testing base were heated to 200°C with the thermoelectrics still attached, they could be permanently damaged.

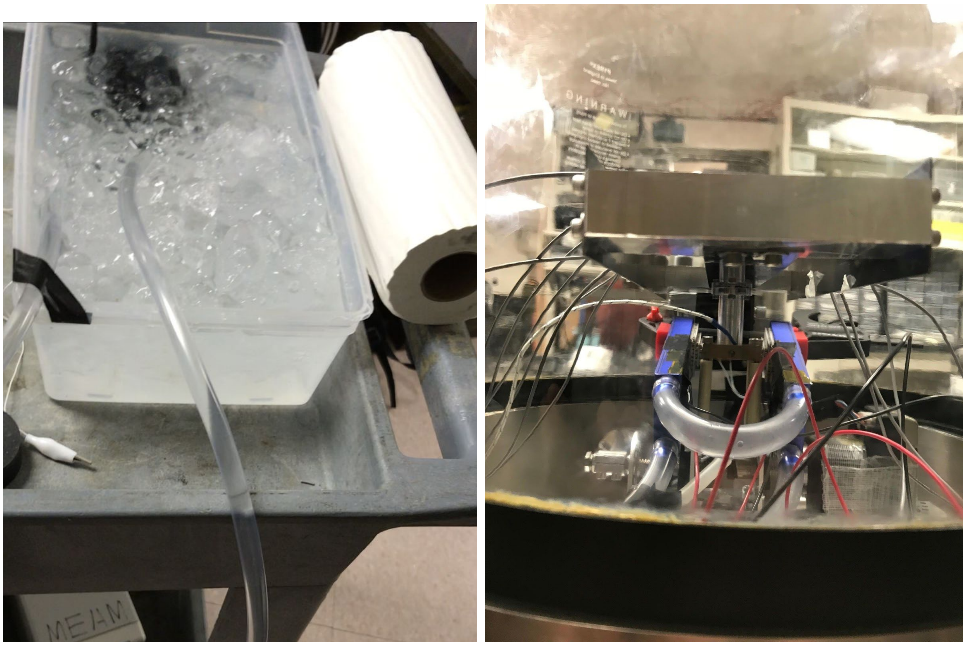

Fig. 35-36: Cooling process full setup 35) ice water reservoir for water-cooled heat sinks 36) SP2402 thermoelectrics in contact with testing base

For the ET Series thermoelectrics, a couple extra steps were needed because the cooling side was too large to contact the testing base without hitting the ceramic spacer first. A copper block with the same dimensions as a side of the testing base and 3 mm thick was machined and attached to each thermoelectric's cold side with thermal adhesive. This copper block could then contact the testing base with the thermal paste in between the two surfaces.

5.4 Data Acquisition Subsystem

5.4.1 Design Data Acquisition

There were several possible methods of testing the normal and lateral force loading on the ball that can be later combined to output a measured friction value. The choice of this subsystem is primarily determined by the accuracy of the various options, as the micro scale we are considering for this tribometer's applicability demands a high level of sensitivity (normal force 10mN - 10N), Other factors to consider in the choice of force sensing mechanisms is the sensitivity to temperature changes. As the substrate might be heated to a maximum of roughly 100 °C and would be conducting heat through the ball upwards into the cantilever, any sensor chosen must have either minimal dependency on the temperature range at which the measurement is conducted, or a predictable relationship that can be accounted for in later computations.

5.4.1.1 Strain Gauges

Strain gauges load cells are based on an elastic element that expands, or contracts, predictably upon the application of force. The elastic element is attached to a resistor component which simultaneously expands with the element. Its resistance value is affected by the strain, and such changes can be measured by a circuit. The material used is usually tool steel, stainless steel, aluminum, or beryllium copper. Since the changes in voltages of a strain gauge is usually miniscule, an amplified setup in the form of a Wheatstone bridge and amplifier circuit, which is explained further below, connected to 4 strain gauges, 2 operating in compression and 2 others operating in tension, is generally used, shown in Fig. 37. Within a certain range they have a predictable response to temperature effects.

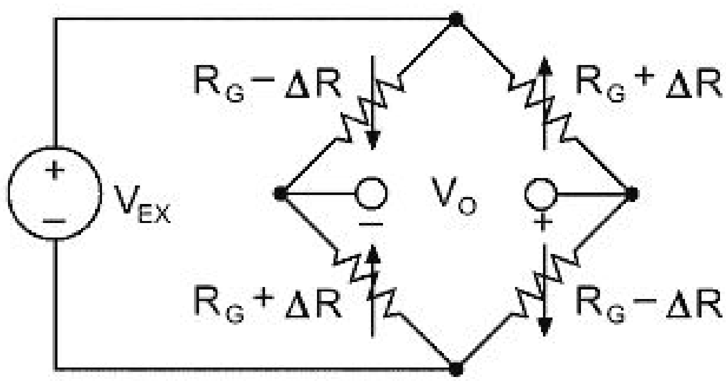

Fig. 37: Wheatstone Bridge of four gauges[18]

5.4.1.2 Piezoelectric Crystals

When a force is exerted on piezoelectric crystals (usually quartz), an electric charge is formed in proportion to the magnitude of the applied force. An amplifier is also necessary here to output a signal large enough to measure. A key difference between piezoelectrics and strain gauges, is that piezoelectrics are active sensors and do no need voltage inputs. Their deflection is minimal, and have a wide temperature range, operating with temperatures of up to 350ºC. Furthermore, piezoelectric transducers can be set to measure forces in multiple dimensions, as shown in Fig. 38. The force is transmitted through the 3 plates, which are cut along specific axes to each measure a directional component of the force vector.

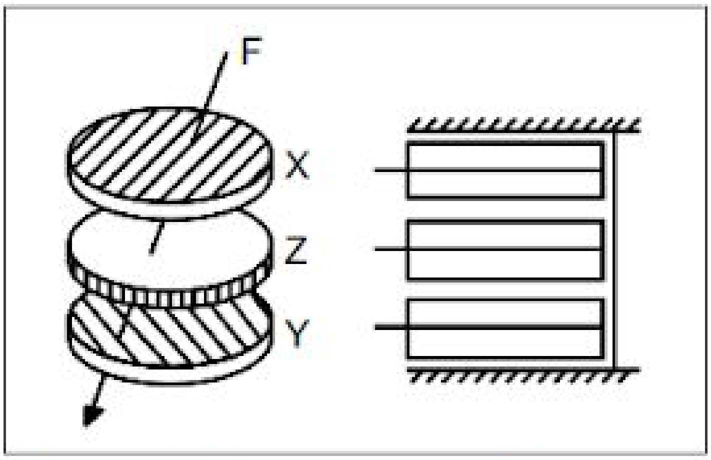

Fig 38: Piezoelectric operating as multidimensional sensor[17]

5.4.1.3 Linear Variable Differential Transducer (LVDT)

LVDTs can be used to measure the displacement of an elastic element, similarly to a strain gauge. It is essentially a transformer which outputs an AC current proportion to the displacement of the magnetic core (Fig. 39). This method is highly resolute, recording as little as 10 mN. However, it is prohibitively costly, costing at least 150$ and is sensitive to temperature changes, operating normally over a range from - 40°C to 80°C.

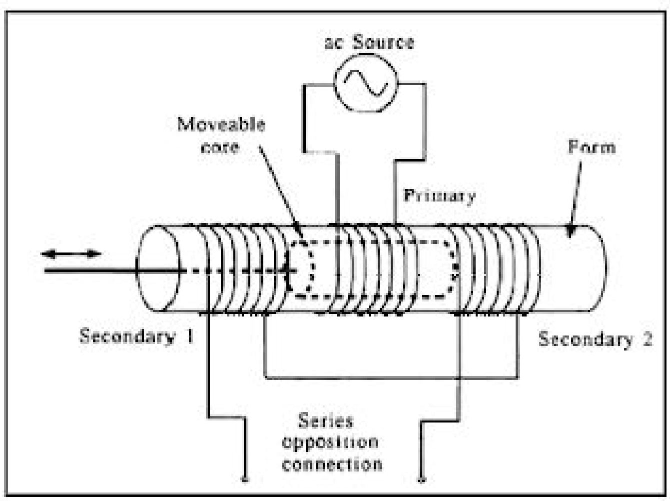

Fig 39: LVDT Setup[17]

Table 9: Comparison of possible data acquisition systems

	Strain Gauge	Piezoelectrics	LVDT
Precision	**Medium**	**Medium**	**Good**
Temperature	**Medium** - highly sensitive to temperature changes, especially at the extremities of range considered (non-linear relationship). However, there are simply and known steps to reduce this.	**Medium** - Wider range, but also sensitive. Behavior is not documented, and would have to be tested.	**Good** - Same normal range of operation as strain gauge, no simple correction. Testing is required.
Design Complexity	**Good** - easily fits into cantilever design	**Medium** - can create multi-dimensional setup.	**Poor** - Highly complex process for installation.
Signal Processing	**Good** - Simple, using Wheatstone bridge and amplifier	**Good** - using charge amplifier	**Medium**
Cost	**Good**	**Good**	**Poor**

The group ultimately chose the strain gauges primarily due to their low cost, simplicity of implementation as well the understanding that the group could find gauges that could operate within the ranges of temperatures the system would experience, which the group arrived at after preliminary testing. This made the largest drawback of the gauges void and thus finalized the decision. The Carpick Group had themselves used gauges in their tribometer design, which was an encouraging sign of their utility. The system that was created as a result of that choice is presented below.

5.4.2 Realization Data Acquisition

The data acquisition system is composed of a hardware and software subsystems. The hardware begins with the strain gauges placed on both the horizontal, which deflect proportionally to the friction application and vertical cantilevers, which deflect proportionally to the normal force. These gauges are then connected in a Wheatstone Bridge setup (In the final iteration, a half bridge was used for the normal force and a full bridge was used for the friction force). This setup is supplied voltage of 10 V by a voltage supplier. The output of the bridge setup is then passed into an amplifier circuit which is seen as a schematic. There are two amplifier circuits, one for the output of the normal force Wheatstone bridge, and one for the output of the friction force bridge. These circuits are also fed a 10 V supply from voltage suppliers. The output then is fed into a data acquisition system which connects with LabVIEW software and is able to process and read the data. To measure temperature, 1000Ω Platinum RTD was placed in a circuit in series with a 3300Ω resistor (needed to lower the current to levels that avoids self-heating of the RTD) and supplied with a 10V supply. The voltage across the RTD is differentiated with changing temperatures and is fed into the data acquisition device and outputted on the GUI after calculation as the current temperature at the hot plate.

5.4.2.1 Strain Gauges

The gauges were chosen with consideration to sensitivity, resilience to the effects of temperature as well as budget. The model ultimately chosen were the CEA-06-062UW-120. The CEA series are general-use gauges, with normal behavior over a temperature range of -75 to 175 C, and an accessible and easily implementable method of adhesion. This was done by purchasing a separate adhesion kit, which was cured upon application at a temperature of 250 °C. It has a resistance of 120Ω, and costed around $6 a gauge, which was well within the budget. Fig. 40 showing the strain gauges installed on the system

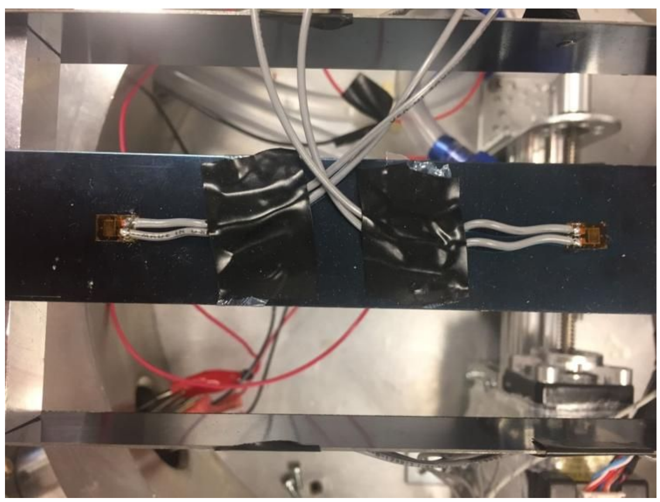

Fig. 40: Strain gauges mounted on the systems cantilever

5.4.2.2 Wheatstone Bridge

The purpose of using a Wheatstone bridge rather than a single strain gauge is twofold. First, the circuit by setting the different strain gauges to change their resistance in opposite directions upon the application of a force, the total signal as a function of the sensitivity to the magnitude of the applied force increases. Furthermore, since gauges are essentially resistors, their resistance is a function of the temperature of the material as a higher temperature causes thermal expansion and thus impacts the shape of the resistor and affects its behavior. Placing strain gauges working in opposite direction, as shown in Fig. 41, in series balances out these changes and essentially acts as a thermal compensation. Due to the extreme temperatures found in the experiment, this was necessary. A half bridge allows for such compensation to a certain level, and a full bridge further protects from the effects of temperature. For the half bridge setups, the group replaced the non-active gauge elements by resistors equal to the nominal resistance of the gauges, at 120 Ω. The circuit diagrams and equations are found in Fig. 42 and 43.

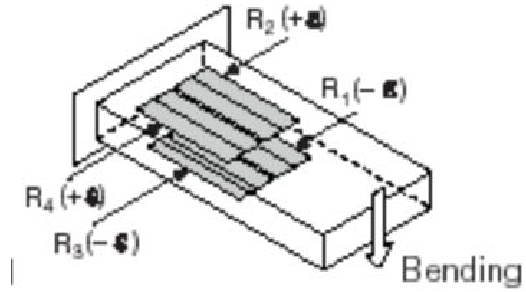

Fig. 41: Cantilever with full bridge setup [19]

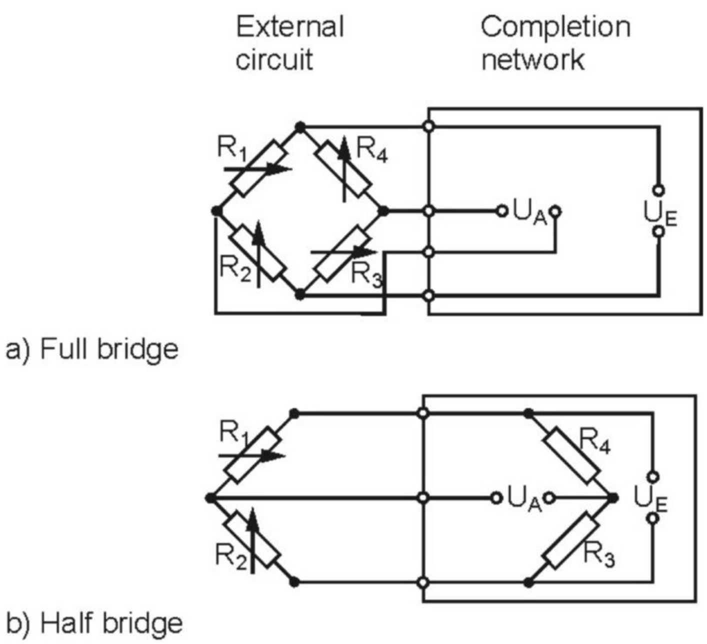

Fig. 42-43: Wheatstone bridge circuit schematic of half and full bridge[20]s

The equations governing the output of a bridge as a function of the strain on the cantilever are:

a) Half Bridge:

$$\frac{V_o}{V_{EX}} = -\frac{GF \cdot \varepsilon}{2} \qquad (5.4.2.2.1)$$

b) Full Bridge:

$$\frac{V_o}{V_{EX}} = -GF \cdot \varepsilon \tag{5.4.2.2.2}$$

5.4.2.3 Amplifier Circuit

The signal outputted from the Wheatstone bridge is in the millivolt scale and thus requires a large amount of amplification to reach a level of differentiation that allows the team to accurately determine the force values. The amplification functions using two op-amps, one operating as a voltage isolator to prevent any excessive current from being drawn from the Wheatstone bridge and the other as a differential amplifier. As such, an amplification circuit shown as a functional schematic in Fig. 44**,** a breadboard circuit schematic in Fig. 45, and as an image in Fig. 46, allows for the amplification of a voltage according to the ratio of the two resistors used. In the final testing setup, we had an amplification of 150.

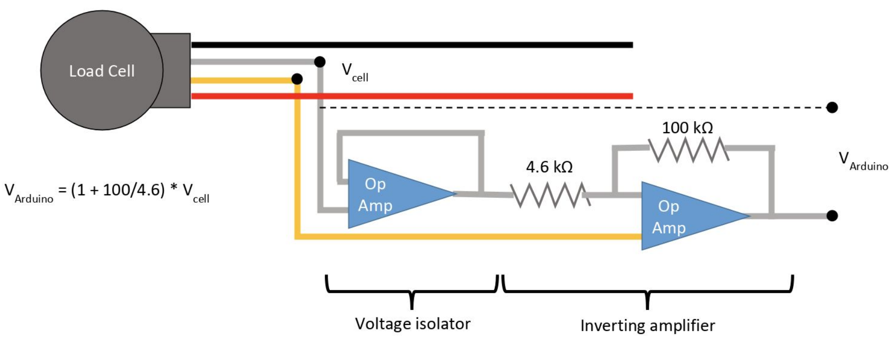

Fig. 44: Functional schematic of the amplifier circuit

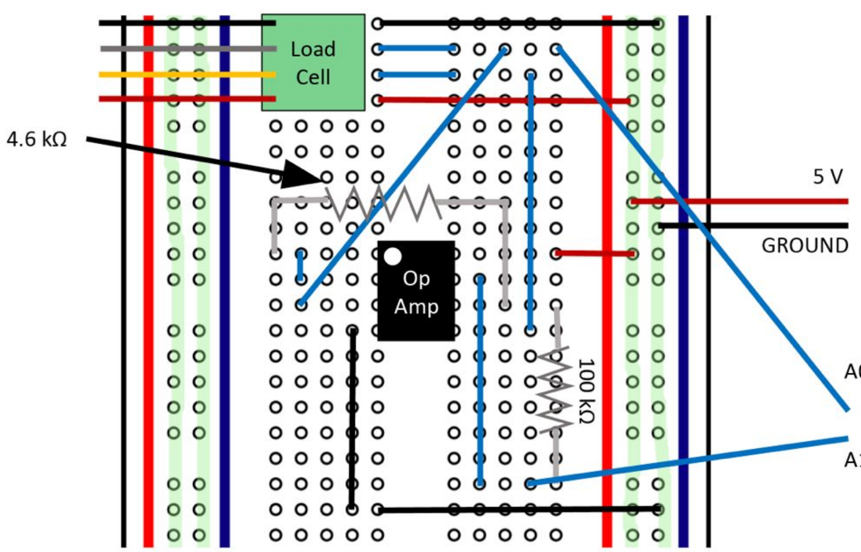

Fig. 45: Breadboard schematic used to create amplifier circuit

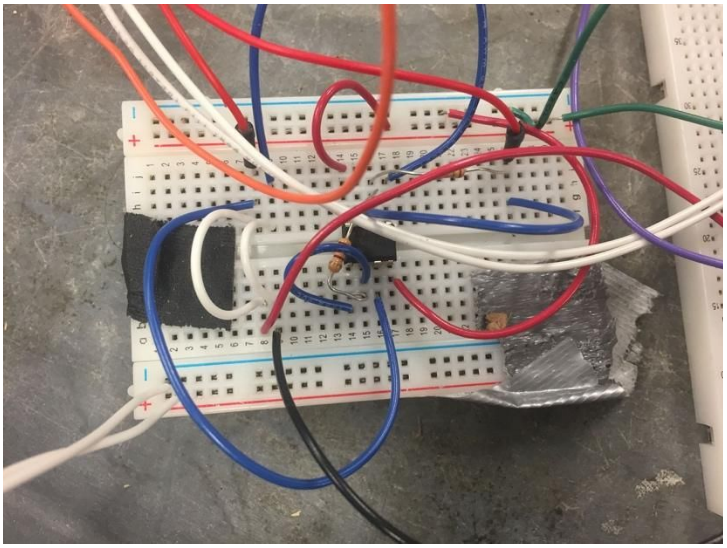

Fig. 46: One of the two amplifier circuits used for signal amplification

5.4.2.4 LabVIEW

The software created on LabVIEW was responsible for processing the voltage inputs explained above into meaningful signal data as well as presenting the data. The reasons LabVIEW was used as opposed to a much simpler Arduino setup is due to the fact that an Arduino is limited to only 10 bits of precision. Scaled across the 5V of the Arduino input range, this meant it could only theoretical detect a minimum of 5 mV. Based on the minimum strain calculations and resulting voltage output, considering amplification can only be done up to the ceiling of 5V, this was simply insufficient. AS such, the group chose the NI USB 6001 to be the data acquisition device, this allowed for 12 bits of measurement as well as the ability to focus on a particular range of voltages if more precision was needed. The NI USB-6001 is shown in Fig. 47.

Fig. 47: NI USB-6001

Firstly, the LabVIEW software allows for calibration of the gauge data. This is due to the fact that there is a linear relationship between the transition from voltage to force which could depend on anything from the initial position of the cantilevers to the voltage inputs to the temperature etc. As such, calibration to determine this relationship must be done before each experiment and involves records the signal output of the system when placed under the force of known magnitude. The coefficients of this linear relationship is then outputted back into LabVIEW to set the relationship and extract force data from the incoming voltage data. To process this data, the software collected 10000 data points every half a second. It then calculates the mean, which eliminates much of the noise. It then calculates the coefficient and outputs the value as an interval graph. The process can be seen as a block diagram in Fig. 48, and the GUI can be seen in Fig. 49.

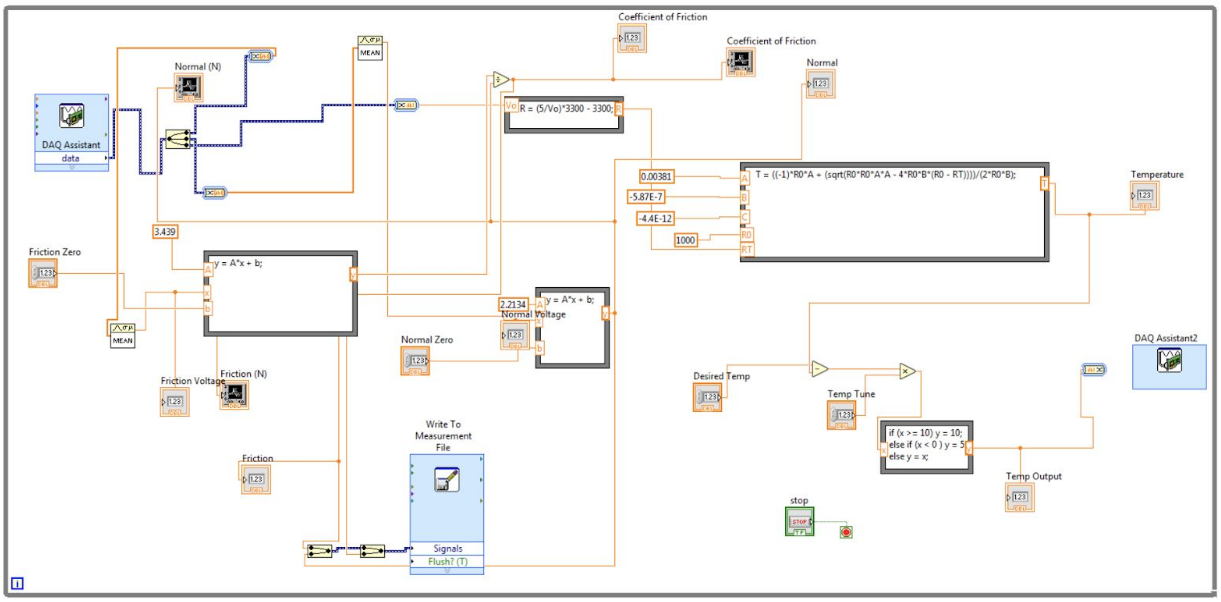

Fig. 48: LabVIEW Software

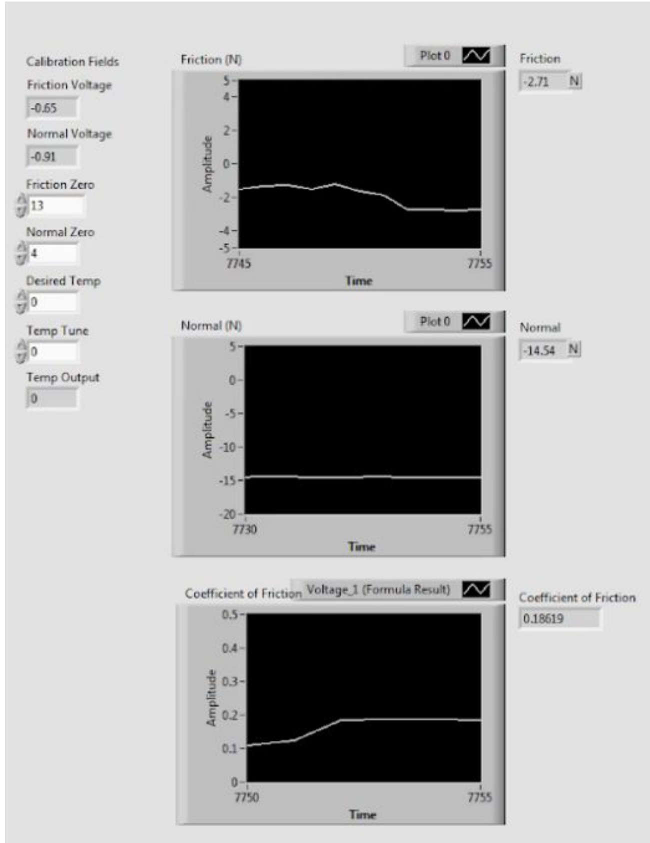

Fig. 49: Graphical User Interface (GUI)

6 Validation and Testing

6.1 Loading Subsystem

6.1.1 Loading Calibration Tests

The primary purpose of the calibration test was to find out the relationship between the voltage read by the DAQ and the force experienced by the system. The results of repeated tests would also determine calibration procedures for the actual usage of the system.

6.1.1.1 Setup

The normal loading calibration test involved flipping the loading hub piece over and loading qualified weights onto the system (Fig. 50). Since the system requirements specify that the system must be able to be loaded from 1 to 10 N, weights ranging from 0.1kg to 1kg were used for this test, as well as collecting a zero value. The lateral test was conducted in a similar manner however rather than loading onto the hub piece, a pulley system was put into place to pull the cantilever system to the side without deflecting it downwards (Fig. 51).

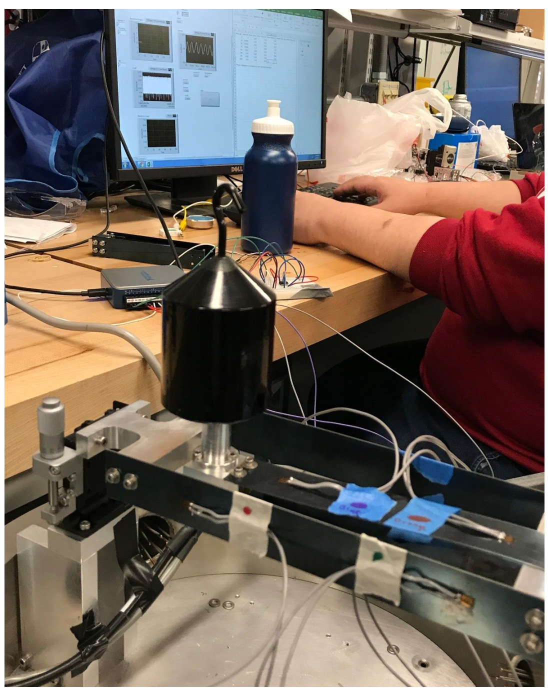

Fig. 50: Normal Loading Calibration Test for 1 kg

Fig. 51: Lateral Loading Calibration Test for 100 g

6.1.1.2 Results

The results as seen in the figures below showed a linear relationship between the loaded forces and the resulting voltage. The gradients between the two tests remained relatively constant though the zero force value fluctuated between two tests. This indicated that for testing procedures, the team would need the ability to either account for the zero force reading or implement a tare function on the GUI. Further testing revealed that the gradient was dependent on the ratio between the resistors used in the amplification circuit.

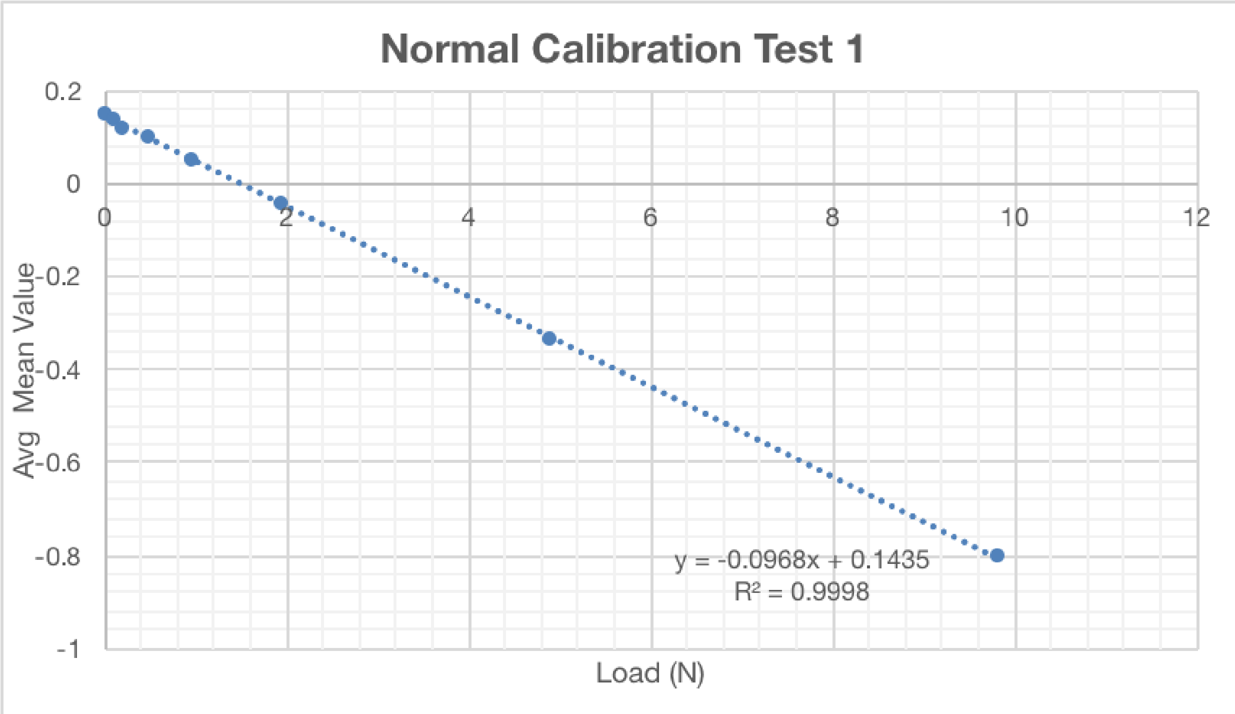

Fig. 52: Normal calibration test 1

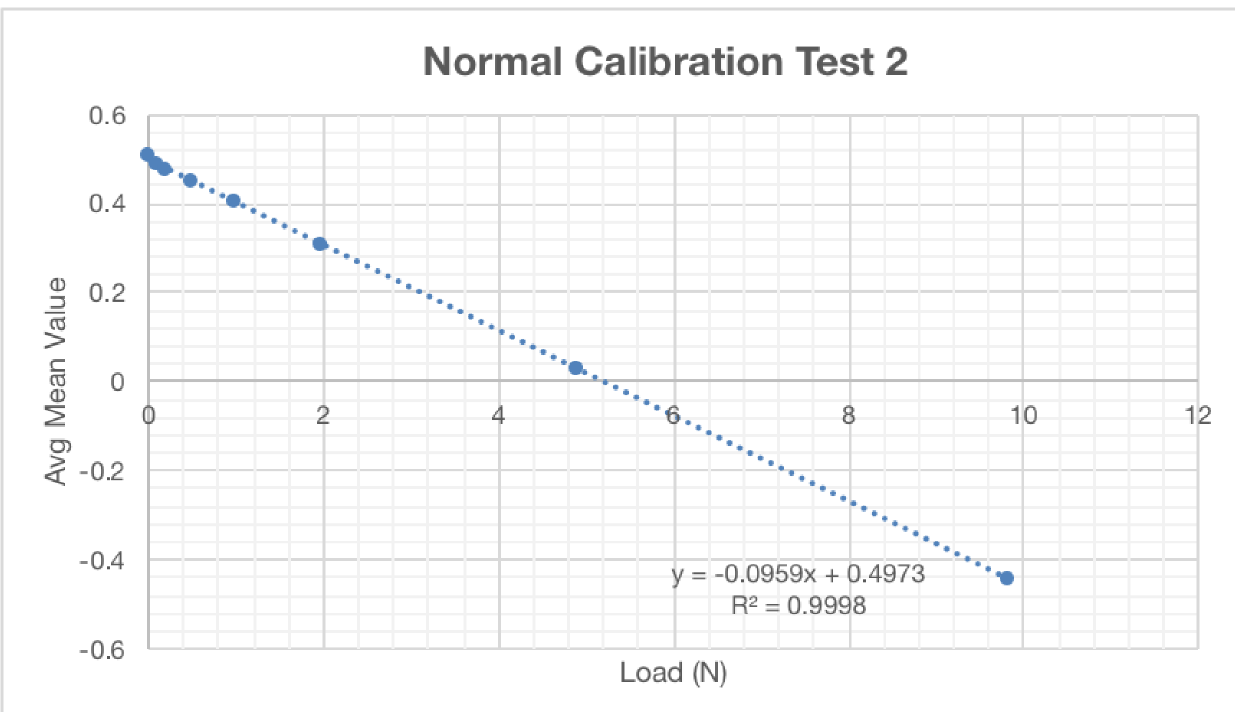

Fig. 53: Normal calibration test 2

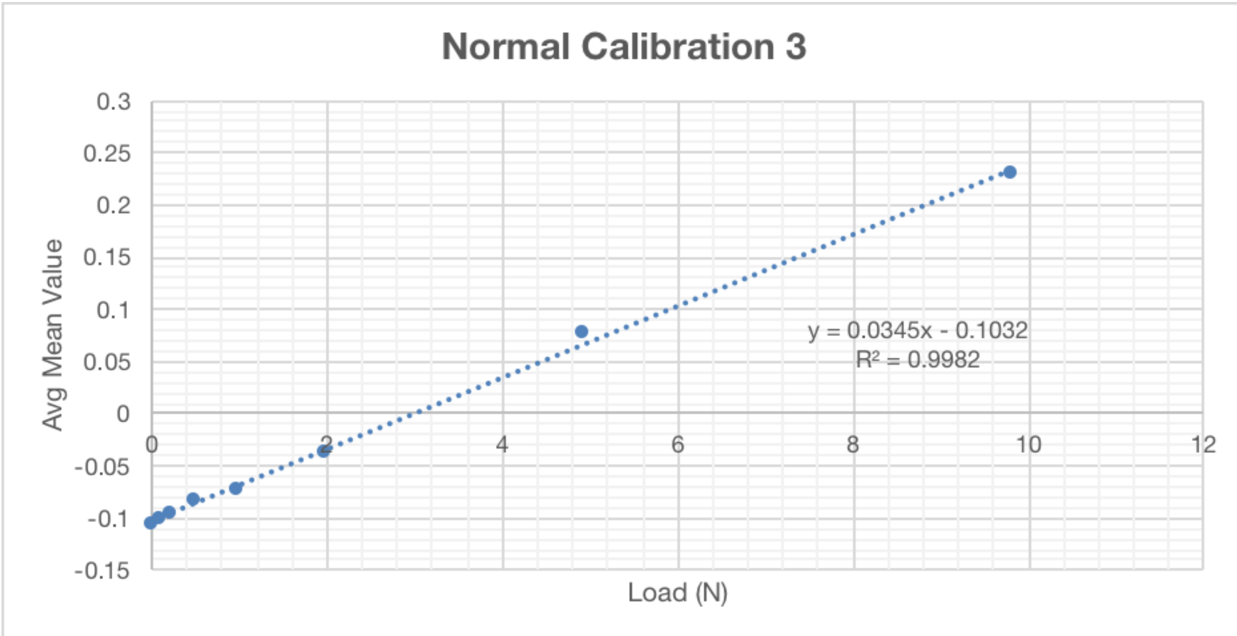

Fig. 54: Normal calibration test 3, different strain gauge ratio from Fig 52 and 53

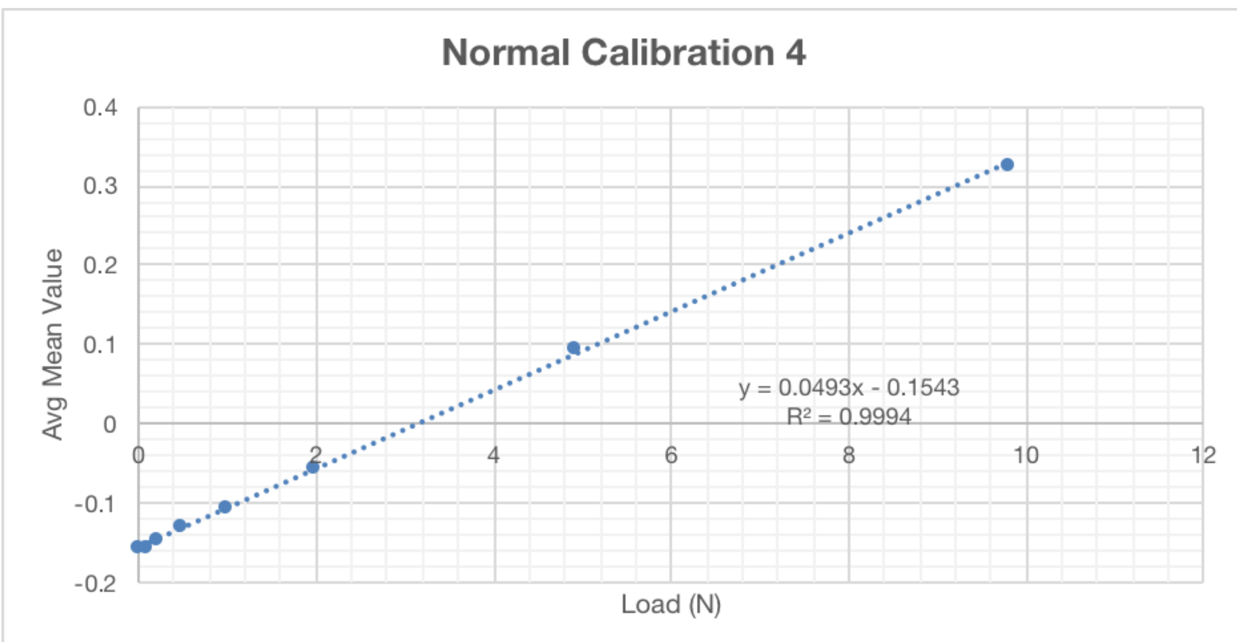

Fig. 55: Normal calibration test 3, different strain gauge ratio from Fig. 52 and 53

6.1.2 MTS Testing

MTS testing was done to verify mathematical simulations about the properties of 1095 Spring Steel. The aim of the test was to conclusively show that not only could Spring

Steel deform under the maximum load without breaking, but that the deformation was elastic and therefore there would be no permanent deformation.

The MTS data as shown below demonstrates that the elastic region of the material far exceeds the maximum load that the system would be subjected to.

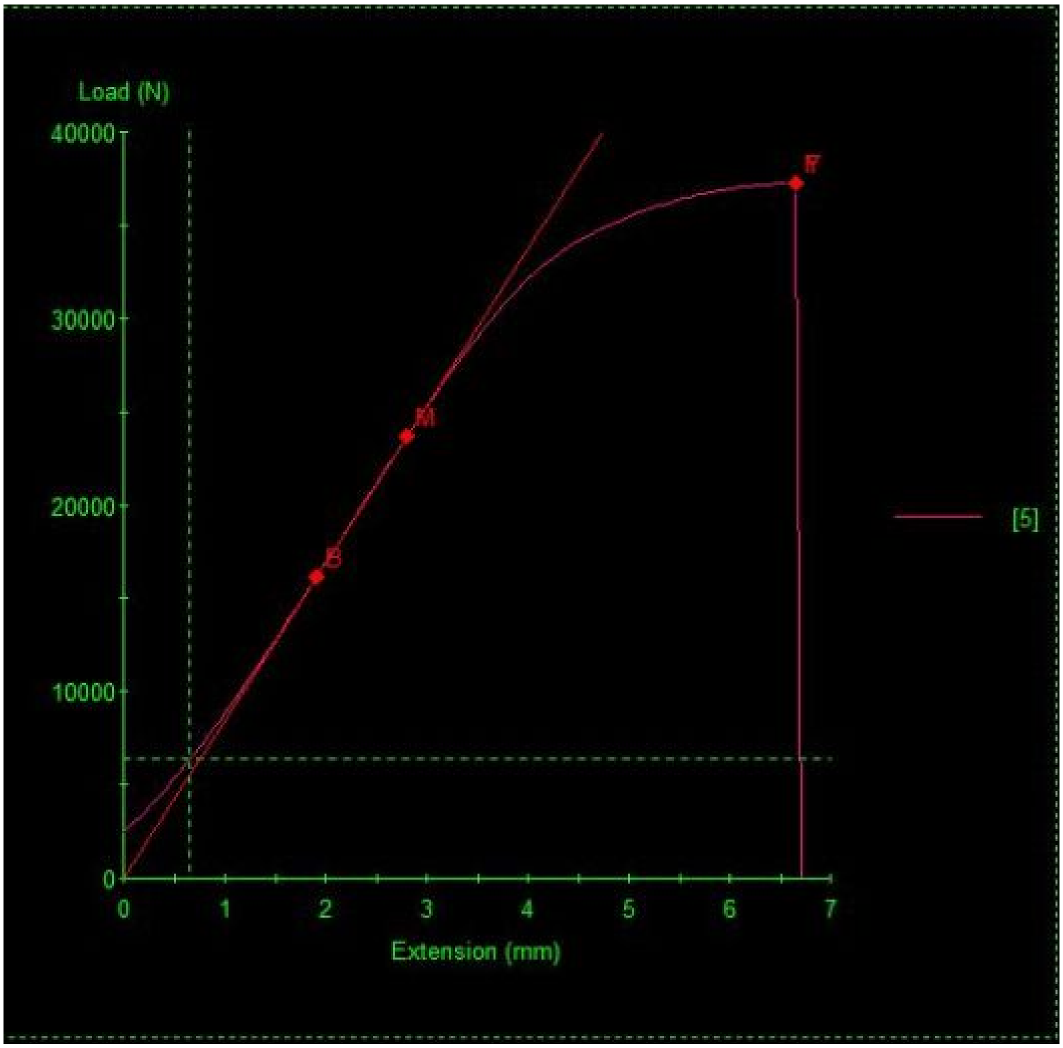

Fig. 56: MTS Data

6.1.3 Long Term Loading Tests

An important parameter for the design to achieve was that the normal load should stay constant over long periods of time since the tribometers are often used in tests that could last multiple hours.

6.1.3.1 Setup

In order to verify this, the team ran the full tribometer for 30 minutes at a frequency of 1 Hz with three different normal loads. The tests were conducted with a layer of PA04 + 0.8% LZ1371 lubricant coating the testing surface, with the testing base heated up to 130°C. This was similar to tests that the Carpick Group had done before. The final results can be seen in the figure below and were exported from LabVIEW.

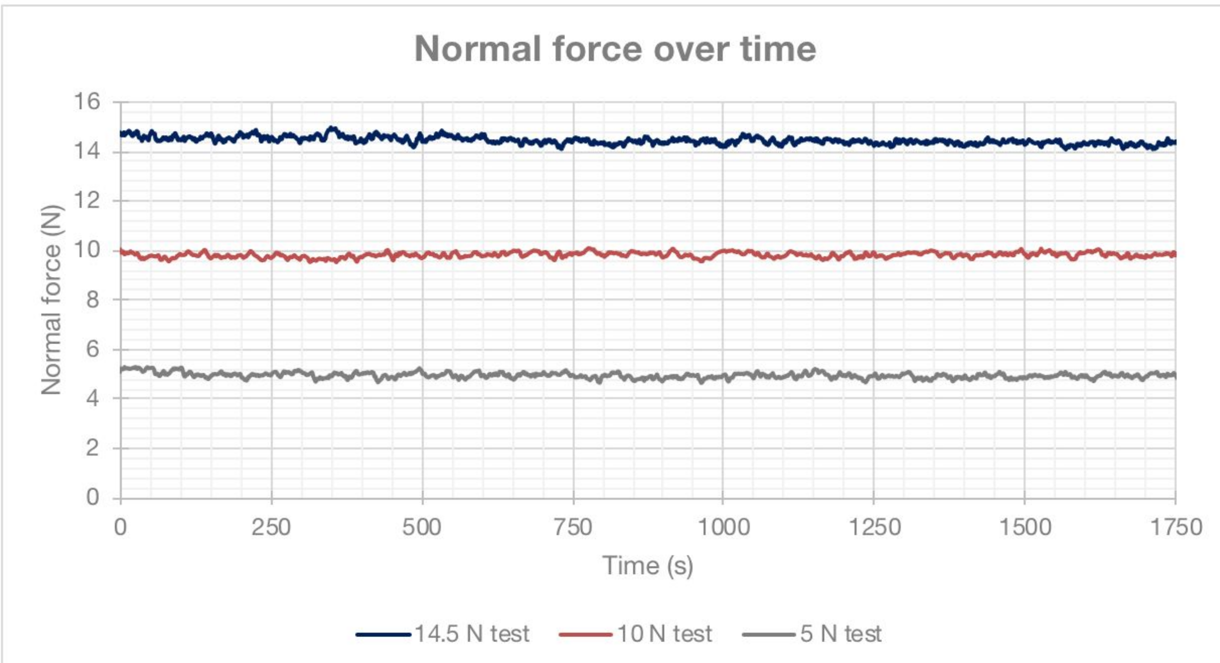

Fig 57: Normal loading test

6.1.3.2 Results

As demonstrated by the horizontal lines in the figure above, the system was capable of applying a relatively constant force over the 30 minute testing period. Although there were slight fluctuations, those fluctuations never exceeded +/- 0.2 N in the worst cases. Thus, the team was relatively confident in it's long-term performance.

6.2 Motion Subsystem

6.2.1 Motion Subsystem Test

For the motion subsystem, the team needed to verify that the reciprocation of the motion is able to achieve 5 mm strokes at the range of 0.5 Hz - 10 Hz.

6.2.1.1 Setup

To verify both the stroke length and frequency ranges, the guiding rail and stepper motor actuator were used to center the carriage system. Using the Lexium software, the stepper motor is able to move the carriage at specific locations across the lead screw. The team used this capability to test the displacements achieved. An excel sheet (Fig. 58) was developed such that the acceleration and velocity values led to an approximation of a sinusoidal wave pattern at the different frequencies. To calculate the acceleration and velocity values needed for the different frequencies, the conversion from revolutions to linear displacement was used for a displacement of 5 mm. For this particular linear actuator, one revolution is equivalent to a linear translation of 6.35 mm. This information was provided by the spec sheet for the actuator. The team verified the number of steps taken in the revolution translated to the real displacement using a caliper.

6.2.1.2 Results

The team was able to verify that the revolution to linear ratio provided in the stepper motor specifications were equal to the real displacement measured. The calculated acceleration and velocity values from Fig. 58, were verified using the internal clock within the Lexium Terminal, which printed out the current time, in seconds, at each cycle of the reciprocation

Frequency (Hz)	V (steps/s)	A (steps/s^2)
0.5	80000	1600000
1	160000	3200000
1.5	240000	4800000
2	320000	6400000
2.5	400000	8000000
3	480000	9600000
3.5	560000	11200000
4	640000	12800000
4.5	720000	14400000
5	800000	16000000
5.5	880000	17600000
6	960000	19200000
6.5	1040000	20800000
7	1120000	22400000
7.5	1200000	24000000
8	1280000	25600000
8.5	1360000	27200000
9	1440000	28800000
9.5	1520000	30400000
10	1600000	32000000

Fig. 58: Velocity and acceleration at different frequencies

6.3 Temperature Subsystem

For the temperature subsystem, multiple tests were conducted throughout the year to validate each individual step.

6.3.1 Single Device Temperature Test

The first set of tests the team conducted was with a finished testing base with spacers sitting on the vacuum chamber surface. The purpose of these tests was to determine the heating or cooling curve of a single heater or thermoelectric and tune the model accordingly. The model would then be able to calculate whether multiple or single heaters or thermoelectrics would be needed.

6.3.1.1 Setup

For the heating test, the heater was attached to the bottom of the testing base with thermal paste and connected via alligator clips and the vacuum chamber port to a 30 V DC power supply operating initially at 2 A and 7 V. The 2 A current level was chosen due to the anticipated 3 A limit for mechanical relays in temperature controllers. Lastly, a K-type thermocouple was wedged between the tab and the testing base to measure temperature. See Fig. KW16 for the setup.

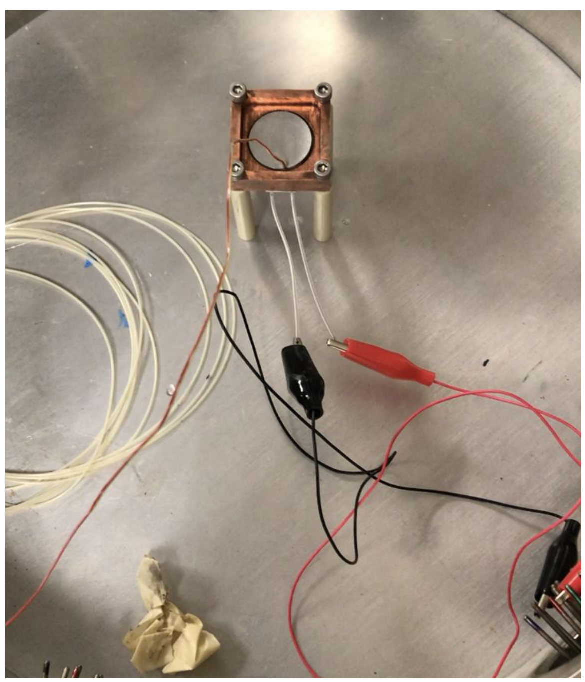

Fig. 59: Heating validation test #1 setup

During the cooling test, a SP2402 thermoelectric with a water-cooled heat sink was clamped onto the side of the testing base, with thermal paste between the thermoelectric and the heat sink, and the thermoelectric and the base. The heat sink was connected via plastic tubing to a 145 GPH pump submerged in an ice water bath. Afterwards, the K-type thermocouple was wedged into the testing base to measure temperature. Then, the thermoelectric was connected to the previous power supply operating at around 3 A, which was determined based on the safe continuous operating level of around 75% of the maximum current rating of 5 A. Finally, the glass dome was placed over the chamber to seal it from the environment, open ports were taped up, and the nitrogen tube was inserted to purge the chamber for two minutes before the start of the cooling process. See Fig. 60 for a rough idea of the setup.

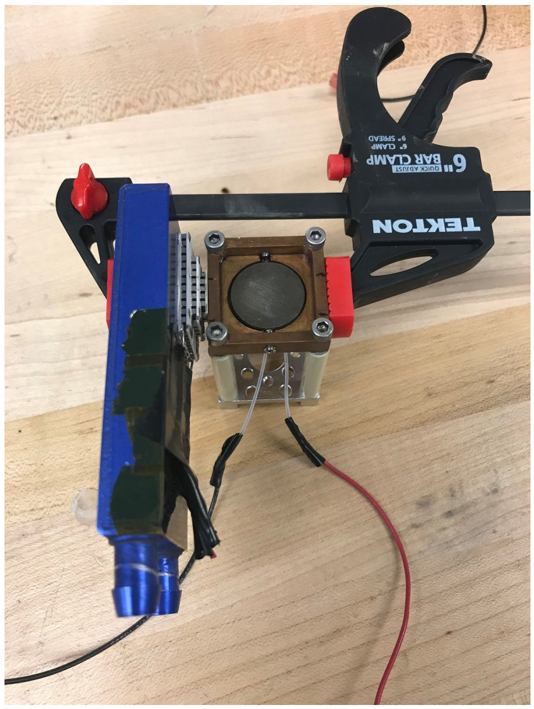

Fig. 60: Post-test reconstruction of cooling test #1 setup. Tubes would have been attached to the heat sink and the testing base would be inside the vacuum chamber.

6.3.1.2 Results

From the cooling data gathered in Fig. 61, the team roughly matched the experimental data curve to the model when projected heat gain from the environment was increased threefold. The error between the two experimental and theoretical curve likely existed because the ice water in the heat sinks cooled the testing base significantly during the first two minutes. When the threefold projected heat gain was applied with two thermoelectrics in the model, the model predicted that the testing base could in fact be cooled to -30°C. Another factor that probably affected performance during the cooling test was the clamp directly contacting the testing base on one side, which increased heat conduction to the base. Thus, the team was fairly confident it could fulfill the -30°C target.

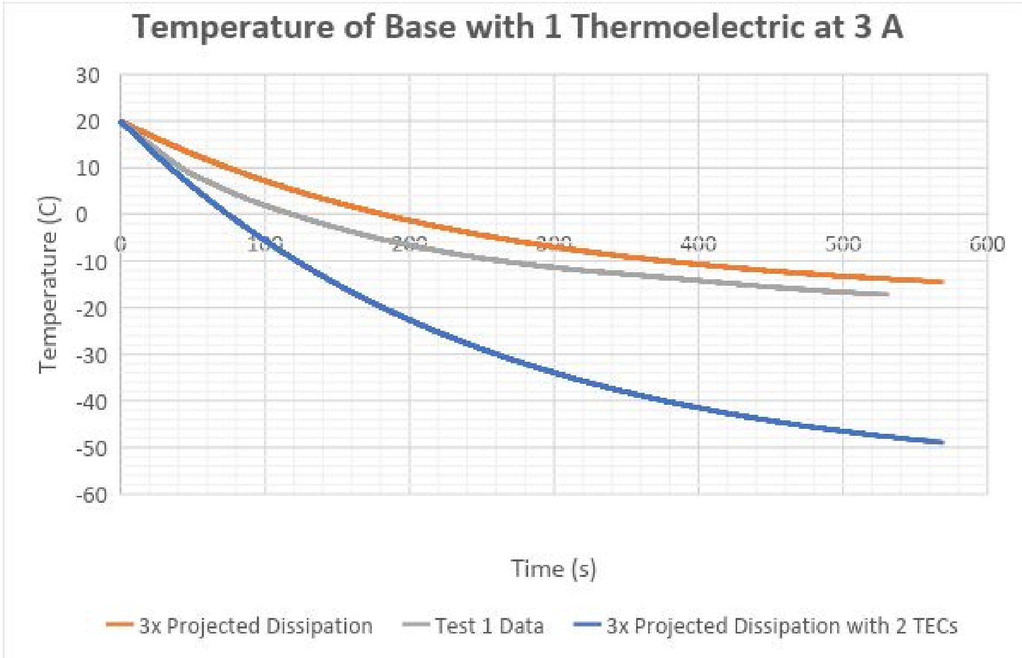

Fig. 61: Predicted and actual temperature of the testing base over time during cooling, test #1

In contrast to the cooling data, the heating data (see Fig. 62) very cleanly matched the model when projected heat loss to the environment was increased twofold. When the data was extrapolated over time, the team realized that 2 A was probably not enough to heat the base up to 200°C. Further adjustments with the model suggested that 2.5 A would suffice for the task though, so future tests would need to be conducted at around that current. Another issue that the heating test raised was that of securing the heater. At around 130°C, the heater fell off the testing base as the thermal paste was not strong enough at that temperature to resist gravity. Future tests would also need a more robust adhesive.

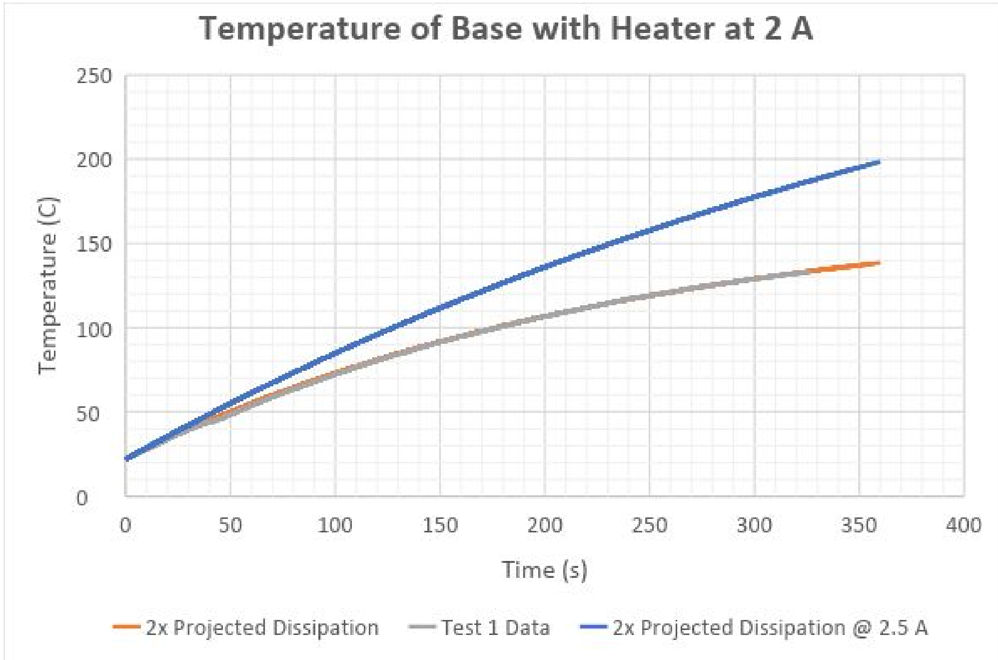

Fig. 62: Predicted and actual temperature of the testing base over time during heating, test #1

6.3.2 Full Subsystem Temperature Test

The second set of temperature tests were conducted with the full temperature setups, but without the cantilever, which had not been finished at that point. The purpose of these tests was to examine whether the full temperature setups could reach the target temperatures.

6.3.2.1 Setup

For the cooling test, two SP2402 thermoelectrics with water-cooled heat sinks were clamped onto the sides of the testing base with thermal paste between the thermoelectrics and the heat sinks, and the thermoelectrics and the base. The heat sinks were connected via plastic tubing to a 145 GPH pump submerged in an ice water bath. Afterwards, a K-type thermocouple was taped onto testing tab to measure temperature. Both thermoelectrics were connected to separate power supplies operating at 3.25 A, as the team attempted to speed up the cooling process while staying within the 3.75 A safe range. Finally, the glass dome was placed over the chamber to seal it from the environment, open ports were taped up, and the nitrogen tube was inserted to purge the chamber for two minutes before the start of the cooling process. See Fig. 63 for an image of the setup.

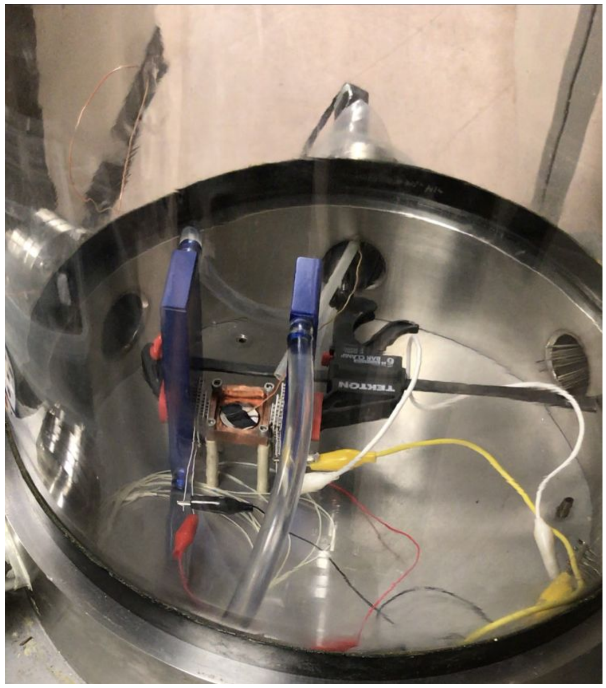

Fig. 63: Cooling validation test #2 setup

The heating test was done some time after the cooling test and unlike the cooling test, the testing base was able to connect to the reciprocating carriage. The heater was attached to the bottom of the testing base this time using with Halnziye thermal adhesive, which was rated up to at least 200°C and connected via alligator clips and the vacuum chamber port to a 30 V DC power supply operating initially at 2.5 A. Lastly, a K-type thermocouple was wedged between the tab and the testing base to measure temperature. See Fig. 64 for the setup.

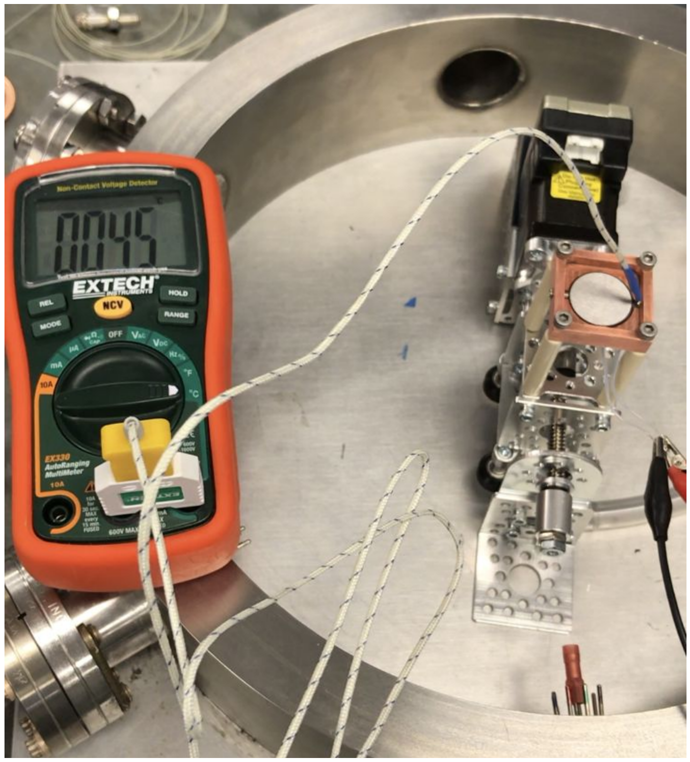

Fig. 64: Heating validation test #2 setup

6.3.2.2 Results

From the data the team gathered during the cooling test (see Fig. 65), it is clear that the temperature of the testing base reached -30°C in around three minutes and even exceeded it by several degrees, which was even better than what the model predicted from the previous set of tests. As a result, the team was relatively confident that the full cooling setup with a cantilever could still reach -30°C. However, the team noticed during the testing that frost was forming, which meant that nitrogen was leaking significantly and the makeshift tape port covers weren't effective. As a result, the team immediately focused on creating more robust covers.

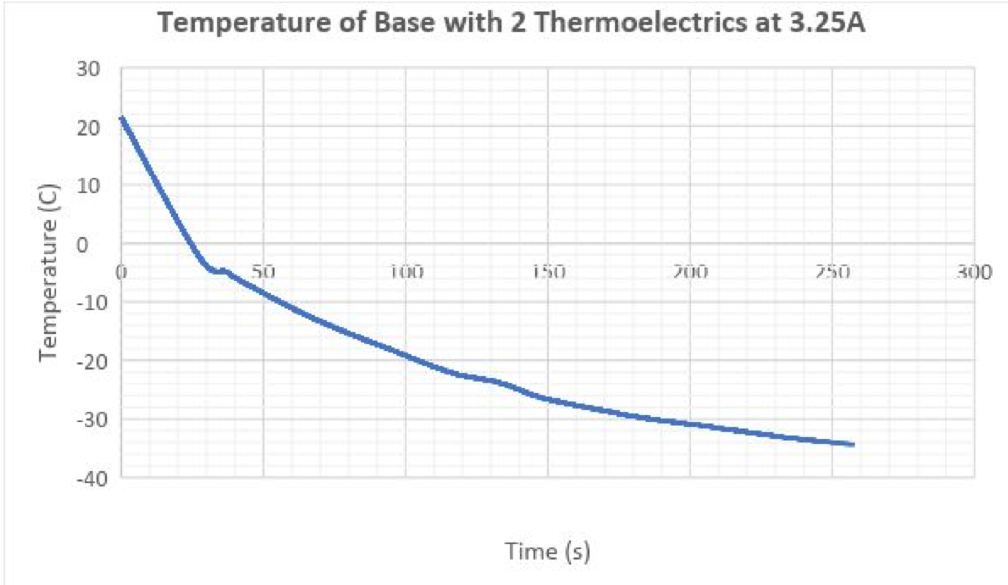

Fig. 65: Actual temperature of the testing base during cooling process, test #2

From the heating test in Fig. 66, it was clear that 200°C was certainly within reach with the heater at 2.5 A. However, although the thermal adhesive performed better than the thermal paste at securing the heater, the adhesive still failed at around 185°C. Thus, the team learned that an adhesive with a temperature limit much higher than 200°C was required.

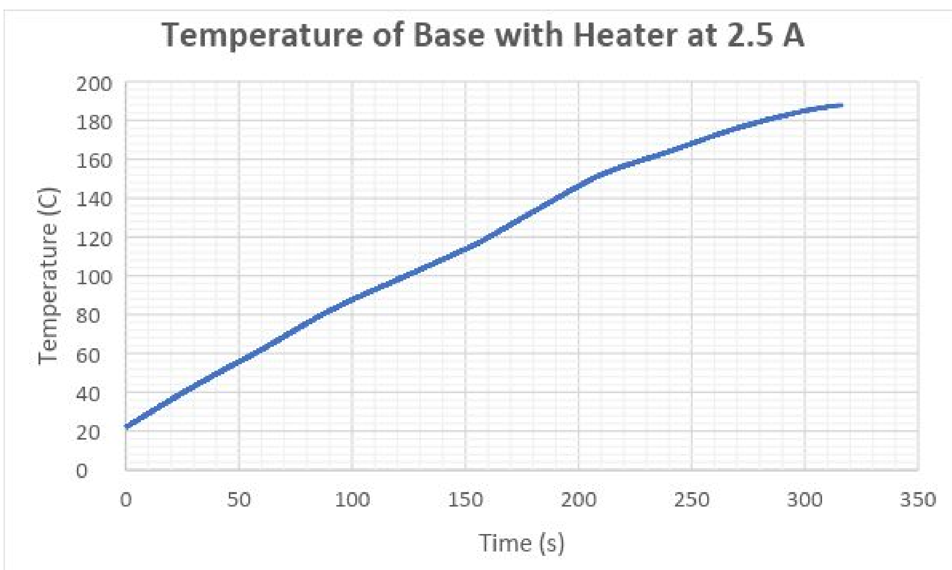

Fig. 66: Actual temperature of the testing base during heating process, test #2

6.3.3 Full Tribometer Temperature Test

The third set of temperature tests were conducted with the full temperature setup and tribometer setup. The purpose of these tests was to examine whether the full tribometer setups could reach the target temperatures.

6.3.3.1 Setup

For the cooling test, two SP2402 thermoelectrics with water-cooled heat sinks were clamped onto the sides of the testing base with thermal adhesives between the thermoelectrics and the heat sinks to permanently secure the two, and thermal paste between the thermoelectrics and the base. The heat sinks were connected via plastic tubing to a 145 GPH pump submerged in an ice water bath. Afterwards, K-type thermocouple was wedged between the tab and the testing base to measure temperature. Both thermoelectrics were connected to separate power supplies operating at 3.7 A, as the team attempted to test up to the maximum capabilities just within the 3.75 A safe range. The micropositioning stage was also adjusted to set the normal force to 10 N to test the most extreme condition. Finally, the glass dome was placed over the chamber to seal it from the environment, port covers were screwed in, and the nitrogen tube was inserted to purge the chamber. When the temperature hit -30°C, the testing base was oscillated back and forth at 1 Hz. See Fig. 67 for an image of the setup.

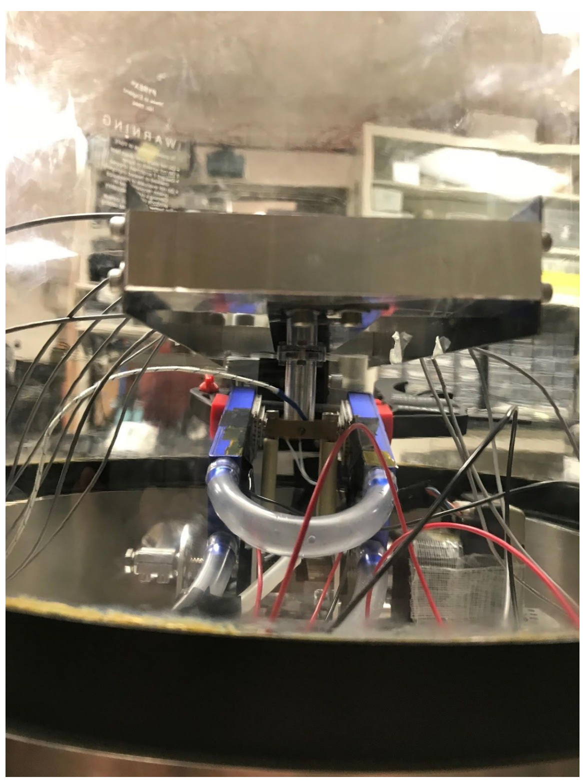

Fig. 67: Cooling validation test #3 setup

The heating test was again done some time after the cooling test and unlike the cooling test, a layer of PA04 + 0.8% LZ1371 lubricant was added to the testing surface. The heater was attached to the bottom of the testing base this time using with OMEGABOND 200 thermal epoxy, which was rated up to at least 260°C and connected via alligator clips and the vacuum chamber port to a 30 V DC power supply operating initially at 2.5 A. When the temperature hit 200°C, the testing base oscillated back and forth at 1 Hz and the was power supply was manually adjusted to keep the temperature near 200°C. The micropositioning stage was also adjusted to set the normal force to 10 N to test the most extreme condition. Lastly, a K-type thermocouple was wedged between the tab and the testing base to measure temperature. See Fig. 68 for the setup.

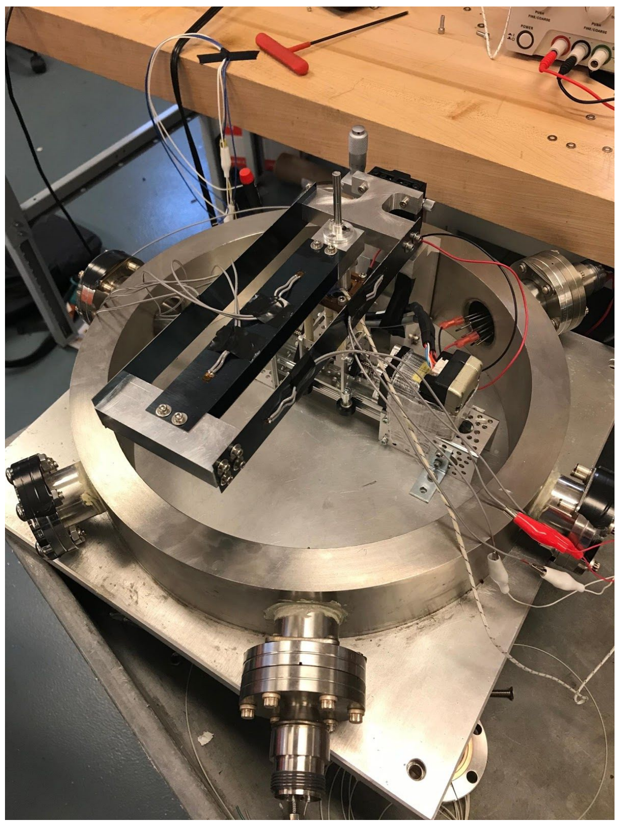

Fig. 68: Heating validation test #3 setup

6.3.3.2 Results

With the full setup oscillating cooling test, the temperature of the testing base was unfortunately unable to stay at around -30°C (see Fig. 69). After the testing base oscillation started when the temperature reached -30°C, the temperature rose to and plateaued at -24°C likely due to the heat generated from friction. If the normal force were lower, the temperature may be able to remain closer to -30°C. One factor that could have contributed to the unexpected result include the thermal adhesive. The thermal adhesive that replaced the thermal paste was lower quality and could have performed relatively poorly at temperatures near 0°C. Another factor was that since guide rails elevated the testing base, the plastic tubing tended to drag the heat sinks downwards, causing part of the thermoelectric cooling surface to lose contact with the testing base. On the positive side, there was no frosting or condensation on the testing surface, which proved the successfulness of the port covers at maintaining low relative humidity. Finally, an abnormality in this test was the fact that the team forgot to shut off the nitrogen valve before starting the test, thus causing an early plateau at around -7°C due to the room temperature nitrogen convecting heat to the base. Once this mistake was realized, the valve was shut off and the temperature immediately started dropping again.

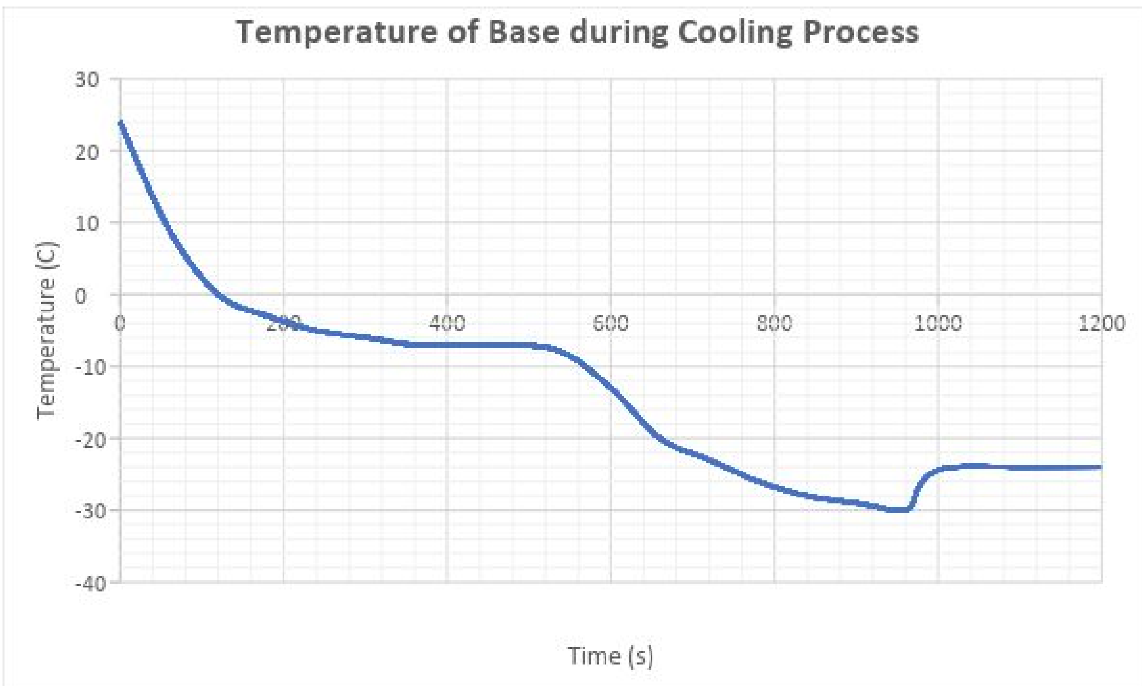

Fig. 69: Actual temperature of testing base during full cooling process, test #3

Unlike the cooling test, the heating test remained successful in reaching 200°C with the full tribometer setup (see Fig. 70). Although manually maintaining the temperature at 200°C was somewhat difficult, the team could safely say that the high temperature goal was achieved.

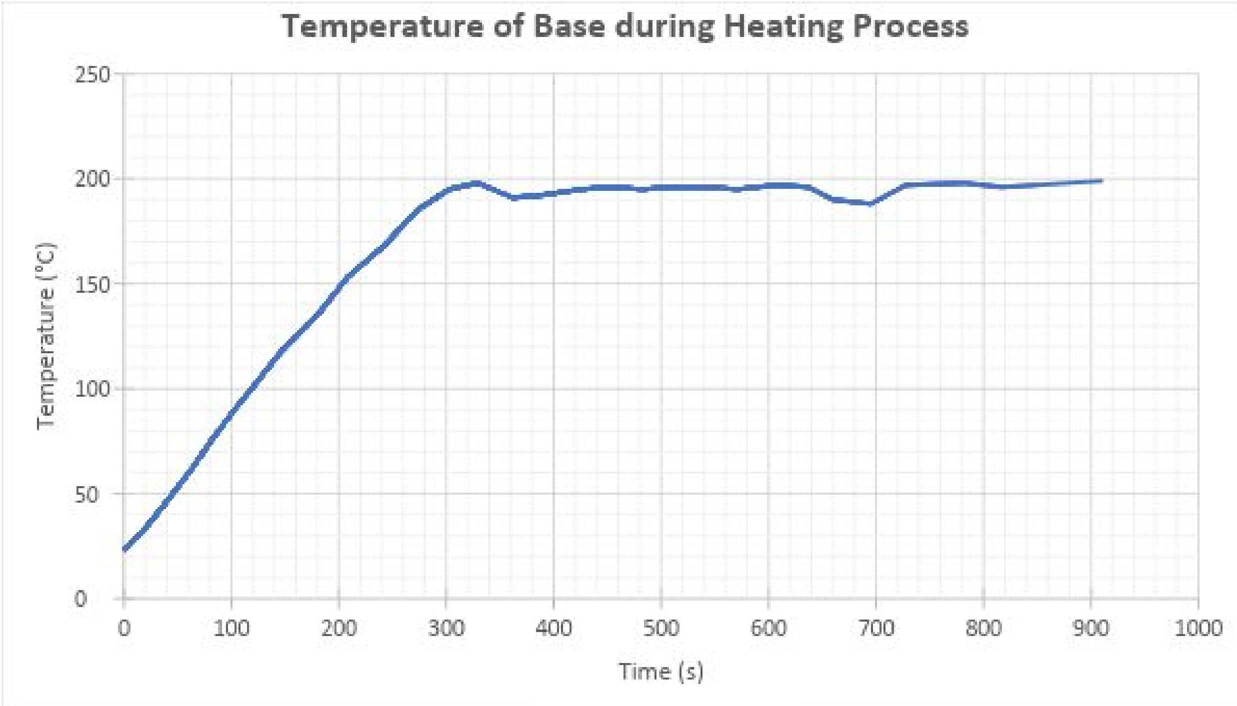

Fig. 70: Actual temperature of testing base during full heating process, test #3

6.3.4 Full Tribometer Cooling Test with ET Series Thermoelectrics

This temperature validation test was conducted only with the low temperature setup, as the high temperature goal had already been reached under more extreme circumstances. The main difference was the use of new thermoelectrics and the addition of lubricant.

6.3.4.1 Setup

The setup for this test was almost the same as the cooling setup for test #3. Two ET Series thermoelectrics with water-cooled heat sinks were clamped onto the sides of the testing base with thermal adhesives between the thermoelectrics and the heat sinks to permanently secure the two, and thermal paste between the thermoelectrics and the base. The heat sinks were connected via plastic tubing to a 145 GPH pump submerged in an ice water bath. Afterwards, a K-type thermocouple was wedged between the tab and the testing base to measure temperature. Both thermoelectrics were connected to separate power supplies operating at 5 A, which was the maximum current from the power supplies. The micropositioning stage was also adjusted to set the normal force to 10 N to test the most extreme condition. A thin layer of PA04 + 0.8% LZ1371 lubricant was then added to cover the testing surface. Finally, the glass dome was placed over the chamber to seal it from the environment, port covers were screwed in, and the nitrogen tube was inserted to purge the chamber. When the temperature plateaued, the base was set to oscillate at 1 Hz.

6.3.4.2 Results

Although the ET Series thermoelectrics were supposed to be more powerful, as seen in Fig. 71, the temperature plateaued at only -23°C and remained there for the duration of the test. The seemingly poorer performance is likely due to the addition of the lubricant. With the lubricant layer, there was a greater contact surface area between the testing base and the testing ball and cantilever, which increased heat conduction to the testing base. If these thermoelectrics were tested without lubricants, their performance would probably exceed that of the SP2402 thermoelectrics. Another factor that could have impeded performance was the small copper block that was attached to the thermoelectric. Since the block could not cover the entire thermoelectric, it was not able to efficiently conduct heat from the testing base. A better designed taper block might perform better. An additional explanation could be that the lubricant was undergoing a phase transition at that time, thus causing the temperature to stay the same. This explanation is supported by the fact that the lubricant appeared to become more of a gel-like texture and the relatively abrupt plateau. If this explanation were the case, -30°C may actually be possible after a longer cooling period.

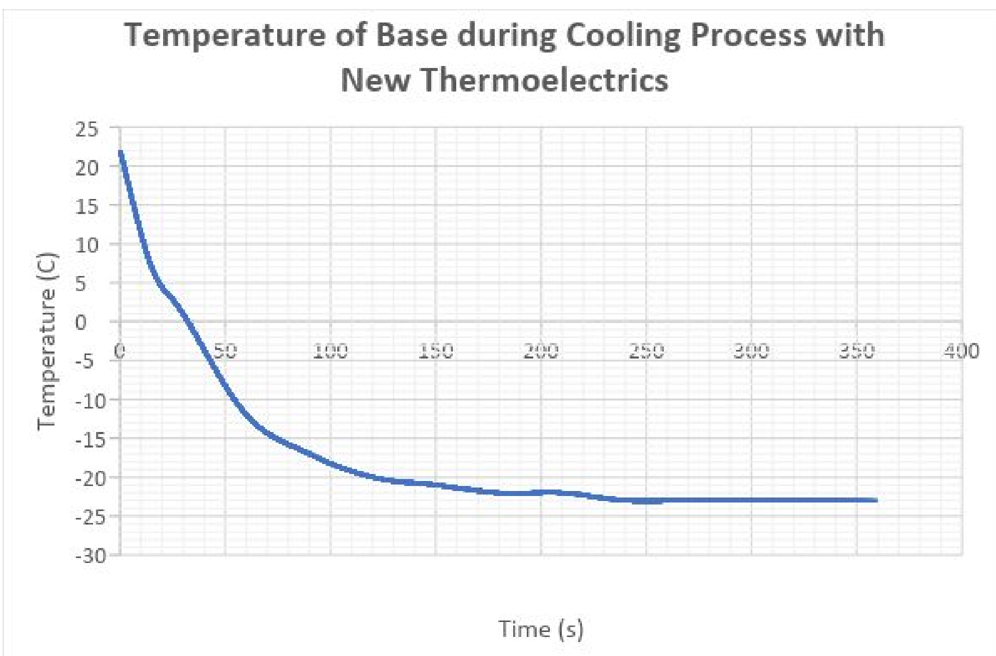

Fig. 71: Actual temperature of testing base during full cooling process, test #4

6.4 Data Acquisition / Full System Validation

6.4.1 Friction Coefficient Data Matching

In order to verify the functionality of the system and the accuracy of the friction coefficient data, the team reached out to the Argonne National Lab who provided the data for a test that the team could replicate. This test would also validate the fluid testing capability.

6.4.1.1 Setup

Their test was conducted with PA04 + 0.8% LZ1371 lubricant on a steel on steel contact heated to 130°C with a contact stress of 1 GPa resulting from a 15.6 N load and 6 mm diameter ball. The team replicated the all of these setup conditions except ball diameter, since the prototype ball hub could only accommodate a 12 mm ball at the time. The figure below is a comparison of the lab results versus those of the cantilever built by the team.

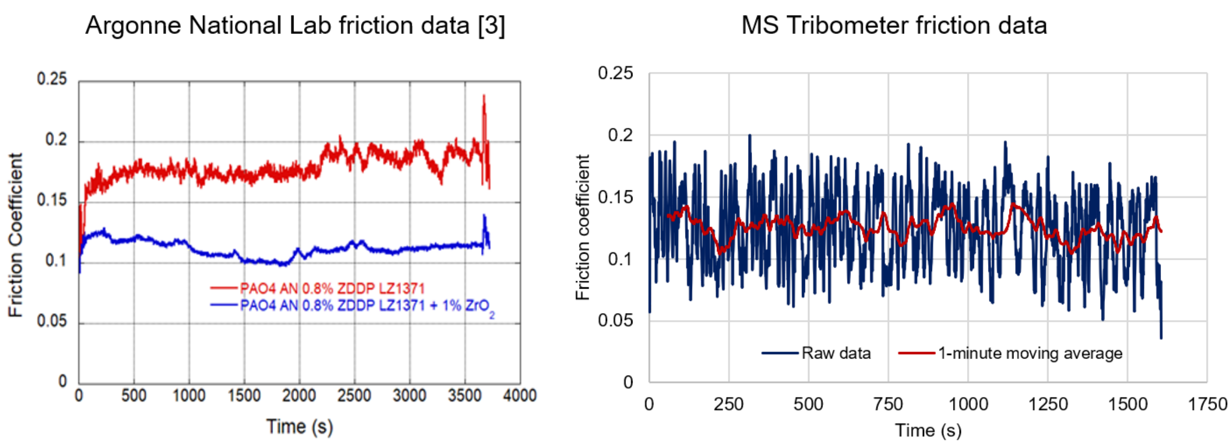

Fig. 72: Normal loading test

6.4.1.2 Results

The data collected by the cantilever built by the team showed more noise than that of Argonne, however a 1-minute moving average showed that the tribometer determined that the coefficient of friction of around 0.12- 0.14, just under the Argonne data which showed a coefficient of friction in the 0.16-0.18 range. This deviation can be accounted for due to the team being unable to recreate the exact contact pressure used by the lab on the system. The 12 mm diameter ball that the team used resulted in a lower contact pressure of around 0.6 GPa, which could have lower the coefficient. Another source of error comes from the region in which the team are working in; in dealing with low coefficients of friction, higher levels of noise are expected and affect results more adversely than regions of higher coefficients of friction. A team attempting to work on this project in the future should re-conduct the tests using the appropriate sized ball as well as with a better filter in place in order to verify the system more completely, however given the data above, the team confidently states that the tribometer functions as intended.

6.4.2 Low End Friction Coefficient Detection

The team also conducted a full test of the tribometer to see if it could reach the low end of the friction coefficient detection range.

6.4.2.1 Setup

The full test of the tribometer was conducted with steel on steel contact heated to 130°C and submerged in a thin layer of PA04 + 0.8% LZ1371 lubricant. The normal load was 10 N, the ball diameter used was 12 mm, and the testing base was reciprocating at 1 Hz. The test was run for a little over 20 minutes.

6.4.2.2 Results

While the 1-minute moving average of the friction coefficient was able to hit around 0.05, there was a lot of noise from the raw data as seen in Fig. 73. This noise could be due the variety of issues previously mentioned or simply due to the difficulty of measuring such low friction coefficients. Another factor that previously wasn't an issue was that the same testing specimen and ball were used from previous tests, and the accumulated wear could have affected the noise levels.

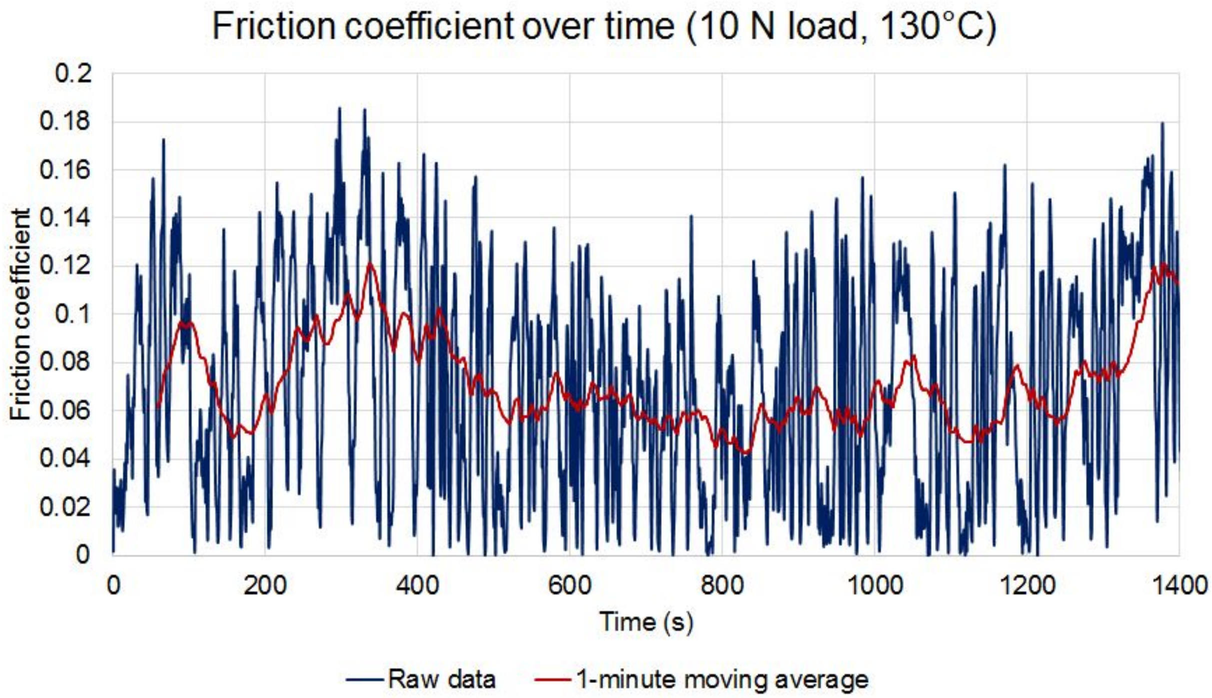

Fig. 73: Low-end friction coefficient testing results

7 Discussion

7.1 Loading Subsystem

7.1.1 Target vs. Accomplished Performance

The loading system had multiple performance targets. The first target was a load range of 10 mN to 10 N and that at any given load, the force remains constant through the duration of testing. The second target is the ability to load balls with diameters ranging from 2 - 12 mm. The final target was to implement a roll/slide functionality that would allow the ball to roll and slip simultaneously and quantify how much rolling was occuring.

Based on the calibration testing done, and the three tests conducted to determine constant forces while the system is running the first targets was hit and even exceeded since the loading system functions at loads greater than 10 N. The current loading system currently only performs with 12 mm balls. The bottom hub piece was designed to be a modular piece, capable of being switched out as necessary, so while the system on its own does not satisfy the target goal of a ball range from 2 - 12 mm, the capability is there if enough of the bottom hubs are made with the modifications necessary to hold other ball diameters. The physical ability for the ball to roll and slip was achieved, however there was no method determined in order to quantify the ratio of roll to slip.

7.1.2 Recommendations

The current system for switching balls involves manufacturing an entire hub and, given the geometry of the system, a significant amount of dismantling in order to replace the bottom hub piece. A future iteration of this device would allow for a better system such that a ball could be more easily inserted and the need for multiple parts would be non-existent. The challenge in designing this part would be that the design would not only need to ensure a fit for multiple sizes, but that there is enough of the ball left exposed to form a contact surface. Some ideas discussed by the team were a plunger like system that would hold the ball in place or some type of adjustable rubber seal that held the ball in place. Other potential solutions could include an iris mechanism that could be adjusted to hold a range of diameters.

It was found that by loosening the steel bar, the ball could roll while the system moved. There was however no means of quantifying the roll to slip ratio meaning that although the functionality is there, it is not useful as there is no means of quantifying the results.

The original design made use of set screws to the ball to roll. The design has potential to work but was not realized due to time constraints. The difficulty with this design is that the design called for the diameter of the ball to be just above the exit hole in the bottom hub. An attempt at this design would require care to ensure that not only is enough of the ball exposed, but that the diameter parallel to the exit hole is high enough such that set screw holes can be drilled through in order to come into contact with it. This however does not solve the issue of quantifying roll to slide ratio. Quantifying roll to slide ratio would likely require the development of some testing procedures.

One final area of potential improvement is the actuation of the loading system such that the loads can be changed mid test or adjusted if necessary. This development would be worthwhile considering the system operates in a closed chamber for some tests.

7.2 Motion Subsystem

7.3.1 Target vs. Accomplished Performance

The current iteration of the team's tribometer is able to hit both the frequency range desired by the Carpick Group (0.5 Hz - 10 Hz) on a 5 mm linear track displacement.

7.3.1 Recommendations

One of the main obstacles the linear motion subsystem faced was the presence of vibrations. From the tests ran, it seemed that the vibrations mainly came from the looseness of the stepper motor on the mounting stand and the vibration of the stepper motor. To minimize the vibration from the interface between the motor and the motor stand, the motor stand would be redesigned such that the pattern brackets are able to properly align with the motor mount and be screw in securely. A possible solution in minimizing the effects of the motor vibration could be the use of some dampening material near the interface between the carriage system and the anti-backlash nut. The combination of these two solutions could significantly reduce the vibrations experienced by the testing base during reciprocation.

Moreover, a desired functionality of a future iteration of the team's tribometer is the ability to track the location of the pin and testing base contact during the tests. To do this, an encoder could be utilized to track the distances the motion system has travelled. Tracking the linear motion would allow for more in depth analysis of the friction testing.

7. 3 Temperature Subsystem

7.3.1 Target vs. Accomplished Performance

The target values for the low and high temperature goals were -30°C and 200°C, respectively. In actuality, the team was able to reach 200°C during the heating process but only -23°C for the cooling process during testing under the most strenuous conditions. Therefore, the team only achieved half of the goal. However, the data from the cooling test of the ET Series thermoelectrics suggested that -30°C may be able to be reached with longer cooling tests or under certain circumstances, such as when there are no fluids. Further validation testing would need to be done to confirm those conclusions.

7.3.2 Recommendations

The biggest issue with the temperature subsystem was the inability to reach -30°C under all testing conditions. To improve on the work accomplished in this report, future teams should spend a lot of time researching and testing different thermoelectrics to identify the optimal one given their physical dimensions, maximum temperature differences, and heat load curves. The contact between the thermoelectrics and the testing base must be as perfect as possible to maximize heat conduction away from the base. This effort may involve machining thin copper blocks with edges that taper to exactly the dimensions of the thermoelectric and the testing base side to minimize thermal resistance.

The second priority for any team building upon the team's progress would be to connect the heater and an RTD sensor to a LabVIEW data acquisition device (DAQ). Since the data acquisition system was entirely shifted to LabVIEW, integrating the temperature control would provide a relatively seamless user interface. The team briefly experimented with this system but did not have enough time to fully integrate it into the GUI and fix all the bugs. With the RTD sensor connected to the LabVIEW DAQ, the temperature data could be automatically recorded and based on certain formulas, output voltage could be transmitted to a separate solid-state relay to turn on or off the heater when appropriate.

Finally, to improve the robustness of the humidity control, proper port covers with air-tight seals should be manufactured rather than laser-cut from acrylic. While the acrylic covers worked for shorter periods of time, there were some gaps in the press-fits and tape coverings that would allow nitrogen to slowly leak out. Airtight port covers would ensure that the nitrogen does not escape. Alternatively, a custom plastic airtight chamber with ports could be built instead of using the vacuum chamber. The new plastic chamber would likely be significantly less expensive than the stainless steel and glass vacuum chamber.

7.4 Fluid Subsystem

7.4.1 Target vs. Accomplished Performance

The final device is able to accommodate liquids and lubricants of a wide range of viscosities in a bath. The team established a goal of testing lubricants with viscosities varying from 1 - 2500 cSt. The team surpassed this goal and can accommodate nearly any lubricant of any viscosity due to the characteristic of the testing base's bath, rather than a flowing mechanism. The bath can comfortably hold up to 2.5 mL of the desired testing lubricant while conducting the test. This is more than adequate as only the point contact must be submerged.

The team regrets that it was unable to incorporate a flow mechanism for the lubricants. This would have been a truly differentiating aspect of the MS Tribometer. However, the team was advised by the Carpick Group at the beginning of the spring semester that the necessity of a fluid flow subsystem was misfounded. They could not think of tangible tests for their current research goals that necessitated the need for circulating lubricants. The team acquiesced to their advice and focused instead on the other aspects of the tribometer. The team ensured to leave a substantial topological footprint inside the vacuum chamber should further customizations include a fluid flow system.

7.4.2 Recommendations

The biggest problem with implementing the fluid flow system was being able to design around the constraints of other subsystems. The fluid flow system would need to be attached to the testing base in some way since it is the reciprocating mechanism. The entire fluid flow system would have to move with the testing base or have tubes going to the surface. If given more time and funds, the first issue that would be addressed is designing a system that fits in with the current setup.

In this setup, the team considers a gravity driven flow mechanism to be the technology of choice. Because of the inherent vibrations in a fluid pump, the team believes a pump would adversely affect the resolution. A basic setup of a gravity fluid flow system involves two reservoirs, one above the testing base and one below. This would allow the flow to be gravity driven, with an adjustable area outlet for the higher reservoir. The adjustable area would allow the user to control the mass flow rate into the testing base. The testing base would then utilize a gravity drain to the lower reservoir. Tubing would need to have a sufficiently large area to accommodate the desired viscosity range of 1 - 2500 cSt. The team recommends use of a COMSOL model to simulate this relatively simple flow.

The second use of the fluid flow system would be able to purge the oil from a previous test. The oil would be purged with water while the testing base heats up slightly in order to dry the surface. A new batch of oil would then be added to the testing base and another test could be performed.

7.5 Data Acquisition Subsystem

7.5.1 Target vs. Actual Performance

Although there was a deviation of 17% between the friction coefficient value the team collected and the value collected by the Argonne National Lab, the difference can likely be attributed to the slightly different testing conditions. The team was thus fairly confident that the tribometer was relatively accurate and could reach higher friction coefficients. On the low end of the friction coefficient detection range, the tribometer was also successful in detecting a friction coefficient of 0.05 as proven in a previous validation test. However, noise levels for both validation tests proved much higher than the 5% objective, with the Argonne test noise around 30-40% and the low-end friction detection test up to 100% noise. Thus, the team did not meet the basic goal of having 5% noise in its result.

7.5.2 Recommendations

Ultimately, the inability to meet the target precision was not due to a resolution limit in the device, but rather due to the large amount of noise originating from the system. As such, the blame cannot lie with a lack of strain sensitivity of the system, the amplitude of the amplification, and the resolution of the data acquisition device. There was simply too much noise to ever even try to isolate a highly sensitive and miniscule measurement. Thus, the question lies in where to eliminate any sources of noise. One possibility is the lack of shielding in the electrical circuits. The two Wheatstone bridges, two amplifiers, RTD circuit were all a crowded mess of intersecting and overlapping wires, built over exposed breadboards where any movement would displace connections and affect resistances. Beyond the interference problems, it meant the system was not conducive to relocation and was quite cumbersome. To tackle this, the group could have designed and ordered integrated PCPs that satisfy the functions required, while in a much more shielded and separated way.

Another important factor is the moment when measurements are taken. The results showed a sinusoidal function with a base value close to the actual value expected. This sinusoidal wave is equivalent to the waveform depicting the motion of the motor, meaning that there are specific moments in the cycle where the recording of measurements should occur. Due to this fact, there should have been a synchronization between the LabVIEW software and the motor, possibly done by an encoder. This would have allowed the team to pick only the base value of this sinusoidal function and arrive at a much less noisy outcome. At that point, precision could have re-emerged as a goal and this could have been achieved by several factors. Firstly, the gauges bought were of relative low-grade and a straightforward improvement on the system would be an upgrade of these gauges. This would not only provide better sensitivity, reducing noise, but also more resilience to temperature and fatigue. This could have also been done in the processing in LabVIEW. However, it would be far better to avoid the inclusion of such results from the start, as in processing they will have still have influence on the outputted data. The final design also had a normal force in a half bridge formation in the final setup, which was due to the fact that a precise measurement of normal force was easier to obtain due the larger magnitude of a normal force as opposed to its resulting friction force. This made the team prioritize the friction force as it was certainly the source of the noisy results. However, in future iterations, a full bridge should be used in all subsystems as it is the optimal setup for increased sensitivity and temperature protecting. Furthermore, while miniscule, the lead wire resistance could have also been factored into the Wheatstone calculations. A simple mathematical analysis was conducted to understand the effects of the resistance in the wires, which reached 0.5 Ω, and found it to be mostly negligible. Still, it would have helped achieve the target level of precision.

7.6 Target vs. Actual Performance Summary

The summary of the actual performance against the target performance is shown below in Table 10.

Table 10: Target vs. actual performance summary

Parameter	Subsystem	Basic Goals	Reach Goals	Actual Results
Load Variation	Loading	10 mN - 10 N		10 mN - 10 N
Ball Diameter Variation	Loading	2 - 12 mm		12 mm but can be changed
Roll-Slide Capability	Loading	Roll or slide	Adjustable roll-slide ratio	Roll or slide
Linear Reciprocation Frequency	Motion	0.5 - 10 Hz		0.5 - 10 Hz
Reciprocation Length	Motion	> 5 mm		> 5 mm
Temperature Range	Temperature	-30°C to 200°C	-50°C to 200°C	-23°C to 200°C, but may go lower
Fluid Testing	Fluid	Static fluid	Flowing fluid	Static fluid
Viscosity Range	Fluid	1 - 2500 cSt		1 - 2500 cSt
Friction Coefficient Detection	Data Acquisition	0.05 - 0.5	0.01 - 0.5	0.05 - 0.5

8 Budget, Donations, and Resources

This project was funded primarily by MEAM Senior Design. The team was given a budget of $2,400 and spent about $2,387 on materials (see Table 11 below for a cost breakdown). A more detailed break-down can be found in Table 12 in the Appendix. The Carpick Group was also a major source of donations and the team would like to greatly thank them. In addition to the donations, the team used Dr. Carpick's laboratory for low temperature testing due to the availability of nitrogen gas and for degreasing the cantilever beams prior to strain gauge installation. While the team had also pursued donations from industry and was in contact with Rtec Instruments, the team didn't end up asking for anything. Finally, the team used many small electrical components such as wiring, resistors, and breadboards from the General Motors Laboratory that the team was based out of.

Table 11: Cost breakdown for the entire project

Paid by / Source	Item / Category	Total Cost / Value
MEAM Senior Design Fund	3x SP2402 Thermoelectric Coolers	723.15
MEAM Senior Design Fund	2x ET Series Thermoelectric Coolers	48.86
MEAM Senior Design Fund	Omega CN32PT-330 Temperature Controller	220.00
MEAM Senior Design Fund	Other Temperature Components	244.59
MEAM Senior Design Fund	Motor and Track Components	241.83
MEAM Senior Design Fund	Other Data Acquisition Components	10.90
MEAM Senior Design Fund	Strain Gauges and Adhesive	270.00
MEAM Senior Design Fund	TADC 491 - SZ Micropositioning Stage	369.24
MEAM Senior Design Fund	Stock Materials	258.78
Carpick Group Donation	Huntington Labs Bell Jar Vacuum Chamber	4,000.00
Carpick Group Donation	MLI3 NEMA 14 Stepper Motor Linear Actuator	800.00
Carpick Group Donation	National Instruments DAQ USB-6001	204.00
Carpick Group Donation	K-Type Thermocouple	10.00
Carpick Group Donation	Thermocouple Reader	30.00
GM Lab	Miscellaneous Electrical Components	40.00
Total		7,471.35

9 Business Analysis

9.1 Value Proposition and Need Summary

Many researchers, in both academia and industry, study friction and wear in a wide variety of environments to better understand and improve efficiencies of mechanical systems. However, commercial friction testing machines can be prohibitively expensive at over $50,000 for cost-conscious research labs and companies and often do not have all the capabilities that researchers desire. Thus, a number of researchers, including 4 out of the 6 researchers interviewed, spend up to half a year or more to build their own lower-cost customizable tribometers. The MS Tribometer is an alternative solution for these researchers in academia and industry looking to cheaply test friction and wear in a wide variety of different environments.

9.2 Target Customer Segments

MS Tribometer is targeted towards researchers at research universities and at smaller companies that conduct R&D on products affected by friction. These researchers likely have smaller budgets for purchasing equipment such as expensive commercially available tribometers and would be more likely to either build their own or buy the MS Tribometer.

9.2.1 Market Size - Universities

According to the Carnegie Classification of Institutions of Higher Education, there are 334 research universities in the US that have moderate to the highest research activity [21]]. Assuming two-thirds of the universities mainly built their tribometers as found in interviews, there is an addressable market of 223 universities. Since the University of Pennsylvania, a major research university, only had one tribology laboratory, it can be assumed that each of the 223 universities has one lab that would require a tribometer. Assuming an useful life of around 8 years for each tribometer, annual demand from universities would likely max out at about 28 tribometers. Given an average selling price of $10,000, the market size would be $280,000. Annual growth rate would likely be between 0% and the GDP growth rate of 2% since tribology labs are relatively steady fixtures in research universities and research university numbers aren't dramatically growing.

9.2.2 Market Size - Industry

The number of members in the Society of Tribologists and Lubrication Engineers can be used as a proxy for the number of companies involved in tribology research. Given that there are more than 15,000 members in industry [22], it can be assumed that half of the members are lubrication engineers that aren't involved in friction testing, leaving 7,500 tribologists. Since there are about 10 researchers in the Carpick Group, it can be assumed that the average lab size is around 10 people. Assuming everyone in those labs is a member of the Society, there are 750 research labs in industry. Using the two-thirds build versus make rate, there would be an addressable market of around 500 laboratories in industry. Assuming again that useful life would be about 8 years, annual demand would be around 63 tribometers. Given an average selling price of $10,000, the market size would be $630,000. Annual growth rate would likely be around the GDP growth rate of 2% since tribology tends to affect relatively mature technologies. While the market size appears small, there is a high likelihood that industry demand was underestimated given the assumptions.

9.3 Competition

Competition in the tribometer manufacturing industry comes mainly from small, specialized manufacturers with a small line of different tribometers or related products. The major players include Anton Paar, PCS, and Rtec Instruments. These players typically build both specialized tribometers and all-in-one tribometers that allow for testing in a variety of environments including in high and low temperatures, with fluids, and with varying contact stresses. However, they are not very customizable for researchers and can be prohibitively expensive. The MS Tribometer would compete primarily on price and the ability to offer the same or slightly wider variety of environments that competitors could offer. The main drawback for the MS Tribometer would be a longer setup time and a slightly less user friendly interface. However, for cash strapped laboratories, this would likely be an acceptable tradeoff.

9.4 Cost

The total cost of the tribometer the team created was around $6,800 as shown in Table 10. For items that weren't fully used in the tribometer, the percentage of the item used was allocated towards the cost. Manufacturing and assembly costs were also included based on the estimated hours needed. Since the annual demand would not likely exceed several hundred, the tribometers would be mostly hand-built. While $6,800 is already very low compared to commercial tribometers, there are further cost reduction opportunities, especially with regards to the vacuum chamber. Cheaper alternative airtight chambers could be either custom designed and manufactured or bought as-is for likely less than $2,000, which would further reduce the cost to $4,800.

Table 12: Cost breakdown for the MS Tribometer

Product	Category	Quantity	Price	Total Price	% Value Used	Cost to Tribometer
Hardened Impact-Resistant S2 Tool Steel Balls	Cantilever / Pillar / Testing Base	1	$9.63	$9.63	2%	$0.19
6061 Aluminum 5/8" Thick, 2" x 48"	Cantilever / Pillar / Testing Base	1	$42.39	$42.39	50%	$21.20
110 Copper Sheet, 6" x 6" x 5/8"	Cantilever / Pillar / Testing Base	1	$115.61	$115.61	4%	$4.62
Spring Steel Shim Stock (1/40")	Cantilever / Pillar / Testing Base	1	$21.53	$21.53	19%	$4.09
Machining Time + Assembly (hrs)	Cantilever / Pillar / Testing Base	40	$25.00	$1,000.00	100%	$1,000.00
Ceramic Standoffs 1/4" OD, 1-1/2" Long	Cantilever / Pillar / Testing Base	4	$6.07	$24.28	100%	$24.28
24 Gauge Wires $/ft	Data Acquisition	30	$0.25	$7.50	100%	$7.50
National Instruments DAQ USB-6001	Data Acquisition	1	$204.00	$204.00	100%	$204.00
Strain Gauges	Data Acquisition	10	$6.00	$60.00	80%	$48.00
Strain Gauge Adhesive	Data Acquisition	1	$150.00	$150.00	5%	$7.50
Resistors	Data Acquisition	13	$0.20	$2.60	100%	$2.60
Op Amps	Data Acquisition	2	$0.57	$1.14	100%	$1.14
Breadboards	Data Acquisition	4	$3.99	$15.96	100%	$15.96
Metal Ceramic Heater, 10x10x1.2mm, 10ohm	Heating and Cooling	1	$16.70	$16.70	50%	$8.35
Honeywell HEL-705-U-1-12-00 RTD Sensor	Heating and Cooling	1	$25.42	$25.42	100%	$25.42
10ft Vinyl Tubing 5/16 ID	Heating and Cooling	1	$4.00	$4.00	100%	$4.00
145 GPH Maxesla Submersible Pump	Heating and Cooling	1	$9.99	$9.99	100%	$9.99
Laird ET Series Thermoelectric Cooler	Heating and Cooling	2	$24.43	$48.86	100%	$48.86
Arctic Silver 5 AS5-3.5G Thermal Paste	Heating and Cooling	1	$6.79	$6.79	100%	$6.79
6 in Tekton Ratchet Bar Clamp	Heating and Cooling	2	$5.51	$11.02	50%	$5.51
Halnziye 10g Thermal Adhesive	Heating and Cooling	1	$7.98	$7.98	20%	$1.60
Aluminum Water Cooling Blocks 40x40	Heating and Cooling	2	$7.99	$15.98	100%	$15.98
Solid-State Relay	Heating and Cooling	1	$8.99	$8.99	100%	$8.99
High-Temperature Tape	Heating and Cooling	1	$6.78	$6.78	100%	$6.78
TADC 401 - SZ	Micropositioning stage	1	$320.00	$320.00	100%	$320.00
Screws for Micropositioning Stage	Micropositioning stage	1	$49.24	$49.24	50%	$24.62
Servocity Order #1	Stepper Motor / Linear Track	1	$48.35	$48.35	100%	$48.35
Servocity Order #2	Stepper Motor / Linear Track	1	$44.07	$44.07	100%	$44.07
Servocity Order #3	Stepper Motor / Linear Track	1	$42.46	$42.46	100%	$42.46
Stepper Motor Linear Actuator	Stepper Motor / Linear Track	1	$800.00	$800.00	100%	$800.00
Vacuum chamber - Huntington Labs	Vacuum Chamber	1	$4,000.00	$4,000.00	100%	$4,000.00
Total						$6,762.85

9.5 Revenue Model

The revenue model for this business would be a simple production model where the company manufacturers the tribometers and sells directly to researchers. Due to low volume, the company could also customize individual tribometers for additional fees. To stay competitive, pricing for the base tribometer would likely need to be less than $10,000 per tribometer.

10 References

[1] VTT Technical Research Centre of Finland. "One-third of car fuel consumption is due to friction loss." ScienceDaily. ScienceDaily, 12 January 2012. [Online]. Available: www.sciencedaily.com/releases/2012/01/120112095853.htm [Accessed: 08-Nov-2017].

[2] D. Singh, F. Gu, J. D. Fieldhouse, N. Singh, and S. K. Singal, “Prediction and Analysis of Engine Friction Power of a Diesel Engine Influenced by Engine Speed, Load, and Lubricant Viscosity,” *Advances in Tribology*, 09-Dec-2014. [Online]. Available: https://www.hindawi.com/journals/at/2014/928015/. [Accessed: 09-Nov-2017].

[3] Hutchings, Shipway: *Tribology: Friction and Wear of Engineering Materials*

[4] Hanaor DA, Gan Y, Einav I (2015) *Contact mechanics of fractal surfaces by spline assisted discretisation*. Int J Solids Struct 59:121–131

[5] “Carpick Group Homepage,” *Carpick Research Group*. [Online]. Available: http://carpick.seas.upenn.edu/. [Accessed: 01-Nov-2017].

[6] Gosvami N. N., Bares J. A., Mangolini F., Konicek A. R.,Yablon D. G., and Carpick R. W. "Mechanisms of antiwear tribofilm growth revealed in situ by single-asperity sliding contacts,", Science, Published online 12 March 2015

[7] Konetschny C. “Tribology: Penn and ExxonMobil address long-standing mysteries behind anti-wear motor oil additive,” *Materialsgate*. [Online]. Available: https://www.materialsgate.de/en/mnews/68233/Tribology+Penn+and+ExxonMobil+address+long-standing+mysteries+behind+anti-wear+motor+oil+additive.html/. [Accessed: 02-Nov-2017].

[8] ASTM G133-05(2016) Standard Test Method for Linearly Reciprocating Ball-on-Flat Sliding Wear, ASTM International, West Conshohocken, PA, 2016, [Online]. Available: https://doi.org/10.1520/G0133-05R16 . [Accessed: 06-Nov-2017]

[9] ASTM G99-17 Standard Test Method for Wear Testing with a Pin-on-Disk Apparatus, ASTM International, West Conshohocken, PA, 2017, [Online]. Available: https://doi.org/10.1520/G0099-17. [Accessed: 06-Nov-2017]

[10] ASTM G115-10(2013) Standard Guide for Measuring and Reporting Friction Coefficients, ASTM International, West Conshohocken, PA, 2013, [Online]. Available: https://doi.org/10.1520/G0115 . [Accessed: 06-Nov-2017]

[11] “Standard Guide for Digital Data Acquisition in Wear and Friction Measurements,” *Scribd*. [Online]. Available: https://www.scribd.com/document/182764290/G-163. [Accessed: 06-Nov-2017].

[12] ASTM G194-08(2013) Standard Test Method for Measuring Rolling Friction Characteristics of a Spherical Shape on a Flat Horizontal Plane, ASTM International, West Conshohocken, PA, 2013,[Online]. Available: https://doi.org/10.1520/G0194 . [Accessed: 06-Nov-2017].

[13] “Piezoelectric Actuators: Components Technologies, Operation.” [Online]. Available: http://www.piezo.ws/pdf/Piezo.pdf. [Accessed: 03-Nov-2017].

[14] “4" Stroke 150lb Force Linear Actuator,” *RobotShop*. [Online]. Available: http://www.robotshop.com/en/firgelli-4-150lb-linea-actuator.html. [Accessed: 07-Nov-2017].

[15] “MLI3 NEMA 14 External Linear Programmable Motion Control IP20,” *Schneider Electric Motion USA*. [Online]. Available: https://motion.schneider-electric.com/mdriveplus/mli3-nema-14-linear-programmable-motion-control-ip20/#1521409510528-eb73afaf-1867. [Accessed: 30-Apr-2018].

[16] “User Interface Software,” *Schneider Electric Motion USA*. [Online]. Available: https://motion.schneider-electric.com/dloads/user-interface-software/. [Accessed: 30-Apr-2018].

[17]“How Is Temperature Affecting Your Strain Measurement Accuracy?,” 15-Mar-2016. [Online]. Available: http://www.ni.com/white-paper/3432/en/. [Accessed: 07-Nov-2017].

[18]“Guide to the Measurement of Force,” National Physical Laboratory, 2013. [Online]. Available: http://www.npl.co.uk/upload/pdf/forceguide.pdf. [Accessed: 07-Nov-2017].

[19]“Wheatstone Bridge,” Load Cell Manufacture. [Online]. Available: https://www.transducertechniques.com/wheatstone-bridge.aspx. [Accessed: 30-Apr-2018].

[20] K. Hoffmann, “Applying the Wheatstone Bridge Circuit,” hbm. [Online]. Available: http://eln.teilam.gr/sites/default/files/Wheatstone bridge.pdf. [Accessed: 30-Apr-2018].

[21] “The Carnegie Classification of Institutions of Higher Education ®,” *Carnegie Classifications | Listings*. [Online]. Available: http://carnegieclassifications.iu.edu/lookup/standard.php. [Accessed: 28-Apr-2018].

[22] Advanced Solutions International, Inc, *Home - Tribology and Lubrication Engineering Society | STLE*. [Online]. Available:

https://www.stle.org/files/Home/files/Default.aspx?hkey=d10dccd9-76c4-4b5d-9236-246b293d0be2. [Accessed: 28-Apr-2018].

11 Appendix

11.1 Engineering Drawings

446-01 MPS Weight
446-02 Micro Support Right
446-03 Micro Support Left
446-04 MPS Holder
446-05 I Beam
446-06 Long Leaf
446-07 Short Leaf
446-08 Leaf Connecter
446-09 Load Cube
446-10 Top Hub
446-11 Bottom Hub
446-12 Testing Base
446-13 Wire Port
446-14 Tubing Port
446-15 Full Assembly
446-16 Testing Base Assembly
446-17 Cantilever Assembly
446-18 MPS Assembly
446-19 Linear Motion Assembly

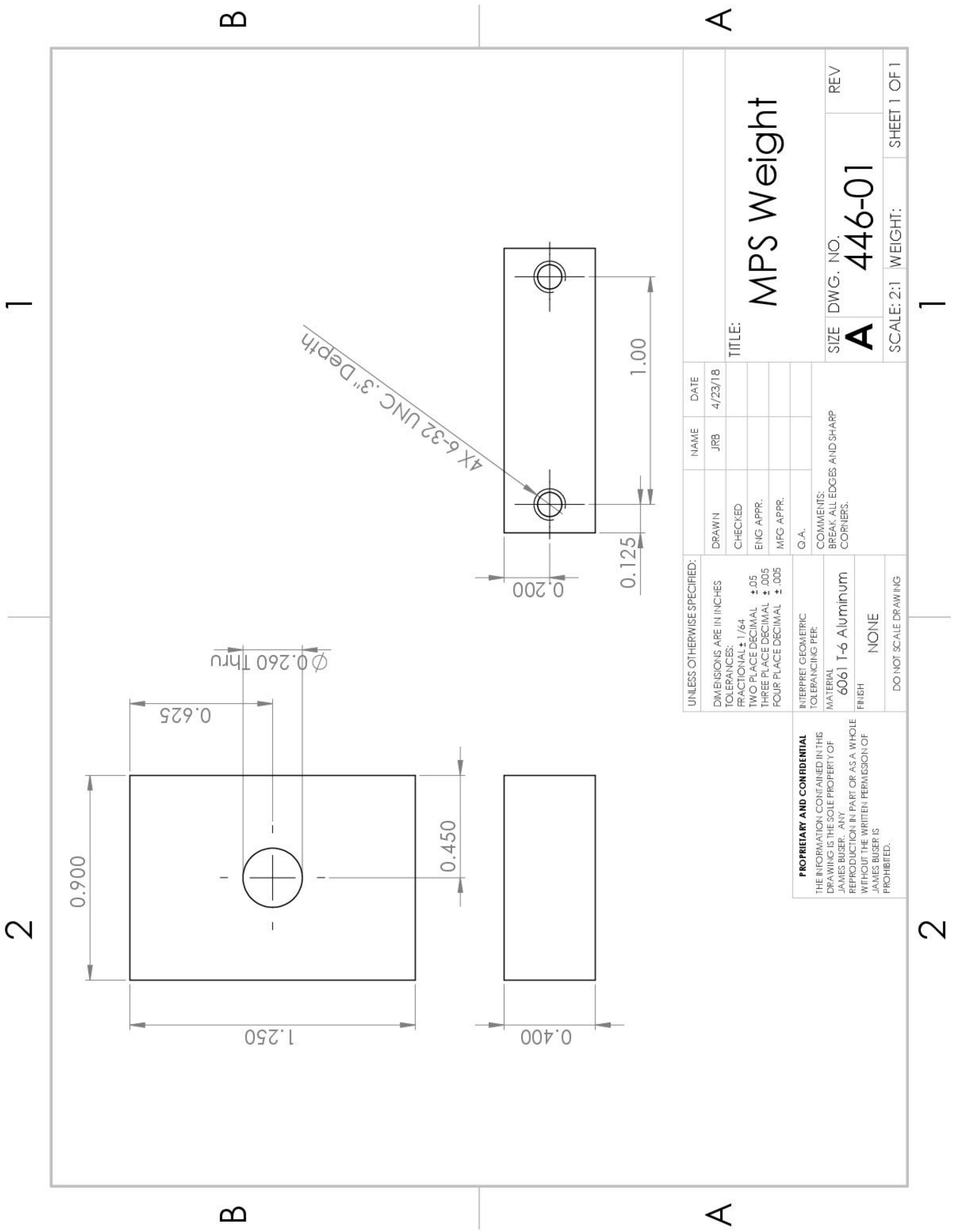

MPS Weight
TITLE:
SIZE A
DWG. NO. 446-01
REV
SCALE: 2:1
WEIGHT:
SHEET 1 OF 1
DRAWN JRB 4/23/18
NAME
DATE
CHECKED
ENG APPR.
MFG APPR.
Q.A.
COMMENTS: BREAK ALL EDGES AND SHARP CORNERS.
UNLESS OTHERWISE SPECIFIED:
DIMENSIONS ARE IN INCHES
TOLERANCES:
FRACTIONAL ± 1/64
TWO PLACE DECIMAL ± .05
THREE PLACE DECIMAL ± .005
FOUR PLACE DECIMAL ± .005
INTERPRET GEOMETRIC TOLERANCING PER:
MATERIAL
6061 T-6 Aluminum
FINISH
NONE
DO NOT SCALE DRAWING
PROPRIETARY AND CONFIDENTIAL
THE INFORMATION CONTAINED IN THIS DRAWING IS THE SOLE PROPERTY OF JAMES BUSER. ANY REPRODUCTION IN PART OR AS A WHOLE WITHOUT THE WRITTEN PERMISSION OF JAMES BUSER IS PROHIBITED.
4X 6-32 UNC .3" Depth
1.00
0.125
0.200
Ø0.260 Thru
0.625
0.900
0.450
1.250
0.400

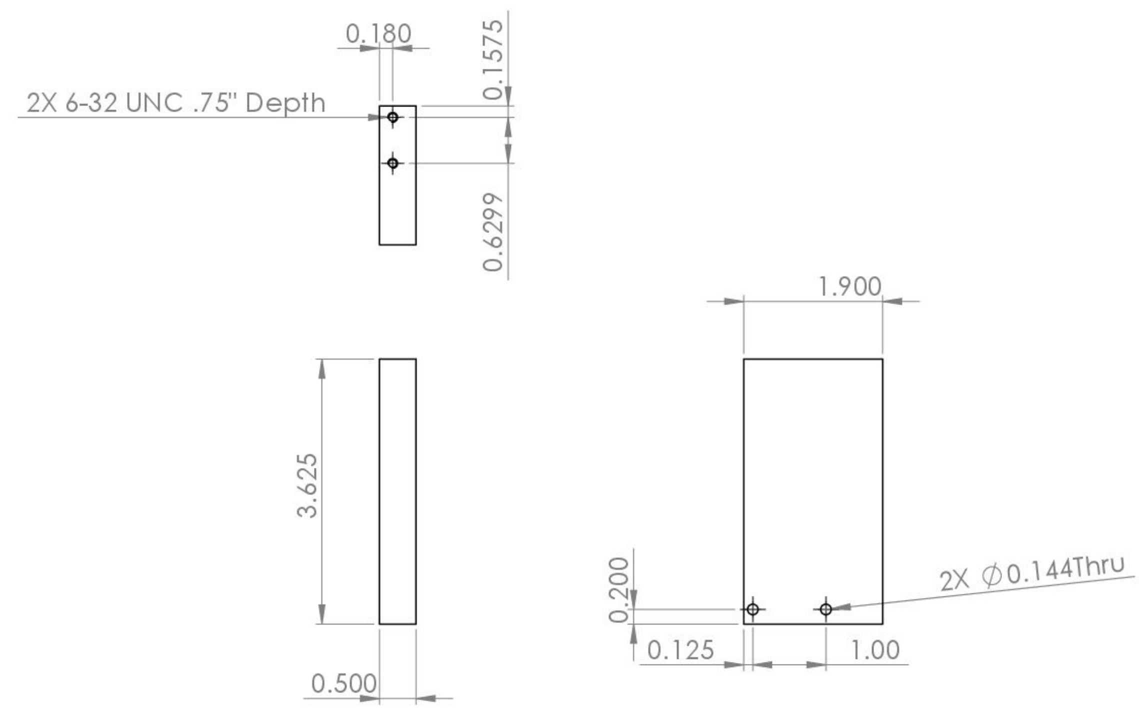

UNLESS OTHERWISE SPECIFIED:		NAME	DATE
DIMENSIONS ARE IN INCHES TOLERANCES: FRACTIONAL ± 1/64 TWO PLACE DECIMAL ± .05 THREE PLACE DECIMAL ± .005 FOUR PLACE DECIMAL ± .005	DRAWN	JRB	4/23/18
	CHECKED		
	ENG APPR.		
	MFG APPR.		
INTERPRET GEOMETRIC TOLERANCING PER:	Q.A.		
MATERIAL 6061 T-6 Aluminum	COMMENTS: BREAK ALL EDGES AND SHARP CORNERS.		
FINISH NONE			
DO NOT SCALE DRAWING			

PROPRIETARY AND CONFIDENTIAL

THE INFORMATION CONTAINED IN THIS DRAWING IS THE SOLE PROPERTY OF JAMES BUSER. ANY REPRODUCTION IN PART OR AS A WHOLE WITHOUT THE WRITTEN PERMISSION OF JAMES BUSER IS PROHIBITED.

TITLE:

Micro Support Right

SIZE	DWG. NO.	REV
A	446-02	
SCALE: 1:1	WEIGHT:	SHEET 1 OF 1

2 1 B A

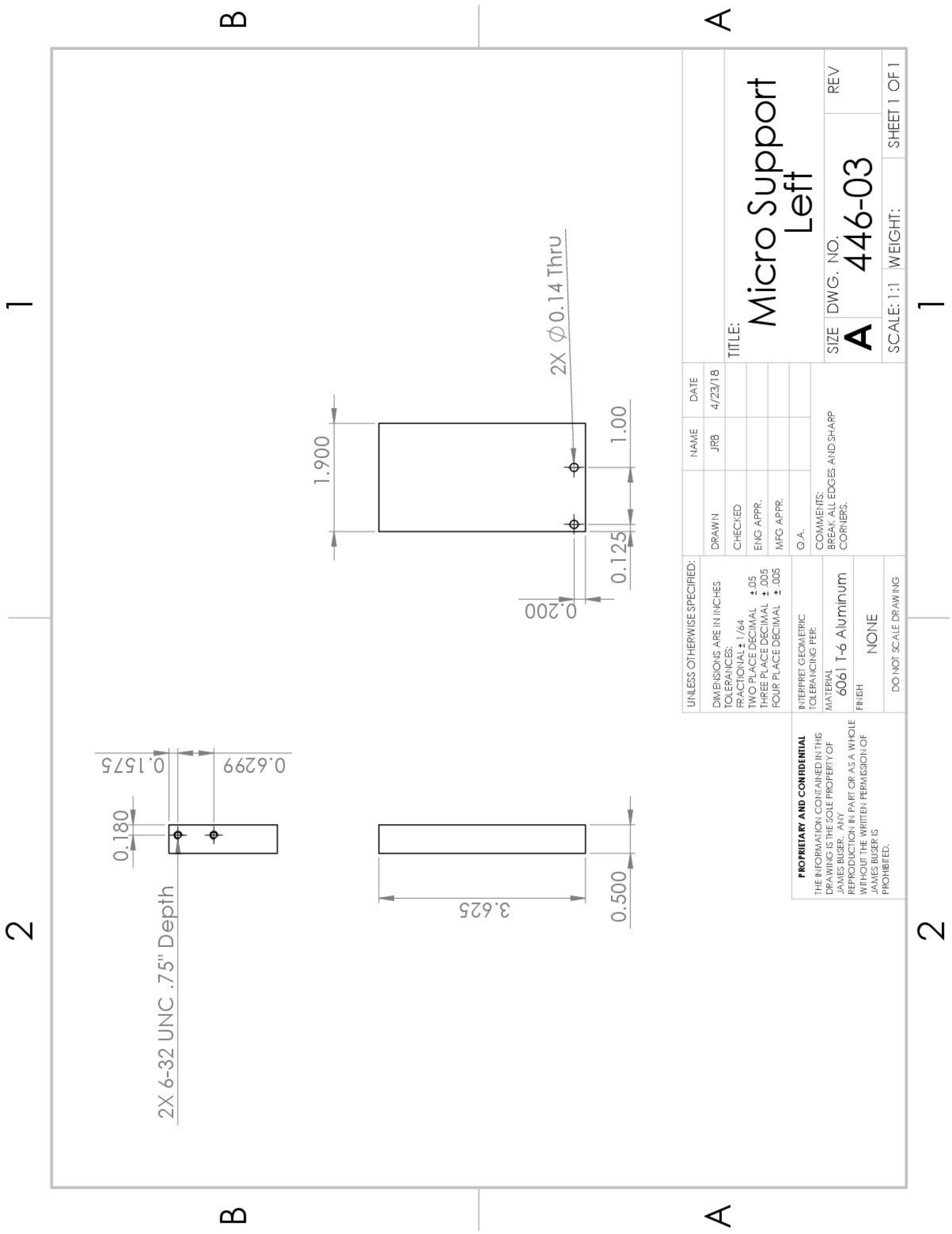
2X 6-32 UNC .75" Depth
0.180
0.1575
0.6299
3.625
0.500
1.900
0.200
0.125
1.00
2X ∅0.14 Thru
UNLESS OTHERWISE SPECIFIED:
DIMENSIONS ARE IN INCHES
TOLERANCES:
FRACTIONAL ± 1/64
TWO PLACE DECIMAL ± .05
THREE PLACE DECIMAL ± .005
FOUR PLACE DECIMAL ± .005
INTERPRET GEOMETRIC TOLERANCING PER:
MATERIAL
6061 T-6 Aluminum
FINISH
NONE
DO NOT SCALE DRAWING
PROPRIETARY AND CONFIDENTIAL
THE INFORMATION CONTAINED IN THIS DRAWING IS THE SOLE PROPERTY OF JAMES BUSER. ANY REPRODUCTION IN PART OR AS A WHOLE WITHOUT THE WRITTEN PERMISSION OF JAMES BUSER IS PROHIBITED.
NAME
DATE
DRAWN
JRB
4/23/18
CHECKED
ENG APPR.
MFG APPR.
Q.A.
COMMENTS:
BREAK ALL EDGES AND SHARP CORNERS.
TITLE:
Micro Support Left
SIZE
A
DWG. NO.
446-03
REV
SCALE: 1:1
WEIGHT:
SHEET 1 OF 1

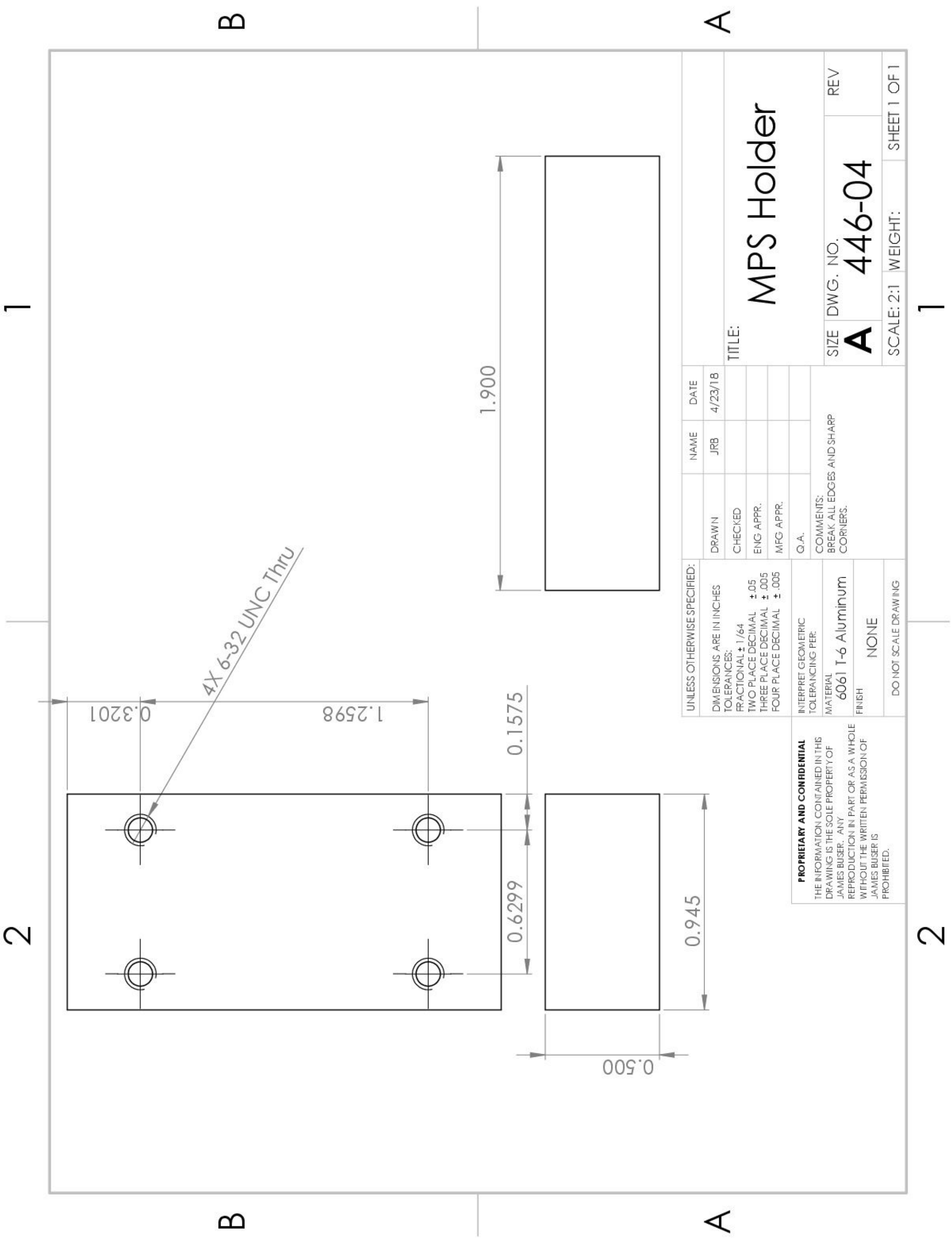
MPS Holder
446-04
4X 6-32 UNC Thru
1.900
0.3201
1.2598
0.1575
0.6299
0.945
0.500
UNLESS OTHERWISE SPECIFIED:
DIMENSIONS ARE IN INCHES
TOLERANCES:
FRACTIONAL ± 1/64
TWO PLACE DECIMAL ± .05
THREE PLACE DECIMAL ± .005
FOUR PLACE DECIMAL ± .005
INTERPRET GEOMETRIC TOLERANCING PER:
MATERIAL
6061 T-6 Aluminum
FINISH
NONE
DO NOT SCALE DRAWING
NAME
DATE
DRAWN
JRB
4/23/18
CHECKED
ENG APPR.
MFG APPR.
Q.A.
COMMENTS:
BREAK ALL EDGES AND SHARP CORNERS.
TITLE:
SIZE
A
DWG. NO.
REV
SCALE: 2:1
WEIGHT:
SHEET 1 OF 1
PROPRIETARY AND CONFIDENTIAL
THE INFORMATION CONTAINED IN THIS DRAWING IS THE SOLE PROPERTY OF JAMES BUSER. ANY REPRODUCTION IN PART OR AS A WHOLE WITHOUT THE WRITTEN PERMISSION OF JAMES BUSER IS PROHIBITED.
A
B
1
2

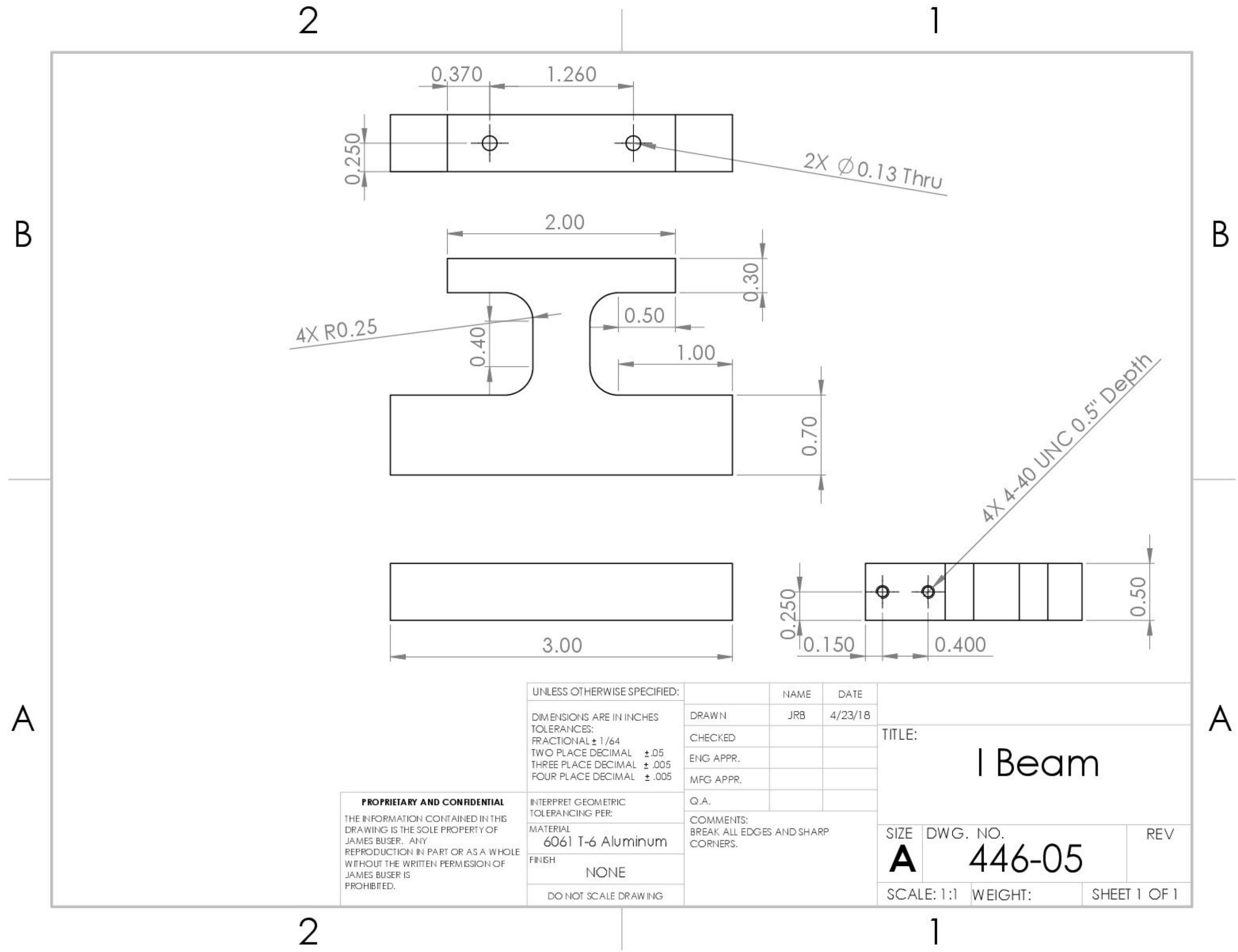

0.370
1.260
0.250
2X ∅0.13 Thru
2.00
0.30
4X R0.25
0.50
0.40
1.00
0.70
4X 4-40 UNC 0.5" Depth
3.00
0.250
0.150
0.400
0.50
UNLESS OTHERWISE SPECIFIED:
DIMENSIONS ARE IN INCHES
TOLERANCES:
FRACTIONAL ± 1/64
TWO PLACE DECIMAL ±.05
THREE PLACE DECIMAL ±.005
FOUR PLACE DECIMAL ±.005
INTERPRET GEOMETRIC TOLERANCING PER:
MATERIAL
6061 T-6 Aluminum
FINISH
NONE
DO NOT SCALE DRAWING
NAME
DATE
DRAWN
JRB
4/23/18
CHECKED
ENG APPR.
MFG APPR.
Q.A.
COMMENTS:
BREAK ALL EDGES AND SHARP CORNERS.
TITLE:
I Beam
SIZE
A
DWG. NO.
446-05
REV
SCALE: 1:1
WEIGHT:
SHEET 1 OF 1
PROPRIETARY AND CONFIDENTIAL
THE INFORMATION CONTAINED IN THIS DRAWING IS THE SOLE PROPERTY OF JAMES BUSER. ANY REPRODUCTION IN PART OR AS A WHOLE WITHOUT THE WRITTEN PERMISSION OF JAMES BUSER IS PROHIBITED.

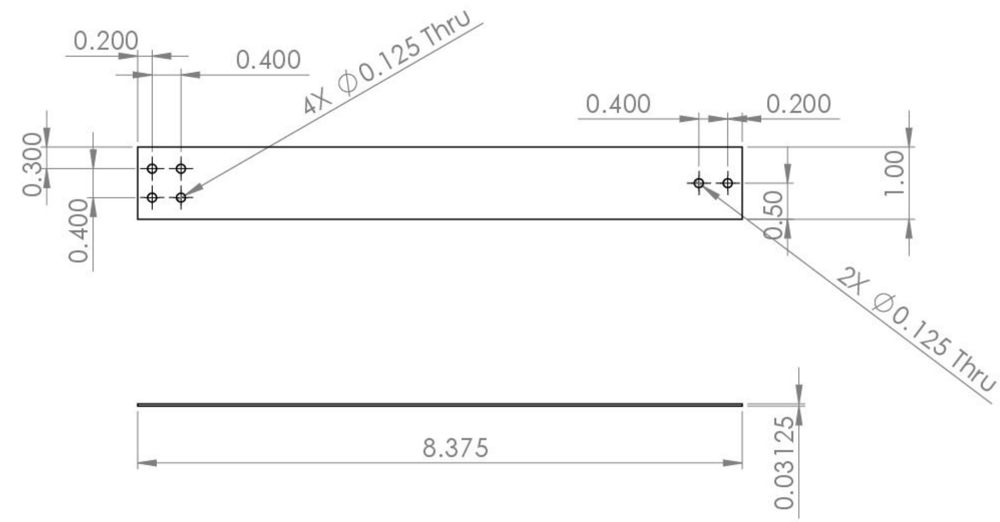

PROPRIETARY AND CONFIDENTIAL

THE INFORMATION CONTAINED IN THIS DRAWING IS THE SOLE PROPERTY OF JAMES BUSER. ANY REPRODUCTION IN PART OR AS A WHOLE WITHOUT THE WRITTEN PERMISSION OF JAMES BUSER IS PROHIBITED.

UNLESS OTHERWISE SPECIFIED:
DIMENSIONS ARE IN INCHES
TOLERANCES:
FRACTIONAL ± 1/64
TWO PLACE DECIMAL ± .05
THREE PLACE DECIMAL ± .005
FOUR PLACE DECIMAL ± .005

INTERPRET GEOMETRIC TOLERANCING PER:

MATERIAL
Spring Steel Shim Stock

FINISH
NONE

DO NOT SCALE DRAWING

	NAME	DATE
DRAWN	JRB	4/23/18
CHECKED		
ENG APPR.		
MFG APPR.		
Q.A.		

COMMENTS:
BREAK ALL EDGES AND SHARP CORNERS.

TITLE:
Long Leaf

SIZE	DWG. NO.	REV
A	446-06	

SCALE: 1:2 | WEIGHT: | SHEET 1 OF 1

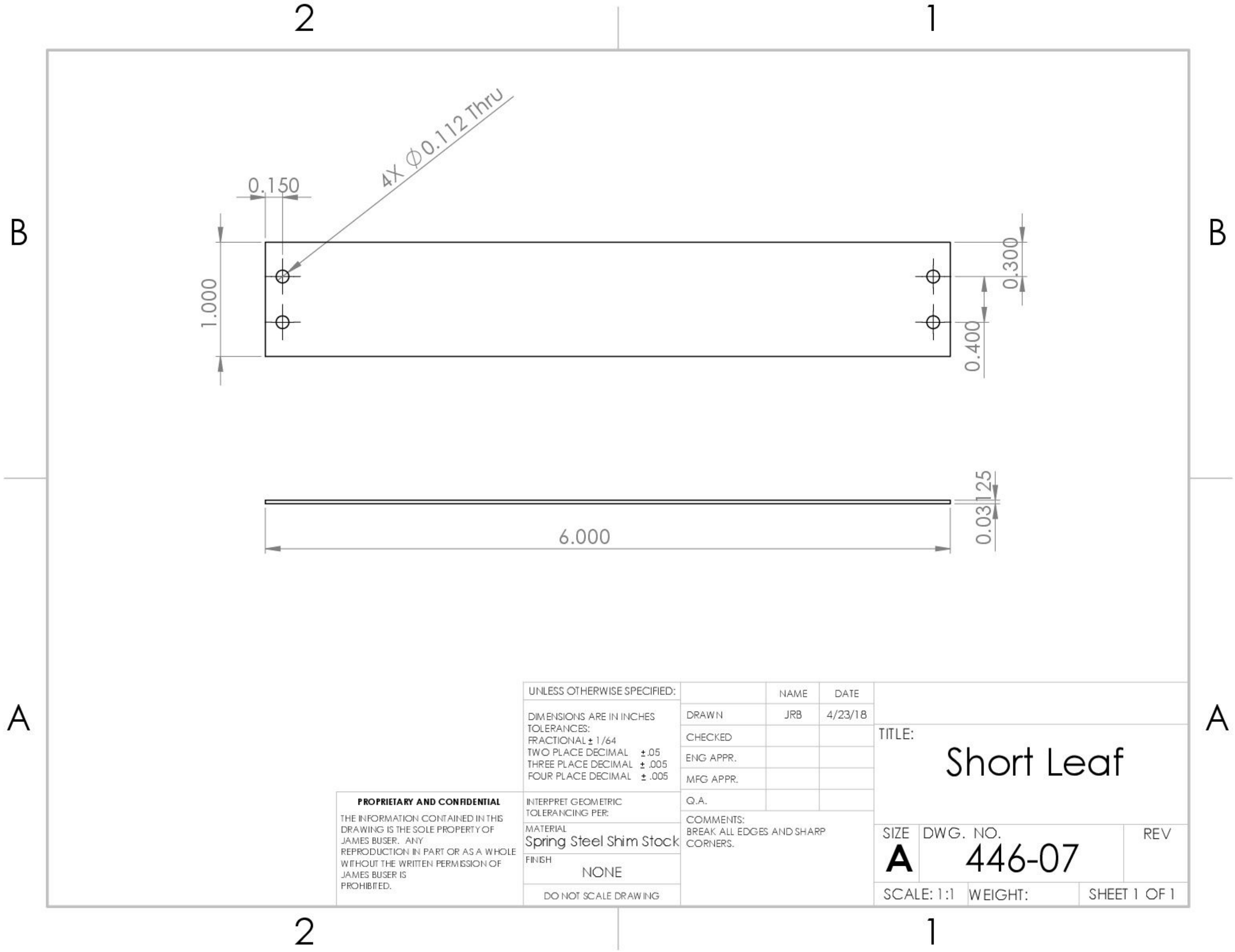
2
1
B
A
4X ⌀0.112 Thru
0.150
1.000
0.300
0.400
0.03125
6.000
UNLESS OTHERWISE SPECIFIED:
DIMENSIONS ARE IN INCHES
TOLERANCES:
FRACTIONAL ± 1/64
TWO PLACE DECIMAL ± .05
THREE PLACE DECIMAL ± .005
FOUR PLACE DECIMAL ± .005
INTERPRET GEOMETRIC TOLERANCING PER:
MATERIAL
Spring Steel Shim Stock
FINISH
NONE
DO NOT SCALE DRAWING
NAME
DATE
DRAWN
JRB
4/23/18
CHECKED
ENG APPR.
MFG APPR.
Q.A.
COMMENTS:
BREAK ALL EDGES AND SHARP CORNERS.
PROPRIETARY AND CONFIDENTIAL
THE INFORMATION CONTAINED IN THIS DRAWING IS THE SOLE PROPERTY OF JAMES BUSER. ANY REPRODUCTION IN PART OR AS A WHOLE WITHOUT THE WRITTEN PERMISSION OF JAMES BUSER IS PROHIBITED.
TITLE:
Short Leaf
SIZE
A
DWG. NO.
446-07
REV
SCALE: 1:1
WEIGHT:
SHEET 1 OF 1

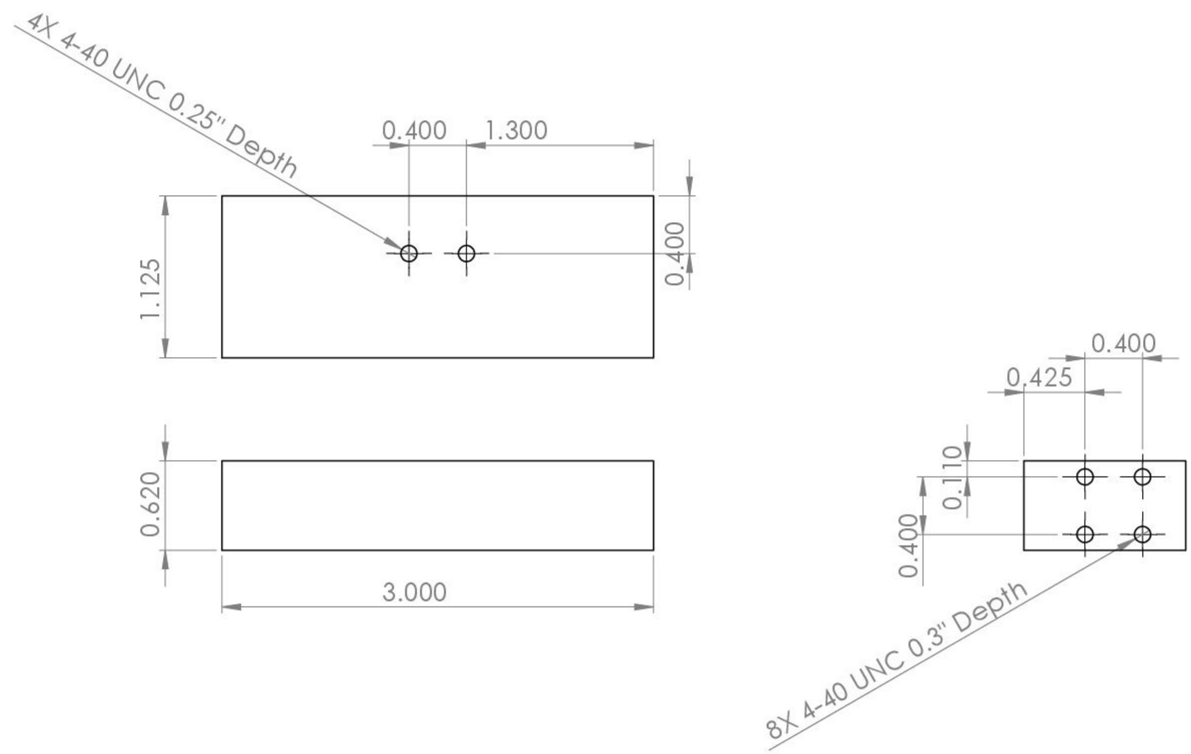

PROPRIETARY AND CONFIDENTIAL

THE INFORMATION CONTAINED IN THIS DRAWING IS THE SOLE PROPERTY OF JAMES BUSER. ANY REPRODUCTION IN PART OR AS A WHOLE WITHOUT THE WRITTEN PERMISSION OF JAMES BUSER IS PROHIBITED.

UNLESS OTHERWISE SPECIFIED:

DIMENSIONS ARE IN INCHES
TOLERANCES:
FRACTIONAL ± 1/64
TWO PLACE DECIMAL ±.05
THREE PLACE DECIMAL ±.005
FOUR PLACE DECIMAL ±.005

INTERPRET GEOMETRIC TOLERANCING PER:

MATERIAL
6061 Aluminum

FINISH
NONE

DO NOT SCALE DRAWING

	NAME	DATE
DRAWN	JRB	4/23/18
CHECKED		
ENG APPR.		
MFG APPR.		
Q.A.		

COMMENTS:
BREAK ALL EDGES AND SHARP CORNERS.

TITLE:
Leaf Connecter

SIZE	DWG. NO.	REV
A	446-08	

SCALE: 1:1 WEIGHT: SHEET 1 OF 1

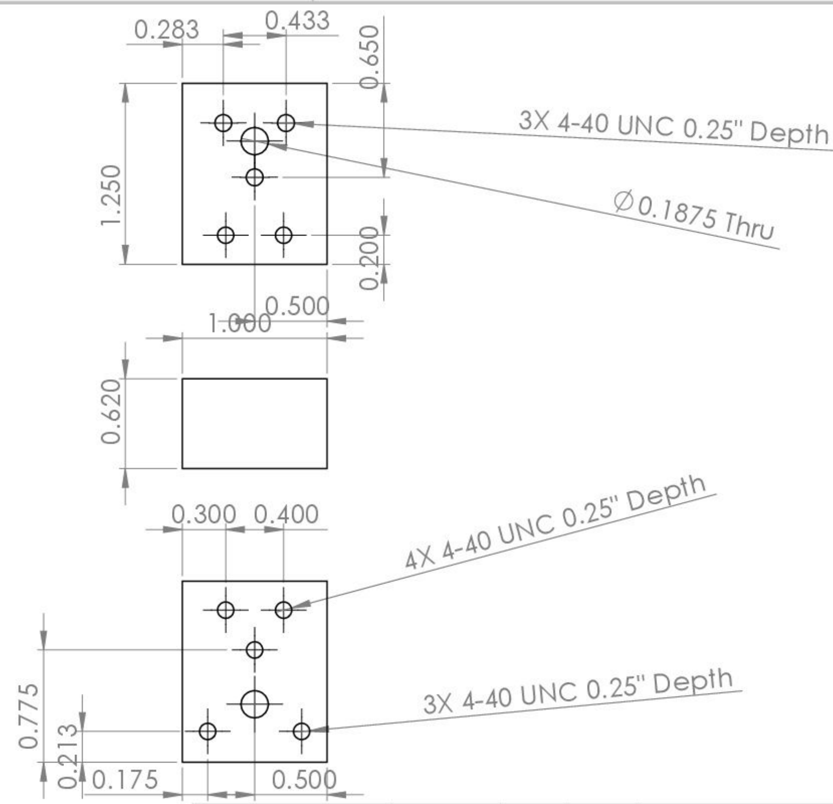

PROPRIETARY AND CONFIDENTIAL

THE INFORMATION CONTAINED IN THIS DRAWING IS THE SOLE PROPERTY OF JAMES BUSER. ANY REPRODUCTION IN PART OR AS A WHOLE WITHOUT THE WRITTEN PERMISSION OF JAMES BUSER IS PROHIBITED.

UNLESS OTHERWISE SPECIFIED:

DIMENSIONS ARE IN INCHES
TOLERANCES:
FRACTIONAL ± 1/64
TWO PLACE DECIMAL ±.05
THREE PLACE DECIMAL ±.005
FOUR PLACE DECIMAL ±.005

INTERPRET GEOMETRIC TOLERANCING PER:

MATERIAL
6061 Aluminum

FINISH
NONE

DO NOT SCALE DRAWING

	NAME	DATE
DRAWN	JRB	4/23/18
CHECKED		
ENG APPR.		
MFG APPR.		
Q.A.		

COMMENTS:
BREAK ALL EDGES AND SHARP CORNERS.

TITLE:

Load Cube

SIZE	DWG. NO.	REV
A	446-09	

SCALE: 1:1 WEIGHT: SHEET 1 OF 1

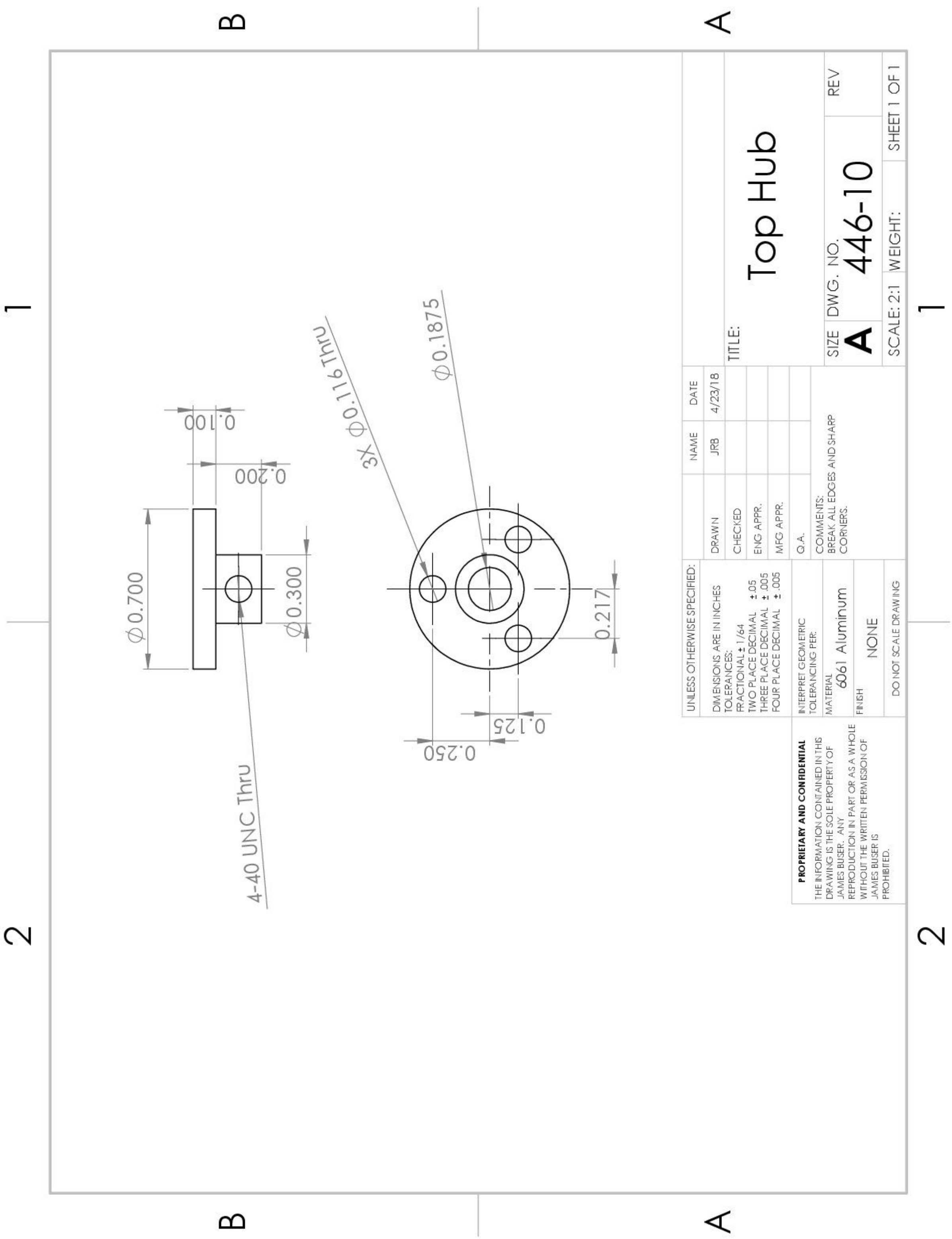
Ø0.700
0.100
0.200
Ø0.300
4-40 UNC Thru
3X Ø0.116 Thru
Ø0.1875
0.217
0.125
0.250
PROPRIETARY AND CONFIDENTIAL
THE INFORMATION CONTAINED IN THIS DRAWING IS THE SOLE PROPERTY OF JAMES BUSER. ANY REPRODUCTION IN PART OR AS A WHOLE WITHOUT THE WRITTEN PERMISSION OF JAMES BUSER IS PROHIBITED.
UNLESS OTHERWISE SPECIFIED:
DIMENSIONS ARE IN INCHES
TOLERANCES:
FRACTIONAL ± 1/64
TWO PLACE DECIMAL ±.05
THREE PLACE DECIMAL ±.005
FOUR PLACE DECIMAL ±.005
INTERPRET GEOMETRIC TOLERANCING PER:
MATERIAL
6061 Aluminum
FINISH
NONE
DO NOT SCALE DRAWING
NAME
DATE
DRAWN
JRB
4/23/18
CHECKED
ENG APPR.
MFG APPR.
Q.A.
COMMENTS:
BREAK ALL EDGES AND SHARP CORNERS.
TITLE:
Top Hub
SIZE
A
DWG. NO.
446-10
REV
SCALE: 2:1
WEIGHT:
SHEET 1 OF 1
A
B
1
2

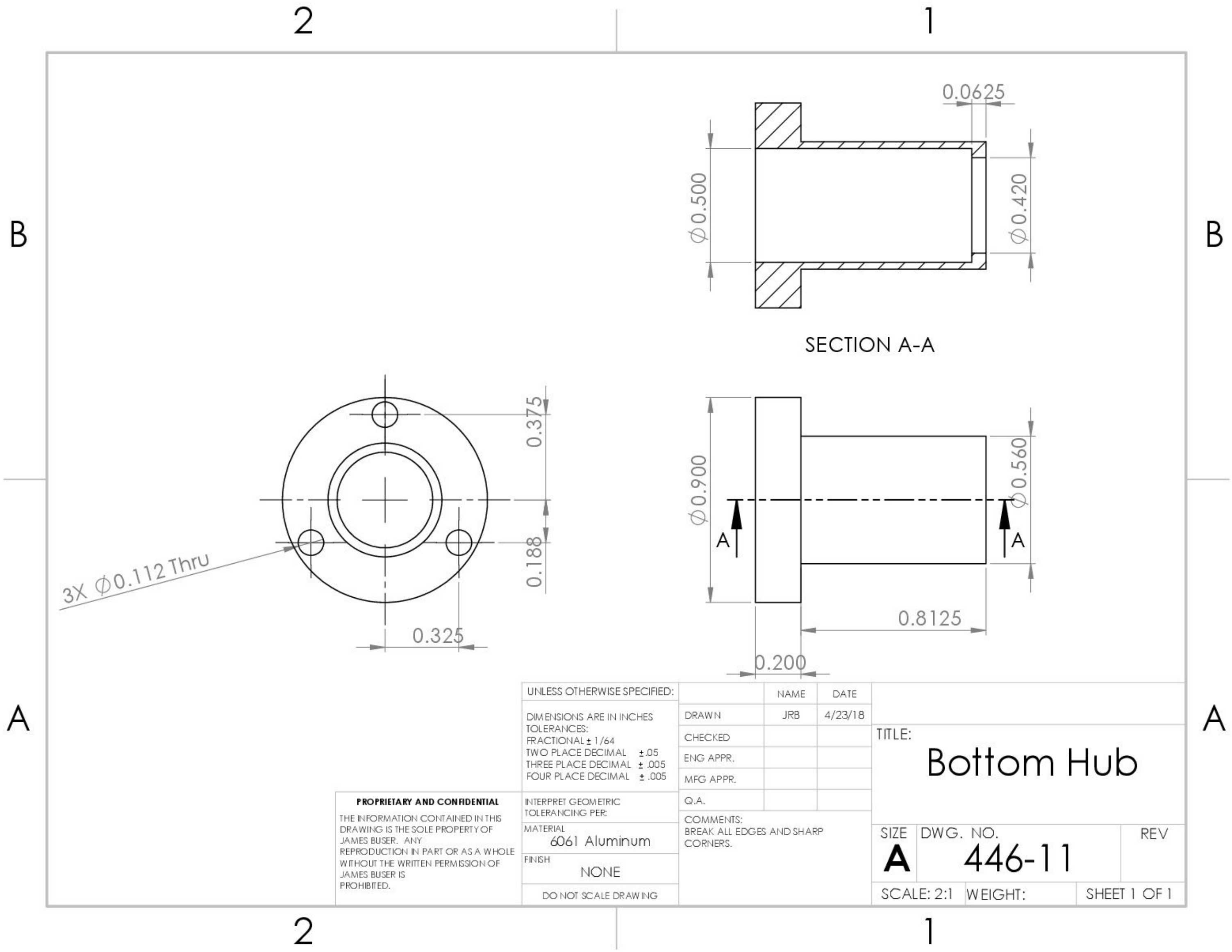
2
1
B
A
0.0625
⌀0.500
⌀0.420
SECTION A-A
0.375
0.188
3X ⌀0.112 Thru
0.325
⌀0.900
⌀0.560
A
A
0.8125
0.200
UNLESS OTHERWISE SPECIFIED:
DIMENSIONS ARE IN INCHES
TOLERANCES:
FRACTIONAL ± 1/64
TWO PLACE DECIMAL ±.05
THREE PLACE DECIMAL ±.005
FOUR PLACE DECIMAL ±.005
NAME
DATE
DRAWN
JRB
4/23/18
CHECKED
ENG APPR.
MFG APPR.
Q.A.
COMMENTS:
BREAK ALL EDGES AND SHARP CORNERS.
TITLE:
Bottom Hub
PROPRIETARY AND CONFIDENTIAL
THE INFORMATION CONTAINED IN THIS DRAWING IS THE SOLE PROPERTY OF JAMES BUSER. ANY REPRODUCTION IN PART OR AS A WHOLE WITHOUT THE WRITTEN PERMISSION OF JAMES BUSER IS PROHIBITED.
INTERPRET GEOMETRIC TOLERANCING PER:
MATERIAL
6061 Aluminum
FINISH
NONE
DO NOT SCALE DRAWING
SIZE
A
DWG. NO.
446-11
REV
SCALE: 2:1
WEIGHT:
SHEET 1 OF 1

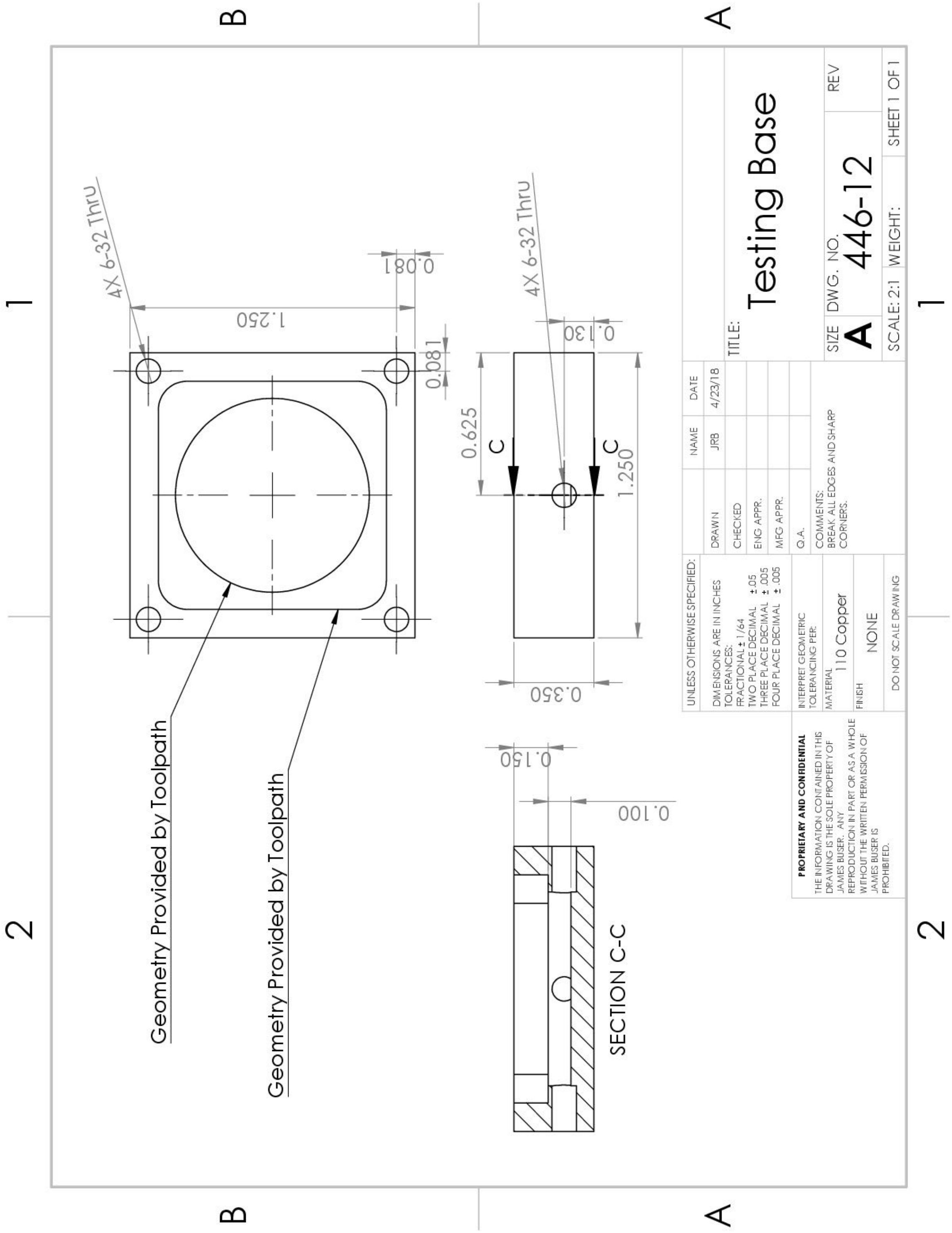

Testing Base
DWG. NO. 446-12
SIZE A
REV
SCALE: 2:1
WEIGHT:
SHEET 1 OF 1
TITLE:
4X 6-32 Thru
4X 6-32 Thru
1.250
0.081
0.081
0.130
0.625
1.250
0.350
0.150
0.100
C
C
SECTION C-C
Geometry Provided by Toolpath
Geometry Provided by Toolpath
UNLESS OTHERWISE SPECIFIED:
DIMENSIONS ARE IN INCHES
TOLERANCES:
FRACTIONAL ± 1/64
TWO PLACE DECIMAL ±.05
THREE PLACE DECIMAL ±.005
FOUR PLACE DECIMAL ±.005
INTERPRET GEOMETRIC TOLERANCING PER:
MATERIAL
110 Copper
FINISH
NONE
DO NOT SCALE DRAWING
NAME
DATE
DRAWN
JRB
4/23/18
CHECKED
ENG APPR.
MFG APPR.
Q.A.
COMMENTS:
BREAK ALL EDGES AND SHARP CORNERS.
PROPRIETARY AND CONFIDENTIAL
THE INFORMATION CONTAINED IN THIS DRAWING IS THE SOLE PROPERTY OF JAMES BUSER. ANY REPRODUCTION IN PART OR AS A WHOLE WITHOUT THE WRITTEN PERMISSION OF JAMES BUSER IS PROHIBITED.

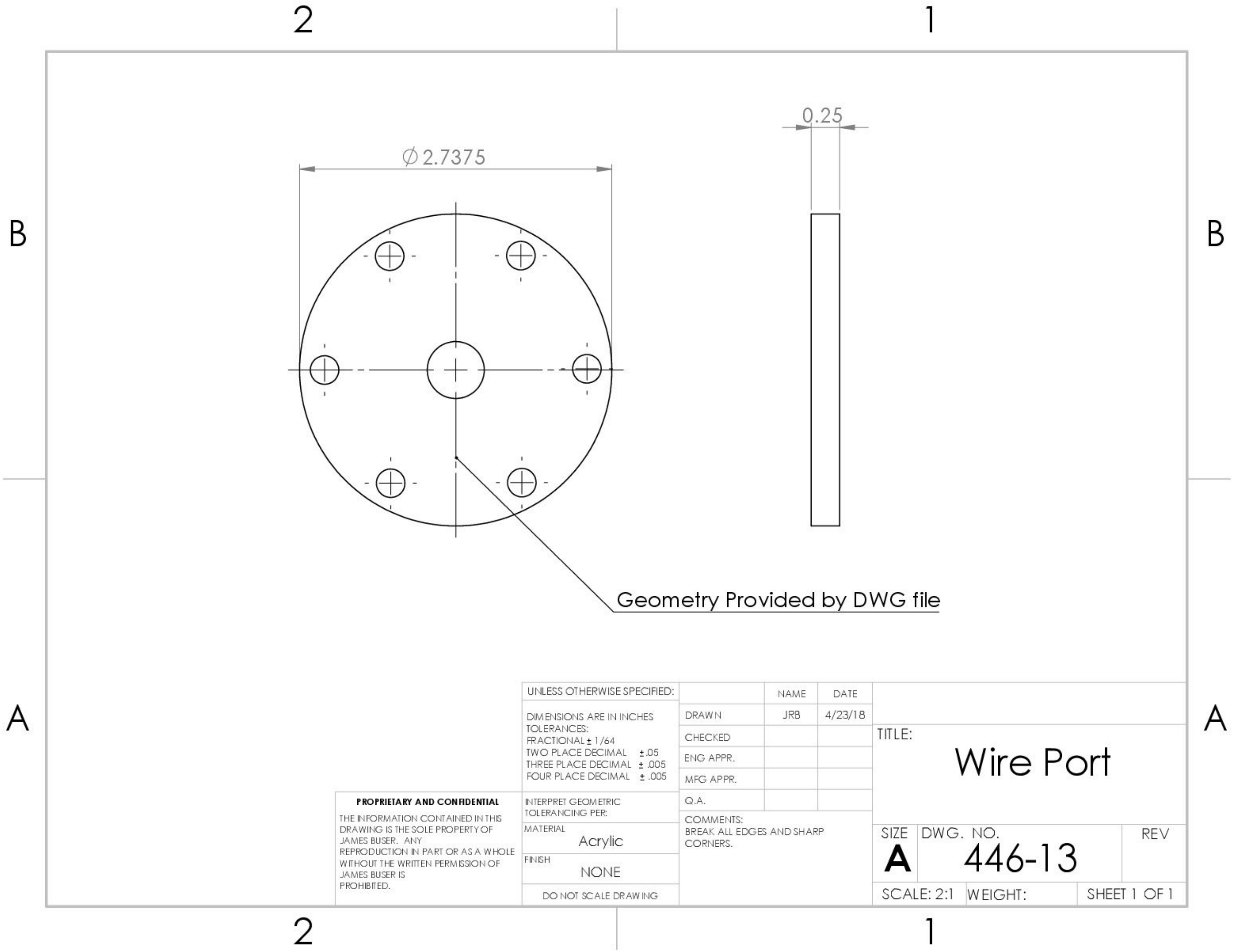
⌀2.7375
0.25
Geometry Provided by DWG file
UNLESS OTHERWISE SPECIFIED:
DIMENSIONS ARE IN INCHES
TOLERANCES:
FRACTIONAL ± 1/64
TWO PLACE DECIMAL ±.05
THREE PLACE DECIMAL ±.005
FOUR PLACE DECIMAL ±.005
INTERPRET GEOMETRIC TOLERANCING PER:
MATERIAL Acrylic
FINISH NONE
DO NOT SCALE DRAWING
NAME DATE
DRAWN JRB 4/23/18
CHECKED
ENG APPR.
MFG APPR.
Q.A.
COMMENTS: BREAK ALL EDGES AND SHARP CORNERS.
TITLE: Wire Port
SIZE A
DWG. NO. 446-13
REV
SCALE: 2:1
WEIGHT:
SHEET 1 OF 1
PROPRIETARY AND CONFIDENTIAL
THE INFORMATION CONTAINED IN THIS DRAWING IS THE SOLE PROPERTY OF JAMES BUSER. ANY REPRODUCTION IN PART OR AS A WHOLE WITHOUT THE WRITTEN PERMISSION OF JAMES BUSER IS PROHIBITED.

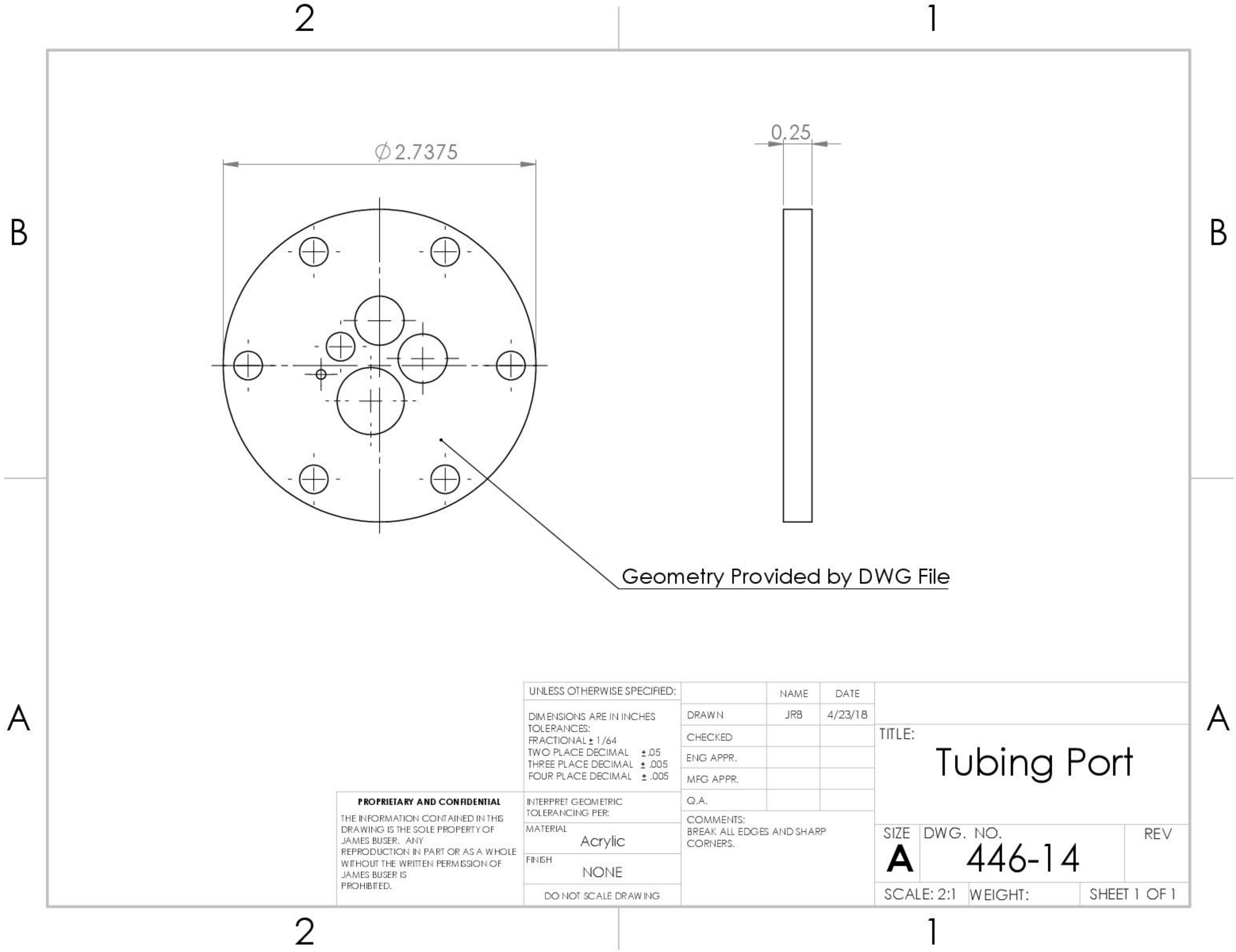

Ø2.7375
0.25
Geometry Provided by DWG File
UNLESS OTHERWISE SPECIFIED:
DIMENSIONS ARE IN INCHES
TOLERANCES:
FRACTIONAL ± 1/64
TWO PLACE DECIMAL ±.05
THREE PLACE DECIMAL ±.005
FOUR PLACE DECIMAL ±.005
NAME
DATE
DRAWN
JRB
4/23/18
CHECKED
ENG APPR.
MFG APPR.
Q.A.
COMMENTS:
BREAK ALL EDGES AND SHARP CORNERS.
INTERPRET GEOMETRIC TOLERANCING PER:
MATERIAL
Acrylic
FINISH
NONE
DO NOT SCALE DRAWING
PROPRIETARY AND CONFIDENTIAL
THE INFORMATION CONTAINED IN THIS DRAWING IS THE SOLE PROPERTY OF JAMES BUSER. ANY REPRODUCTION IN PART OR AS A WHOLE WITHOUT THE WRITTEN PERMISSION OF JAMES BUSER IS PROHIBITED.
TITLE:
Tubing Port
SIZE
A
DWG. NO.
446-14
REV
SCALE: 2:1
WEIGHT:
SHEET 1 OF 1

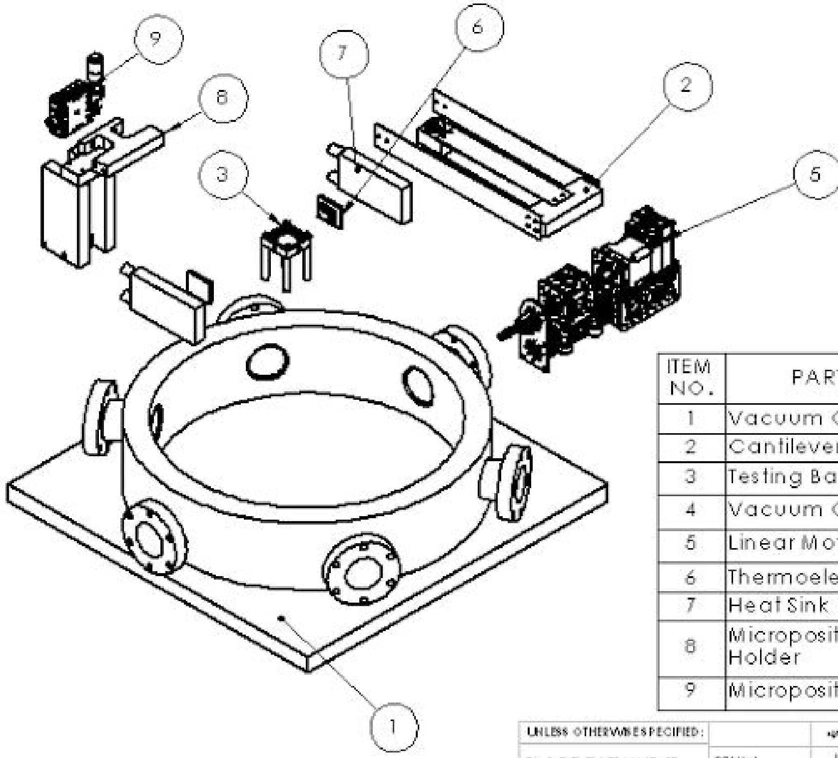

ITEM NO.	PART NUMBER	DESCRIPTION	QTY.
1	Vacuum Chamber Base		1
2	Cantilever		1
3	Testing Base		1
4	Vacuum Chamber Top		1
5	Linear Motion Stage		1
6	Thermoelectric		2
7	Heat Sink		2
8	Micropositioning Stage Holder		1
9	Micropositon Stage		1

	NAME	DATE
DRAWN	JRB	4/30/18
CHECKED		
ENG APPR.		
MFG APPR.		
Q.A.		
COMMENTS:		

UNLESS OTHERWISE SPECIFIED:
DIMENSIONS ARE IN INCHES
TOLERANCES:
FRACTIONAL ±
ANGULAR: MACH ± BEND ±
TWO PLACE DECIMAL ±
THREE PLACE DECIMAL ±
INTERPRET GEOMETRIC TOLERANCING PER:
MATERIAL
FINISH
James Buser
DO NOT SCALE DRAWING

NEXT ASSY | USED ON
APPLICATION

TITLE:
Full Assembly

SIZE A | DWG. NO. 446-15 | REV
SCALE: 1:12 | WEIGHT: | SHEET 1 OF 1

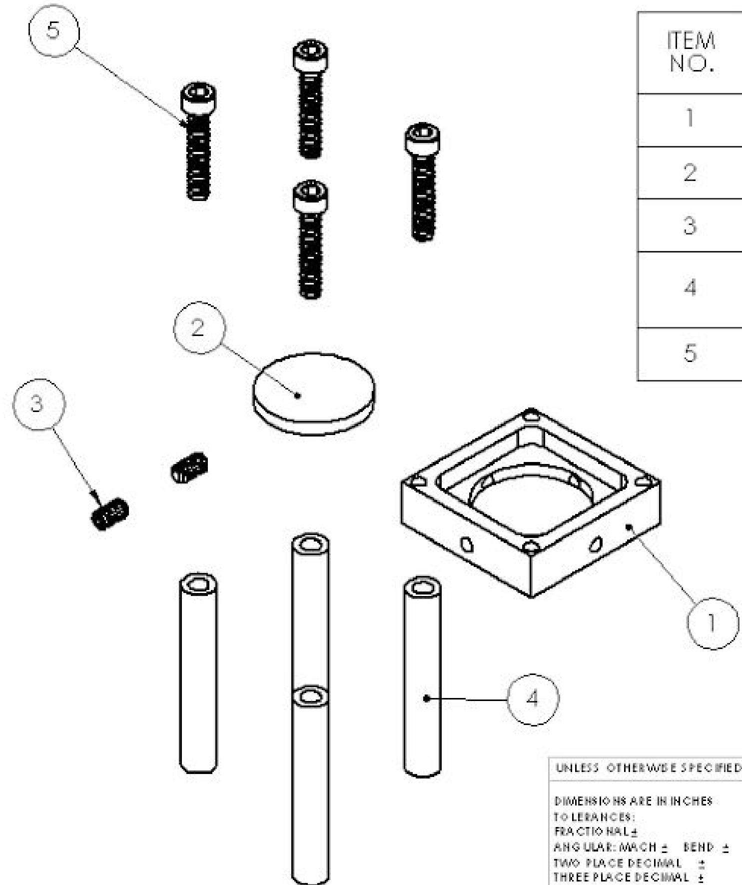

ITEM NO.	PART NUMBER	DESCRIPTION	QTY.
1	Testing Base		1
2	Tab		1
3	6-32 Set Screws		2
4	Ceramic Spacers		4
5	6-32 3/4" Screws		4

	NAME	DATE
DRAWN	JRB	4/30/18
CHECKED		
ENG APPR.		
MFG APPR.		
Q.A.		

COMMENTS:

UNLESS OTHERWISE SPECIFIED:
DIMENSIONS ARE IN INCHES
TOLERANCES:
FRACTIONAL ±
ANGULAR: MACH ± BEND ±
TWO PLACE DECIMAL ±
THREE PLACE DECIMAL ±

INTERPRET GEOMETRIC TOLERANCING PER:
MATERIAL
FINISH James Buser
DO NOT SCALE DRAWING

NEXT ASSY | USED ON
APPLICATION

PROPRIETARY AND CONFIDENTIAL
THE INFORMATION CONTAINED IN THIS DRAWING IS THE SOLE PROPERTY OF <INSERT COMPANY NAME HERE>. ANY REPRODUCTION IN PART OR AS A WHOLE WITHOUT THE WRITTEN PERMISSION OF <INSERT COMPANY NAME HERE> IS PROHIBITED.

TITLE:
Testing Base Assembly

SIZE A | DWG. NO. 446-16 | REV

SCALE: 1:2 | WEIGHT: | SHEET 1 OF 1

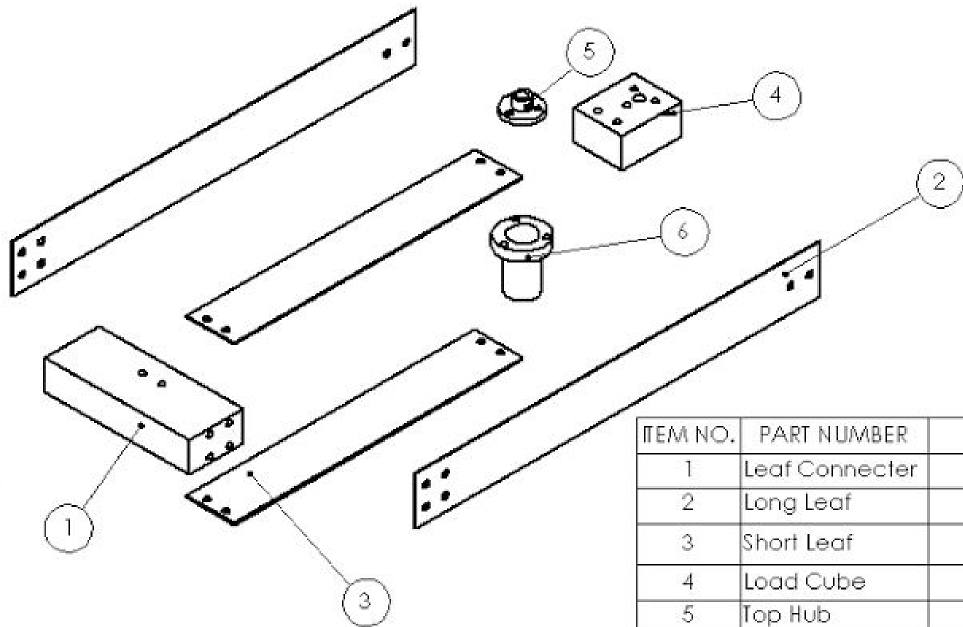

ITEM NO.	PART NUMBER	DESCRIPTION	QTY.
1	Leaf Connecter		1
2	Long Leaf		2
3	Short Leaf		2
4	Load Cube		1
5	Top Hub		1
6	Bottom hub		1

UNLESS OTHERWISE SPECIFIED:

DIMENSIONS ARE IN INCHES
TOLERANCES:
FRACTIONAL ±
ANGULAR: MACH ± BEND ±
TWO PLACE DECIMAL ±
THREE PLACE DECIMAL ±

INTERPRET GEOMETRIC TOLERANCING PER:

MATERIAL

FINISH James Buser

DO NOT SCALE DRAWING

	NAME	DATE
DRAWN	JRB	4/30/18
CHECKED		
ENG APPR.		
MFG APPR.		
Q.A.		
COMMENTS:		

TITLE:

Cantilever Assembly

SIZE A DWG. NO. 446-17 REV

SCALE: 1:4 WEIGHT: SHEET 1 OF 1

NEXT ASSY USED ON
APPLICATION

PROPRIETARY AND CONFIDENTIAL
THE INFORMATION CONTAINED IN THIS DRAWING IS THE SOLE PROPERTY OF <INSERT COMPANY NAME HERE>. ANY REPRODUCTION IN PART OR AS A WHOLE WITHOUT THE WRITTEN PERMISSION OF <INSERT COMPANY NAME HERE> IS PROHIBITED.

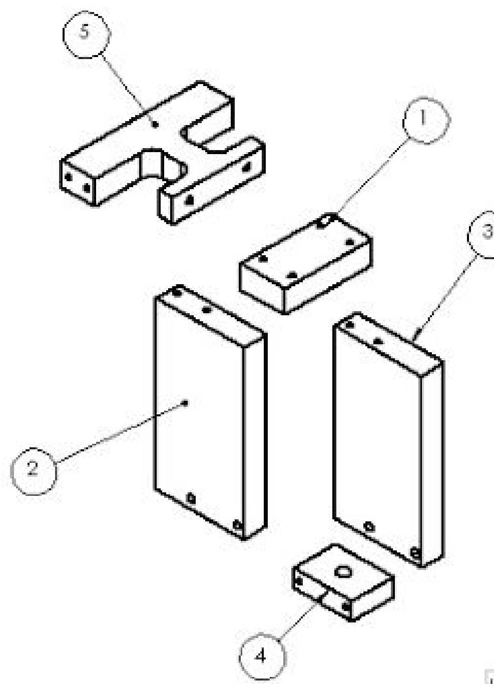

ITEM NO.	PART NUMBER	DESCRIPTION	QTY.
1	MPS Holder		1
2	Micro Support Left		1
3	Micro Support Right		1
4	MPS Weight		1
5	I Beam		1

DRAWN JRB 4/30/18

FINISH James Buser

TITLE: MPS Assembly

SIZE A DWG. NO. 446-18 REV

SCALE: 1:4 WEIGHT: SHEET 1 OF 1

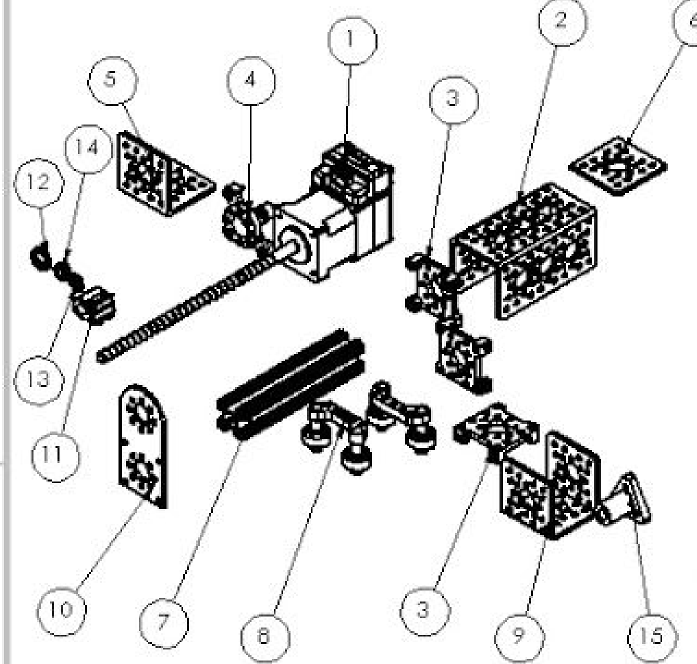

ITEM NO.	PART NUMBER	DESCRIPTION	QTY.
1	MDrive14		1
2	Motor Stand		1
3	Side Mount		3
4	Motor Mount		1
5	L-Shaped Pattern Bracket		1
6	Square Bracket		1
7	X-Rail		1
8	V-Wheel		2
9	Carriage Bracket		1
10	Shaft Bracket		1
11	Shaft Coupler		1
12	Shaft Collar		1
13	Spacer		1
14	Shaft Bearing		1
15	Anti-backlash Nut		1

	NAME	DATE
DRAWN	JFB	4/30/18
CHECKED		
ENG APPR.		
MFG APPR.		
Q.A.		
COMMENTS:		

UNLESS OTHERWISE SPECIFIED: DIMENSIONS ARE IN INCHES TOLERANCES: FRACTIONAL ± ANGULAR: MACH ± BEND ± TWO PLACE DECIMAL ± THREE PLACE DECIMAL ±

INTERPRET GEOMETRIC TOLERANCING PER:

MATERIAL

FINISH James Buser

DO NOT SCALE DRAWING

NEXT ASSY | USED ON

APPLICATION

PROPRIETARY AND CONFIDENTIAL

TITLE: Linear Motion Assembly

SIZE A | DWG. NO. 446-19 | REV

SCALE: 1:8 | WEIGHT: | SHEET 1 OF 1

11.2 Additional Appendix Items

All Purchases

Date	Item	Category	Quantity	Price	Total Price
11/10/2017	304 Stainless Steel Sheet, 6" x 6", 3/8 Thick	Stock materials	1	$22.96	$22.96
11/10/2017	Hardened Impact-Resistant S2 Tool Steel Balls	Stock materials	1	$9.63	$9.63
11/10/2017	6061 Aluminum 5/8" Thick, 2" x 48"	Stock materials	1	$42.39	$42.39
11/19/2017	SunFounder Metal Gear Digital RC Servo Motor	Motor	2	$11.99	$23.98
11/21/2017	Marlow Industries SP2402-01AB Thermoelectric Module	Thermoelectrics	1	$241.05	$241.05
11/28/2017	T5 Series Dust-Free Timing Belt	Linear Track Parts	1	$5.79	$5.79
11/28/2017	Dry-Running Mounted Sleeve Bearings for Extreme Misalignment	Linear Track Parts	6	$4.42	$26.52
11/28/2017	Linear Motion Shaft	Linear Track Parts	2	$5.93	$11.86
11/28/2017	T5 Series Timing Belt Pulley	Linear Track Parts	2	$9.46	$18.92
11/29/2017	Elegoo UNO R3 Board ATmega328P ATMEGA16U2 with USB Cable for Arduino	Arduino Board	1	$10.90	$10.90
1/16/2018	110 Copper Sheet, 6" x 6" x 5/8"	Stock materials	1	$115.61	$115.61
1/19/2018	Metal Ceramic Heater, 10x10x1.2mm, 10ohm	General temperature materials	1	$16.70	$16.70
1/22/2018	Omega CN32PT-330 Temperature Controller	Temperature controllers	1	$220.00	$220.00
1/22/2018	Honeywell HEL-705-U-1-12-00 RTD Sensor	General temperature materials	1	$25.42	$25.42
1/24/2018	Aluminum Water Cooling Blocks 40x120x12mm	General temperature materials	3	$14.98	$44.94
1/24/2018	10ft Vinyl Tubing 5/16 ID	General temperature materials	1	$4.00	$4.00
1/24/2018	145 GPH Maxesla Submersible Pump	General temperature materials	1	$9.99	$9.99
1/24/2018	Qunqi NEMA17 Stepper Motor bipolar 4 leads 40mm 1.5A 39Ncm	Motor	1	$12.99	$12.99
1/24/2018	Qunqi L298N Motor Drive Controller Board Module Dual H Bridge DC Stepper For Arduino	Motor	1	$6.89	$6.89
2/5/2018	Spring Steel Shim Stock	Stock materials	1	$23.33	$23.33
2/5/2018	Marlow Industries SP2402-01AB Thermoelectric Module	Thermoelectrics	2	$241.05	$482.10
2/6/2018	Arctic Silver 5 AS5-3.5G Thermal Paste	General temperature materials	1	$6.79	$6.79
2/6/2018	6 in Tekton Ratchet Bar Clamp	General temperature materials	2	$5.51	$11.02
2/15/2018	Halnziye 10g Thermal Adhesive	General temperature materials	1	$7.98	$7.98
2/21/2018	10ft Cablera Power Cord Extension	General temperature materials	1	$10.11	$10.11
2/21/2018	10 pcs 3.15A 250 V Glass Fuses 20 x 5mm	General temperature materials	1	$6.39	$6.39
2/21/2018	5 pcs Screw Cap 5 x 20mm Fuse Holder	General temperature materials	1	$5.44	$5.44
2/21/2018	Siemens SPDT Relay 3A 120VAC	General temperature materials	1	$11.82	$11.82
2/22/2018	AluminumWater Cooling Blocks 40x80	General temperature materials	2	$13.98	$27.96
2/28/2018	TADC 401 - SZ	Micropositioning stage	1	$320.00	$320.00
2/28/2018	Spring Steel Shim Stock (1/32")	Stock materials	1	$23.33	$23.33
2/28/2018	Spring Steel Shim Stock (1/40")	Stock materials	1	$21.53	$21.53
3/12/2018	Servocity Order #1	Linear Track Parts	1	$48.35	$48.35
3/13/2018	Servocity Order #2	Linear Track Parts	1	$44.07	$44.07
3/15/2018	Strain Gauges	Strain Gauges	10	$6.00	$60.00
3/19/2018	Screws for micropositioning stage	Micropositioning stage	1	$49.24	$49.24
3/21/2018	Servocity Order #3	Linear Track Parts	1	$42.46	$42.46
3/28/2018	25A 3-32V DC Solid State Relay and Heat Sink	General temperature materials	1	$8.99	$8.99
3/28/2018	Kapton high temperature tape	General temperature materials	1	$6.78	$6.78
4/2/2018	L5 Ceramic spacers 1/4" OD	General temperature materials	4	$6.07	$24.28
4/3/2018	Strain Gauge Adhesive	Strain Gauges	1	$150.00	$150.00
4/5/2018	Strain Gauges	Strain Gauges	10	$6.00	$60.00
4/10/2018	ET Series Laird thermoelectrics	Thermoelectrics	2	$24.43	$48.86
4/10/2018	40x40mm Water cooling heat sinks	General temperature materials	2	$7.99	$15.98

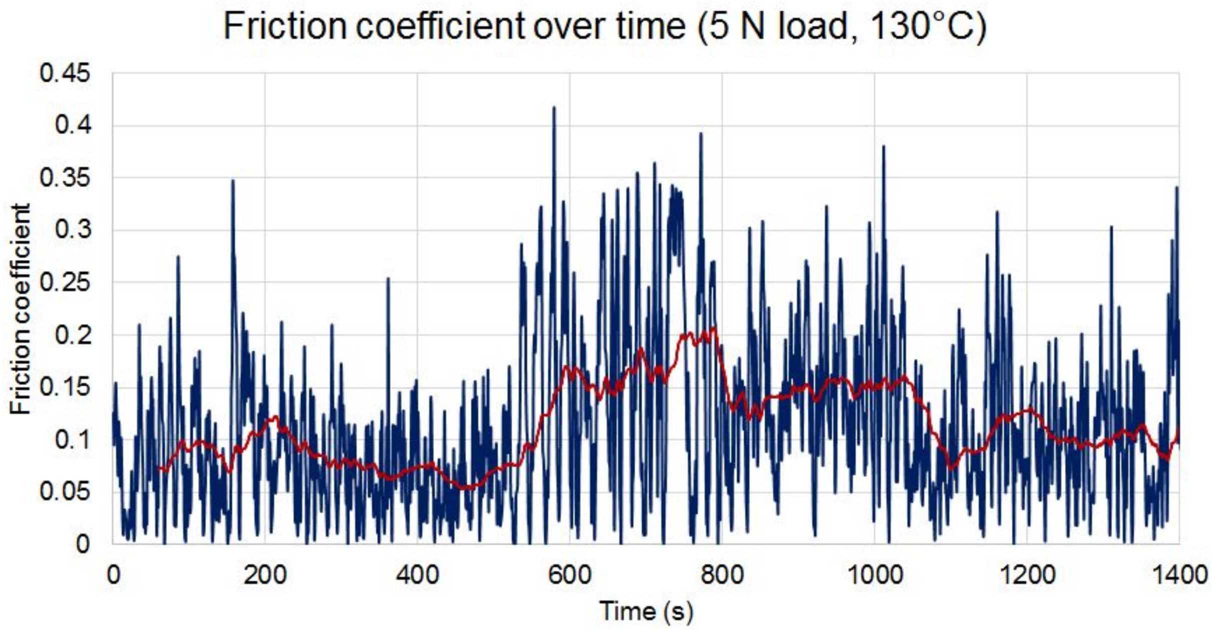

Friction coefficient over time (5 N load, 130°C)
Friction coefficient
Time (s)
0.45
0.4
0.35
0.3
0.25
0.2
0.15
0.1
0.05
0
0
200
400
600
800
1000
1200
1400

Beam Equations Matlab Script

```
E = 68.9e9; % Pa, Aluminium 6061

int = .0254/16;
e_max_vert = 0;
e_max_hori = 0;
boptH = 0;
hoptH = 0;
boptV = 0;
hoptV = 0;
Optimal = zeros(10, 5);
i = 1;
for l =0.05: .05: .5; % m, length
for b = int:int:0.127; % m

for h =int:int:0.127; %
I_vert = b * h^3 / 12; % m^4. longer dim is vertical
I_hori = h * b^3 / 12; % m^4. longer dim is horizontal

mu = linspace(0.1,10,100); % desired 0.05 to 0.5
Fn = 0.1:0.1:10; % N
Ff = Fn .* mu; % Possible friction values

% Vertical

delta_vert = (Fn * l^3) / (3 * E * I_vert); % deflection
e_vert = (l * Fn * h) / (2 * E * I_vert); % max strain (at edge)

if e_max_vert < max(e_vert) && max(e_vert) < 5000 *10^-6;
     e_max_vert = max(e_vert);
     boptH = b;
     hoptH = h;
end


% Horizontal

delta_hori = (Ff * l^3) / (3 * E * I_hori); % deflection
e_hori = (l * Ff * b) / (2 * E * I_hori); % max strain (at edge)

if e_max_hori< max(e_hori) && max(e_hori) < 5000 *10^-6;
      e_max_hori = max(e_hori);
      boptV = b;
     hoptV= h;
end

end
end
Optimal(i,1) = l;
Optimal(i,2)= boptH;
Optimal(i,3) =hoptH;

 Optimal(i,4)= boptV ;
 Optimal(i,5) =hoptV;

 i = i +1;
 end
```

Cantilever Optimization

	Horizontal beam		Vertical Beam	
Length of Bar (m)	b (m)	h (m)	b (m)	h (m)
0.05	0.0048	0.0016	0.0016	0.0349
0.1	0.0079	0.0016	0.0016	0.0349
0.15	0.0111	0.0016	0.0016	0.0349
0.2	0.0016	0.0048	0.0016	0.0349
0.25	0.0175	0.0016	0.0016	0.0349
0.3	0.0175	0.0016	0.0016	0.0349
0.35	0.0175	0.0016	0.0048	0.027
0.4	0.0175	0.0016	0.0048	0.027
0.45	0.0175	0.0016	0.0111	0.0063
0.5	0.0175	0.0016	0.0111	0.0063

Testing Base Temperature Model - Heating

Convection Cooling Losses			
Air @ 300K			
thermal conductivity	k	0.0259	W/mK
Prandtl number	Pr	0.707	
kinematic viscosity	v	1.59E-05	m^2/s
gravity	g	9.81	m/s^2
fluid temp	Tinf	295	K
surface temp	Ts	473	K
base perimeter	P	0.127	m
length scale	L	0.008	m
coeff of thermal expansion	beta	0.003	1/K
rayleigh number	Ra	8,289	
convection coefficient	h	16.81	
convection resistance	R conv	30.35	
Copper base			
base length	l	0.0318	m
base width	w	0.0318	m
base top area	A top	0.0010	m^2
base thickness	t	0.00889	m
base side area	A side	0.0008645	m^2
cavity length	l	0.02540	m
cavity width	w	0.02540	m
cavity height	h	0.00381	m
cavity vertical area	A cavity	0.00059	m^2
total area	A total	0.00198	m^2
	Qdot-conv	-5.865	W

Conduction Cooling Losses			
Grade L5 Ceramic and Carbon Steel Screw Support - Spacer Top/Bo			
base surface temp	Ts	473	K
environment temp	Tinf	295	K
thermal conductivity	k	2.9	W/mK
area of spacer	A	8.70E-05	m^2
height of spacer - w/ screw	L	0.01905	m
spacer resistance	R ceramic	75.5	K/W
area of steel screw	A	3.87E-05	m^2
screw thermal conductivity	k	16.2	W/mK
screw resistance	R screw	29.6	K/W
spacer and screw resistance	R top - bot	21.3	K/W
		10.65594	
Spacer Middle			
area of spacer middle	A	0.000127	m^2
height of spacer - w/o screw	L	0.01905	m
spacer w/o screw resistance	R middle	51.86	K/W
total resistance	R total	73.12	K/W
	Qdot-cond	-2.434	W

Temperature over Time Calculation (Lumped Capacitance)					
Copper base					
base length	l	0.0318	m		
base width	w	0.0318	m		
base thickness	t	0.0089	m		
base area	A	0.0010	m^2		
base volume	V base	8.96E-06	m^3		
cavity length	l	2.54E-02	m		
cavity width	w	2.54E-02	m		
cavity height	h	3.81E-03	m		
cavity volume	V cavity	2.46E-06	m^3		
net base volume	V total	6.5E-06	m^3		
thermal conductivity	k	385	W/mK		
density	rho	8960	kg/m^3		
heat capacity	c_p	385	J/kgK		
constant a	a	0.05	0.05	0.05	
constant b	b	22.43	22.43	22.43	
constant c	c	(214.49)	(214.49)	(535.14)	

Testing Base Temperature Model - Cooling

Convection Cooling Losses			
Nitrogen Gas (N2) @ 300K			
thermal conductivity	k	0.0259	W/mK
Prandtl number	Pr	0.716	
kinematic viscosity	v	1.59E-05	m^2/s
gravity	g	9.81	m/s^2
surface temp	Ts	223	K
fluid temp	Tinf	295	K
base perimeter	P	0.127	
length scale	L	0.008	
coeff of thermal expansion	beta	0.003	
rayleigh number	Ra	3,408	
convection coefficient	h	8.6523	W/(m^2*K)
convection resistance	R conv	59.11	K/W
copper			
base length	l	0.0318	m
base width	w	0.0318	m
base top area	A top	0.0010	m^2
base thickness	t	0.00889	m
base side area	A side	0.000564515	m^2
cavity length	l	0.02540	m
cavity width	w	0.02540	m
cavity height	h	0.00381	m
cavity vertical area	A cavity	0.00039	m^2
total area	A total	0.00193597	m^2
thermal conductivity	k	385	W/mK
	Qdot-gas conv	1.218	W

Conduction Cooling Losses			
Grade L3 Ceramic and Carbon Steel Screw Support - Spacer Top/Bottom			
base surface temp	Ts	223	K
environment temp	Tinf	295	K
thermal conductivity	k	2.9	W/mK
area of spacer	A	8.70E-05	m^2
height of spacer - w/ screw	L	0.01905	m
spacer resistance	R ceramic	75.5	K/W
area of steel screw	A	5.97E-05	m^2
screw thermal conductivity	k	16.2	W/mK
screw resistance	R screw	29.6	K/W
spacer and screw resistance	R top - bottom	21.3	K/W
		10.65395972	
Spacer Middle			
area of spacer middle	A	0.000128677	m^2
height of spacer - w/o screw	L	0.01905	m
spacer w/o screw resistance	R middle	51.86	K/W
total resistance	R total	73.12	K/W
	Qdot-cond	0.9846629436	

Temperature over Time Calculation (Lumped Capaci				
304 stainless steel base				
base length	l	0.0318	m	
base width	w	0.0318	m	
base thickness	t	0.0089	m	
base area	A	0.0010	m^2	
base volume	V base	8.96E-06	m^3	
cavity length	l	2.54E-02	m	
cavity width	w	2.54E-02	m	
cavity height	h	3.81E-03	m	
cavity volume	V cavity	2.46E-06	m^3	
net base volum	V total	6.504E-06	m^3	
density	rho	8960	kg/m^3	
heat capacity	c_p	385	J/kgK	
constant a	a	0.03		0.09
constant b	b	22.43		22.43
constant c	c	228.82		76.27